

**Characterization of the moonlighting function of the  
plastid pyruvate dehydrogenase complex in  
*Chlamydomonas reinhardtii***



**Dissertation**

zur Erlangung des Grades eines Doktors der Naturwissenschaften

an der Fakultät für Biologie

der Ludwig-Maximilians-Universität München

vorgelegt von

**Daniel Neusius**

München, 28. Juli 2020

Erstgutachter: Prof. Dr. Jörg Nickelsen

Zweitgutachter: Prof. Dr. Peter Geigenberger

Tag der Abgabe: 28.07.20

Tag der mündlichen Prüfung: 19.11.20

**TABLE OF CONTENT**

|   |    |
|---|----|
| Summary.....  | 4  |
| Zusammenfassung .....   | 6  |
| I. Introduction .....   | 8  |
| I.1. Origin and evolution of chloroplasts .....                 | 8  |
| I.2. Function of the chloroplast.....                           | 9  |
| 1.2.1 Fatty acid synthesis.....                                 | 9  |
| 1.2.2. Oxygenic photosynthesis .....                            | 10 |
| I.3. <i>Chlamydomonas reinhardtii</i> - A model organism .....  | 12 |
| I.4. Chloroplast gene expression.....                           | 13 |
| I.4.1. RNA metabolism in the chloroplast .....                  | 13 |
| I.4.2. Translation.....   | 14 |
| I.4.3. <i>psbA</i> gene expression .....                        | 16 |
| I.5. Moonlighting enzymes.....                                  | 18 |
| I.5.1 The pyruvate dehydrogenase complex.....                   | 18 |
| I.5.2. DLA2, a moonlighting enzyme.....                         | 21 |
| I.6. Lysine acetylation, an advancing regulatory mechanism..... | 22 |
| I.7. Aims of this study .....                                   | 24 |
| II. Material & Methods.....                                     | 25 |
| II.1. Material.....   | 25 |
| II.1.1. Chemicals.....  | 25 |
| II.1.2. Oligonucleotides .....                                  | 26 |
| II.1.3. Plasmids .....  | 26 |
| II.1.4. Enzymes.....  | 26 |
| II.1.5. Kits.....   | 26 |
| II.1.6. <i>Escherichia coli</i> strains .....                   | 26 |
| II.1.7. <i>Chlamydomonas reinhardtii</i> strains.....           | 27 |

|   |    |
|---|----|
| II.1.8. Antibodies .....  | 27 |
| II.1.9. Software and online tools .....   | 28 |
| II.2. Methods .....   | 28 |
| II.2.1. Growth and harvesting of bacterial strains .....  | 28 |
| II.2.2. Growth and harvesting of <i>C. reinhardtii</i> strains .....  | 28 |
| II.2.3. Chlorophyll fluorescence analysis of <i>C. reinhardtii</i> strains .....  | 29 |
| II.2.4. Drop plating test.....  | 29 |
| II.2.5. Nucleic acid methods.....   | 29 |
| II.2.6. Protein methods .....   | 32 |
| III. Results .....  | 40 |
| III.1. Mode of RNA-binding of DLA2 .....  | 40 |
| III.1.1. Protein structure of DLA2 .....  | 40 |
| III.1.2. Multiple domains are involved in RNA-binding of DLA2 .....   | 41 |
| III.1.3. E3BD is crucial for RNA recognition .....  | 45 |
| III.2. Is reversible lysine acetylation regulating DLA2 function?.....  | 47 |
| III.2.1. Differential acetylation of DLA2 <i>in vivo</i> .....  | 47 |
| III.2.2. Evolutionary conservation of K197 might enable lysine acetylation-dependent regulation in photosynthetic organisms.....              | 48 |
| III.2.3. Acetylation at K197 of DLA2 does not influence RNA-binding affinity <i>in vitro</i>  | 50 |
| III.3. Generation of a <i>dla2</i> mutant using the CRISPR/Cas9 system .....  | 52 |
| III.3.1. Complementation of the <i>dla2</i> mutant with a construct encoding an HA-tagged DLA2 version restores growth on minimal medium..... | 54 |
| III.3.2. Loss of DLA2 does not lead to severe changes in lipid and fatty acid accumulation in the presence of acetate .....                   | 57 |
| III.4. Analysis of mutants mimicking the acetylation state of K197 of DLA2 <i>in vivo</i> .....   | 59 |
| III.4.1. Modification of the acetylation state of K197 leads to altered growth under photoautotrophic conditions .....                        | 59 |
| III.4.2. The acetylation state of K197 influences cpPDC activity.....   | 62 |

|  |     |
|--|-----|
| III.4.3. cpPDC complex stability is influenced by acetylation of K197 within the E3BD .....                      | 63  |
| III.4.4. Lysine acetylation leads to membrane attachment of DLA2 .....   | 65  |
| III.4.5. K197 acetylation results in an increased RNP complex formation <i>in vivo</i> .....                     | 67  |
| III.4.6. Knockout of <i>DLA2</i> results in a reduction of D1 synthesis for PSII <i>de novo</i> biogenesis ..... | 72  |
| IV. Discussion .....   | 76  |
| IV.1. Mode of RNA-binding of DLA2.....   | 76  |
| IV.2. DLA2 is essential for growth of <i>C. reinhardtii</i> under photoautotrophic growth conditions .....       | 78  |
| IV.3. Lysine acetylation is regulating the moonlighting function of DLA2 .....                                   | 79  |
| IV.3.1. Acetylation of K197 leads to cpPDC disassembly.....  | 79  |
| IV.3.2. Acetylation of K197 leads to RNP complex formation .....   | 81  |
| IV.3.3. DLA2 is regulating D1 synthesis for PSII <i>de novo</i> biogenesis .....                                 | 85  |
| IV.4. Evolutionary conservation of DLA2's moonlighting function and regulation .....                             | 88  |
| IV.5. Conclusion and future perspectives.....  | 89  |
| V. References.....   | 90  |
| VI. Appendix .....   | 108 |
| List of abbreviations .....  | 127 |
| Curriculum Vitae .....   | 130 |
| Danksagung .....   | 132 |
| Eidesstattliche Erklärung .....  | 134 |

## SUMMARY

Chloroplast gene expression depends greatly on nuclear gene products which are imported into plastids and regulate gene expression on various levels. This thesis aimed to further characterize such a factor in *Chlamydomonas reinhardtii*, namely the dihydrolipoamide acetyltransferase (DLA2) of the chloroplast pyruvate dehydrogenase complex (cpPDC). DLA2 has previously been shown to possess a moonlighting activity in chloroplast gene expression besides its catalytic function in providing acetyl-CoA for plastid fatty acid synthesis. Under mixotrophic conditions, i.e. in the presence of light and acetate, DLA2 was shown to form a ribonucleoprotein (RNP) complex involving the *psbA* mRNA.

The data presented in this thesis show that two domains, the putative E3-binding domain (E3BD) and the catalytic domain, are crucial for RNA-binding of DLA2. While the catalytic domain is decisive for overall RNA-binding affinity, the E3BD is responsible for RNA specificity by recognizing an A-rich region in the 5' UTR of the *psbA* mRNA.

The generation of a *dla2* mutant using the CRISPR/Cas9 system recently established for *C. reinhardtii* enabled the analysis of the two functions of DLA2 in more detail and showed that the absence of DLA2 results in inhibition of photoautotrophic growth. Moreover, the analysis of lysine acetylation of the proteome of *C. reinhardtii* revealed that a lysine residue at position 197 (K197) in the E3BD of DLA2 is increasingly acetylated in the presence of acetate. Complementation of the generated *dla2* mutant with DLA2 versions containing amino acid substitutions at K197 which mimic constitutive acetylation or deacetylation showed that the acetylation state of K197 regulates PDC activity and thereby RNP formation. The data reveal that acetylation at K197 leads to disassembly of the cpPDC and a concomitant formation of the membrane bound RNP complex involving DLA2 and the *psbA* mRNA. Moreover, the first report of Förster resonance energy transfer (FRET) microscopy detecting RNA-protein interaction in *C. reinhardtii* shows that the RNP complex is mainly localized around the pyrenoid where the *de novo* biogenesis of photosystem II (PSII) at translation zones is located. Sulfur depletion-dependent degradation followed by reaccumulation of PSII could confirm that DLA2 is involved in the D1 synthesis for *de novo* biogenesis of PSII. Interestingly, analysis of the FRET microscopy data under photoautotrophic conditions suggest that the RNP complex is not exclusively formed under mixotrophic conditions and that acetylation at K197 of DLA2 is rather regulating RNP complex accumulation.

In conclusion, the data presented in this thesis significantly enhances the understanding of the RNA-binding mode of DLA2 and identify reversible lysine acetylation as the key

mechanism for regulation of DLA2 functions. Furthermore, the data gives final proof for DLA2 function in regulation of *psbA* gene expression and thereby the role of DLA2 as integrator protein, coordinating carbon metabolism and gene expression in the chloroplast in response to environmental conditions.

## ZUSAMMENFASSUNG

Die plastidäre Genexpression hängt zu einem großen Teil von kerncodierten Proteinen ab, die in Chloroplaste importiert werden und dort die Genexpression auf verschiedenen Ebenen regulieren. Diese Arbeit zielte darauf ab solch ein Protein, nämlich die Dihydrolipoamid-S-Acetyltransferase (DLA2) des plastidären Pyruvatdehydrogenase (PDH) Komplexes, in der Grünalge *Chlamydomonas reinhardtii* näher zu charakterisieren. Frühere Studien zeigen, dass DLA2 zusätzlich zu seiner eigentlichen Funktion in der Produktion von Acetyl-CoA für die plastidäre Fettsäuresynthese noch eine zweite Funktion in der plastidären Genexpression besitzt und somit ein *moonlighting* Enzym ist. Hierbei wurde gezeigt, dass unter mixotrophen Bedingungen, also in Anwesenheit von Licht und Acetat als externer Kohlenstoffquelle, DLA2 mit der *psbA* mRNA einen Ribonukleoproteinkomplex (RNP-Komplex) bildet.

Die in dieser Dissertation präsentierten Daten belegen, dass zwei Domänen immens wichtig für die RNA-Bindung von DLA2 sind, die potenzielle E3-Bindedomäne (E3BD) sowie die katalytische Domäne. Während die katalytische Domäne entscheidend für die generelle RNA-Bindefähigkeit von DLA2 ist, ist die E3BD für die Spezifität der Bindung zuständig, indem sie eine Adenin-reiche Sequenz in der 5' UTR der *psbA* mRNA erkennt und bindet.

Die Herstellung einer *dla2* Mutante mit Hilfe des kürzlich für *Chlamydomonas* etablierten CRISPR/Cas9 Systems ermöglichte eine genauere Analyse der beiden Funktionen von DLA2 und zeigte, dass ohne DLA2 kein photoautotrophes Wachstum mehr möglich ist. Des Weiteren führte die Analyse des *Chlamydomonas* Proteoms bezüglich Lysin-Acetylierung zur Identifizierung eines sich in der E3BD befindenden Lysin-Restes (K197), der in der Anwesenheit von Acetat zunehmend acetyliert wird. Die *dla2* Mutante wurde daraufhin mit DLA2-Versionen komplementiert, die einen Aminosäureaustausch an K197 enthielten, um die konstitutiv acetylierte oder nicht-acetylierte Form nachzuahmen. Es konnte gezeigt werden, dass der Acetylierungsstatus von K197 die PDH-Aktivität und damit einhergehend die RNP-Bildung reguliert. Die in dieser Arbeit gezeigten Daten verdeutlichen, dass Acetylierung an K197 zu einer Disassemblierung des PDH-Komplexes und damit gleichzeitig zu einer Bildung des Membran-assoziierten RNP-Komplexes führt, welcher DLA2 und die *psbA* mRNA beinhaltet. Die, unseres Wissens nach, erste Durchführung von Förster-Resonanzenergietransfer (FRET) Mikroskopie, die zur Detektion von RNA-Protein-Interaktionen in *C. reinhardtii* genutzt wurde, zeigte, dass der RNP-Komplex zu einem großen Teil um den Pyrenoid angeordnet ist. Dies ist ebenjener Ort, an dem die de-novo-Synthese von Photosystem II (PSII) an den sogenannten Translationszonen stattfinden soll. Des Weiteren

wurden Experimente durchgeführt, bei denen durch Schwefelverarmung ein PSII-Abbau herbeigeführt wurde, um die anschließende PSII de-novo-Synthese in Bezug auf D1 isoliert betrachten zu können. Diese bestätigten, dass DLA2 die D1 Synthese reguliert, welche für die de-novo-Biogenese von PSII benötigt wird. Interessanterweise zeigen die Daten der FRET Mikroskopie, welche unter photoautotrophen Bedingungen aufgenommen wurden, dass der RNP-Komplex nicht wie zuvor gedacht nur unter mixotrophen Bedingungen gebildet wird und dass die Acetylierung an K197 von DLA2 die Anreicherung des Komplexes reguliert.

Abschließend lässt sich sagen, dass die Daten, welche im Rahmen dieser Arbeit präsentiert werden, zum umfassenderen Verständnis der DLA2-RNA-Bindung beitragen und die reversible Lysin-Acetylierung als den entscheidenden Regulationsmechanismus für die DLA2 Funktionen identifizieren. Des Weiteren beweisen die Daten endgültig die Beteiligung von DLA2 an der Regulation der *psbA* Genexpression und somit die Rolle von DLA2 als Schnittstelle, die den Kohlenstoffmetabolismus und die Genexpression im Chloroplasten, abhängig von äußeren Einflüssen, verbindet und koordiniert.

## I. INTRODUCTION

### I.1. Origin and evolution of chloroplasts

Like mitochondria, chloroplasts descend from an event of primary endosymbiosis. This so-called endosymbiotic theory was first postulated by Mereschkowsky (1905) but the attention it received from the scientific community was limited. Since the repostulation by Margulis (1967) the theory gained broader acceptance. Nowadays, we know that mitochondria descend from an  $\alpha$ -proteobacterium-like prokaryote which was taken up by a host cell around 1.5 - 2.2 billion years ago. 1.2 – 1.5 billion years ago a eukaryotic host cell engulfed a cyanobacterium-like cell leading to the formation of the first plastids and by this the first photosynthetic eukaryotic cell (Figure 1). This means that all plastids derive from one endosymbiotic event (McFadden and van Dooren, 2004; for a review on endosymbiosis see Gould et al., 2008).

Over time and evolution, the new derived organisms had to cope with the complexity of having two or even three genomes, therefore extensive restructuring was necessary. This process involved the loss of unrequired or redundant genes and the huge translocation of genes from the inherited genomes to the nucleus (Bock and Timmis, 2008). Because of this lateral gene transfer, more than 98 % of the chloroplast proteins of nowadays plants and algae are encoded in the nucleus with only 99 expressed genes left in the plastome of *Chlamydomonas reinhardtii* (Maul et al., 2002). Most of the remaining chloroplast genes code for proteins involved in photosynthesis but also other important chloroplast functions, like fatty acid synthesis or gene expression (Sato et al., 1999). For all photosynthetic complexes, the small size of the plastome led to a combination of protein subunits which are encoded in the plastome and of proteins encoded in the nucleus. Even the arguably most important enzyme in photosynthesis, the ribulose-1,5-bisphosphate carboxylase/oxygenase (Rubisco), or plastid ribosomes consist of both plastid and nuclear-encoded subunits (Sato et al., 1999; Barkan and Goldschmidt-Clermont, 2000). As most chloroplast proteins are translated by cytosolic ribosomes, there is a crucial need for an efficient protein import system into chloroplasts. This system is assisted by cytosolic proteins which keep proteins in an importable state and targeting them to the import machinery which consists of the TOC (Translocon at the outer envelope of chloroplasts) and the TIC (Translocon at the inner envelope of chloroplasts) complex (Jarvis and Soll, 2002). Most of the nucleus-encoded chloroplast proteins have a cleavable N-terminal sequence for targeting to the chloroplast, although many proteins targeted to the outer chloroplast membrane miss such a transit peptide (Strittmatter et al., 2010).

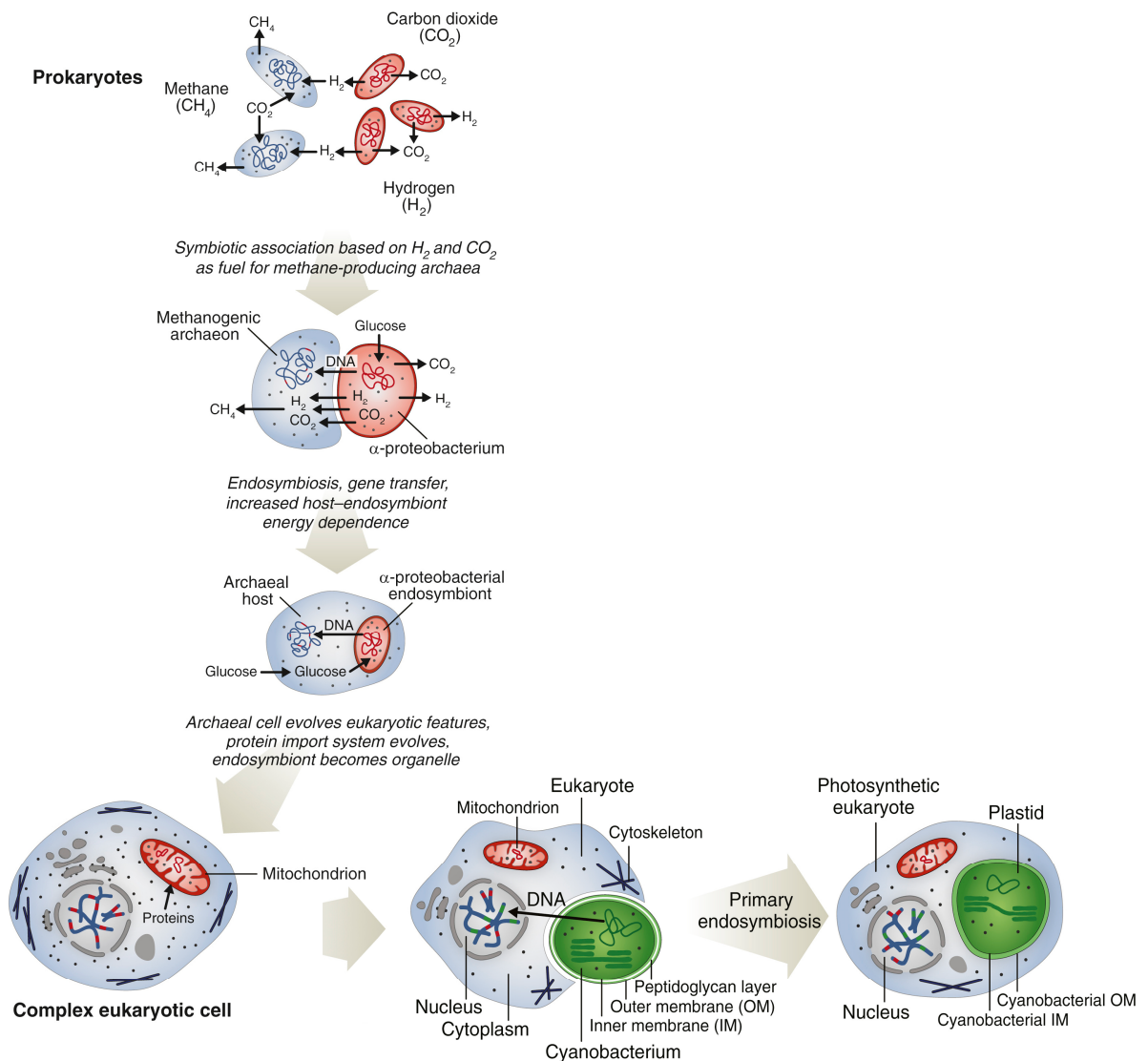


**Figure 1: Scenario for the origin of the first eukaryotic photosynthetic cell.**

The two major primary endosymbiotic events resulting in the formation of mitochondria and chloroplasts followed by lateral gene transfer are shown. Adapted from Archibald (2015).

## I.2. Function of the chloroplast

### 1.2.1 Fatty acid synthesis

Chloroplasts contain and fulfill many essential pathways and functions like assimilation of nitrogen and sulfur, synthesis of fatty acids and amino acids, and above all photosynthesis. While fatty acid synthesis takes place in the cytosol of non-photosynthetic eukaryotes, in most plant and algae species it is exclusively performed in the chloroplast (Rawsthorne, 2002). The first and rate-limiting step of fatty acid synthesis is the formation of malonyl-CoA from acetyl-CoA by acetyl-CoA carboxylase in an ATP-dependent way. The sequential steps of fatty acid synthesis which, in short, consist of chain elongation by the addition of acetyl residues to the



Photosystem II (PSII) is the first complex in the electron transport chain and exists as a dimer in its active form with the monomer consisting of at least 27 to 28 subunits (Figure 2; Dekker and Boekema, 2005). Photons are absorbed by the attached light-harvesting complexes (LHCs) leading to an energy transfer to a chlorophyll molecule in the PSII reaction center which is built by the core proteins D1 and D2 (Nelson and Junge, 2015). The excited electron is subsequently transferred via plastoquinone to the second photosynthetic complex, the cytochrome *b<sub>6</sub>/f* complex. Missing electrons in the PSII core are immediately filled up by the oxidization of H<sub>2</sub>O at the oxygen-evolving complex (Suga et al., 2015). Afterwards, the electron at the cytochrome *b<sub>6</sub>/f* complex is transferred via plastocyanin to the third photosynthetic complex, photosystem I (PSI) (Nelson and Ben-Shem, 2005). Here, another photon is absorbed by the attached LHCs and the energy is transferred to the PSI core for a second charge separation. Via several chlorophylls, a quinone and several iron sulfur clusters, the electron is passed through PSI to reduce ferredoxin, a soluble electron carrier protein at the stromal side of PSI (Melkozernov et al., 2006). Subsequently, the ferredoxin is used for reduction of NADP<sup>+</sup> at the ferredoxin-NADP<sup>+</sup> reductase to generate the important reducing equivalent NADPH (Mulo, 2011). During the transport of the electrons along the ETC, protons are released into the thylakoid lumen and generate, together with protons released at the photolysis of H<sub>2</sub>O, a proton gradient across the thylakoid membrane. This proton motive force is used by the fourth photosynthetic complex, the ATP synthase, to synthesize adenosine triphosphate (ATP) from adenosine diphosphate (ADP) and phosphate (Nelson and Junge, 2015).

In the light-independent reaction, the chemical energy fixed in the light-dependent reaction in form of NADPH and ATP is used for the synthesis of carbohydrates (Buchanan, 2016). The so-called Calvin-Benson-Bassham cycle was first described in 1950 (Bassham et al., 1950). The first and most important phase is the carbon fixation. Carboxylation of ribulose-1,5-bisphosphate catalyzed by Rubisco leads to the fixation of CO<sub>2</sub> and the production of two molecules 3-phosphoglycerate. In phase two, a phosphorylation and a reduction step lead to the production of glyceraldehyde-3-phosphate which can be used for the synthesis of glucose and other metabolic processes. In phase 3, ribulose-1,5-bisphosphate is regenerated for the fixation of another CO<sub>2</sub> molecule (Eberhard et al., 2008; Buchanan, 2016). As oxygenic photosynthesis and especially the light-dependent reaction is crucially depending on light and other abiotic factors, there are many levels of regulation, adaptation and reorganization in response to environmental stimuli (reviewed in Michelet et al., 2013; and in Minagawa and Tokutsu, 2015).

### **I.3. *Chlamydomonas reinhardtii* - A model organism**

Along *Synechocystis* sp. PCC 6803, *Physcomitrella patens*, *Arabidopsis thaliana* and *Nicotiana tabacum*, *Chlamydomonas reinhardtii* is one of the most studied model organisms in photosynthetic research (Nickelsen and Kuck, 2000). It is a small unicellular, biflagellate green alga with a size of about 10  $\mu\text{m}$  (Figure 3). It has a single cup-shaped chloroplast which makes it extremely useful in the analysis of chloroplast mutants (Harris, 1989). Furthermore, *Chlamydomonas* is a haploid organism which makes it easy to analyze nuclear gene mutants as well. Solely, the gene specific generation of nuclear mutants was impracticable, as homologous recombination only occurs at extremely low frequency in the *Chlamydomonas* nucleus. Therefore, the recent establishment of the CRISPR/Cas9 system for *C. reinhardtii* was a breakthrough for the future characterization of many factors (Greiner et al., 2017). Furthermore, the recent creation of an online mutant insertion line library facilitated the analysis of many proteins once again (Li et al., 2016). Another important benefit is that the asexual reproduction of *C. reinhardtii* results in short generation times under favorable conditions. When the conditions are unfavorable, *C. reinhardtii* is also able to perform a sexual life cycle resulting in the recombination of the genetic material of different mating types ( $\text{mt}^-$  and  $\text{mt}^+$ ) which can be used for crossing of mutants (Ferris and Goodenough, 1994; Jiang and Stern, 2009). Moreover, *C. reinhardtii* cannot just grow photoautotrophically, but also mixo- and heterotrophically using acetate as carbon source, enabling the analysis of photosynthetic mutants. Another advantage of *C. reinhardtii* is that the three genomes are sequenced and transformation methods are established for all of them (Gray and Boer, 1988; Maul et al., 2002; Merchant et al., 2007). Even methods for the isolation of mitochondria and chloroplasts are established. The chloroplast of *C. reinhardtii* contains an eyespot which enables it to detect directions of light sources to perform phototaxis (Thompson et al., 2017). Another structure and target of a lot of research within the plastid of *C. reinhardtii* is the pyrenoid, a non-membrane-bound phase separated organelle, which is found in the chloroplast of most algae and a group of non-vascular plants (Brown Jr. and Arnott, 1970; Wang et al., 2015). With its high accumulation of Rubisco and a carbon concentrating mechanism, the pyrenoid is a special site of carbon fixation (Zhan et al., 2018; Itakura et al., 2019; Wunder et al., 2019).

Taken together, with the recent establishment of the CRISPR/Cas9 system, the single chloroplast and the short generation time, *C. reinhardtii* is an ideal model organism for the analysis of nuclear encoded factors in the chloroplast.

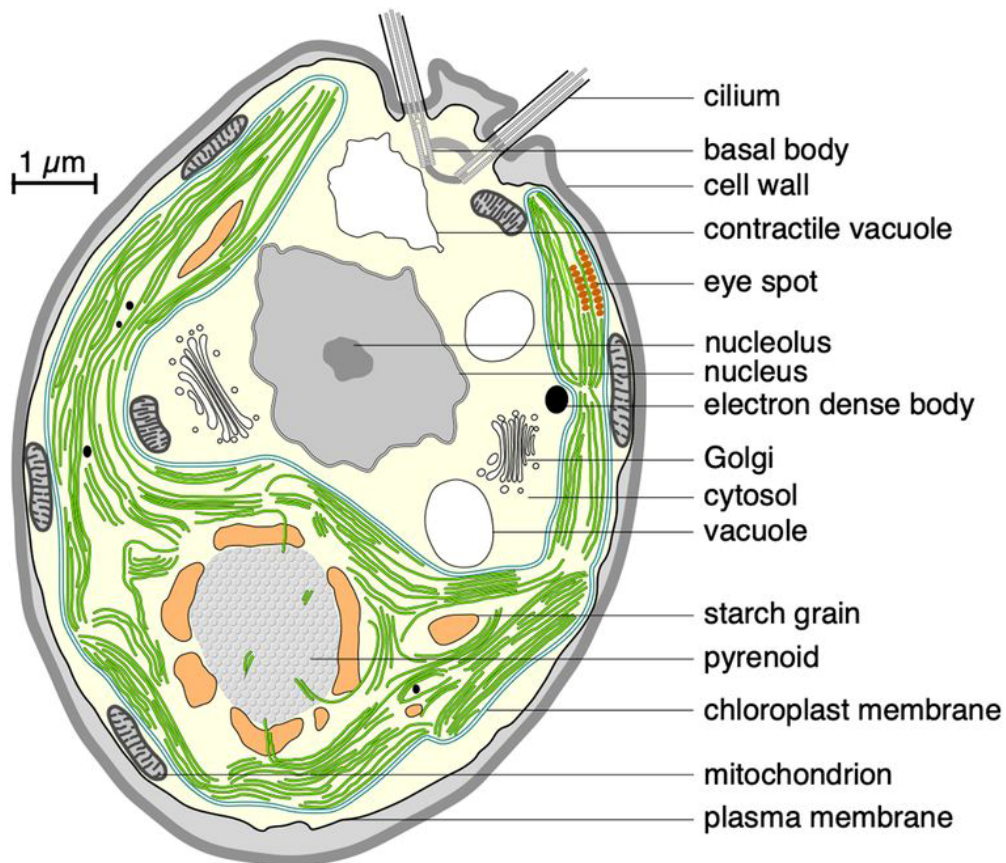


**Figure 3: Schematic overview of a *Chlamydomonas reinhardtii* cell (Salomé and Merchant, 2019).** Drawing of a *C. reinhardtii* cell based on a TEM image. Thylakoid membranes are depicted in green. The Rubisco-packed pyrenoid is depicted in grey within the chloroplast and is surrounded by a starch sheath (orange).

## I.4. Chloroplast gene expression

### I.4.1. RNA metabolism in the chloroplast

As outlined before, the three genomes in plant and algal cells combined with lateral gene transfer raises the need for a tight co-regulation of plastid with nuclear gene expression. Thus, chloroplast gene expression is very complex and differs significantly from eukaryotic or prokaryotic gene expression systems (Barkan and Goldschmidt-Clermont, 2000).

In higher plants and mosses, the first step of chloroplast gene expression, the transcription, is performed by two RNA polymerases, a nuclear-encoded (NEP) and a plastid-encoded RNA polymerase (PEP) (Hess et al., 1993). In contrast to that, *C. reinhardtii* and some other green algae possess only a PEP which is a multienzyme complex of four different subunits (Eberhard et al., 2002; Maul et al., 2002; Derelle et al., 2006). Furthermore, there is only one characterized sigma like transcription factor in green algae while higher plants often possess much more (Allison, 2000; Carter et al., 2004).

The next step of plastid gene expression is the processing of transcripts including RNA-editing, maturation of 5' and 3' ends, splicing of introns, polyadenylation, binding of RNA-binding proteins and other post-transcriptional modifications (Herrin and Nickelsen, 2004). RNA editing is a common step in plants, but this process seems to be completely absent in chlorophyte algae such as *Chlamydomonas* (Stern et al., 2010). There are also just three intron containing genes in the *C. reinhardtii* plastome (*psbA*, *psaA*, and 23S rRNA) which is much less than in most angiosperms (Plant and Gray, 1988; Maul et al., 2002). The quantity of genes transcribed in polycistronic primary transcripts was also thought to be greatly reduced compared to higher plants (Drapier et al., 1998; Stern and Drager, 1998). However, recent data show that this number might have been underestimated for years (Cavauiolo et al., 2017). These polycistronic transcripts are cleaved into monocistronic transcripts by ribonucleases (Hashimoto et al., 2003; Stoppel et al., 2011). An example of such a ribonuclease is the polynucleotide phosphorylase (PNPase) which is additionally the sole polyadenylation enzyme in *C. reinhardtii* (Yehudai-Resheff et al., 2007; Zimmer et al., 2009). Polyadenylation occurs in all three major RNA classes (mRNA, rRNA and tRNA) in the chloroplast of *C. reinhardtii* and is mainly thought to be a part of an RNA decay pathway (Komine et al., 2000; Komine et al., 2002). 5' and 3' untranslated regions (UTRs) are another aspect especially important for stability or degradation of transcripts (Stern et al., 2010). Binding of proteins to the RNA or secondary structures positioned at transcript ends like stem-loops are often involved in protection from exonucleolytic digest (Barkan, 2011). In the last 20 years a bulk of RNA-binding proteins has been characterized which bind to the 5' UTR and are involved in the processing of RNA or increasing the stability by hampering 5' → 3' exonuclease activity and with that define the position of the mature 5' end (Drager et al., 1998; Boudreau et al., 2000; Vaistij et al., 2000; Hammani et al., 2012; Jalal et al., 2015; Wang et al., 2015; Douchi et al., 2016; Viola et al., 2019). Nevertheless, half-lives of chloroplast mRNAs are generally long when compared to their bacterial counterparts which creates a need for additional levels of regulation of plastome expression (Barkan, 2011).

#### I.4.2. Translation

A lot of these additional regulation mechanisms occur at the level of translation and especially of translation initiation, which is the next step of gene expression. Chloroplast translation in general already differs significantly from the eukaryotic cytosolic process, as chloroplast ribosomes have a 70S composition like their prokaryotic counterparts because of their endosymbiotic origin. But despite their common ancestry chloroplast ribosomes differ significantly from bacterial ribosomes e.g. by having additional subunits (reviewed in Marin-

Navarro et al., 2007). In chloroplasts and bacteria, a purine-rich sequence, the so-called Shine-Dalgarno (SD) sequence, precedes about two thirds of the reading frames (Shine and Dalgarno, 1974; Drechsel and Bock, 2010; Scharff et al., 2017). This SD sequence interacts with a pyrimidine-rich sequence in the 16S rRNA to ensure the accurate positioning of the ribosome. The absence of such an SD sequence in one third of chloroplast and many bacterial genes together with experimental data suggest that there is also an SD-independent translation initiation (Scharff et al., 2011; Nakagawa et al., 2017). Nevertheless, the final impact of the SD sequence on chloroplast translation initiation was and is still a matter of discussion, as there is evidence that not all SD or SD-like sequences are essential for translation initiation of the respective transcripts (Mayfield et al., 1994; Hirose and Sugiura, 1996; Nickelsen et al., 1999). Another fact supporting the hypothesis that SD sequences are more dispensable in chloroplasts than in bacteria is, that the landscape of characterized factors involved in regulation of plastid translation and especially in translation initiation is huge and still growing. In the last 20 years there have been many publications identifying RNA-binding proteins which influence translation of chloroplast encoded proteins, e.g. TBC2, RBP40, TCA1, TDA1, TAB1 and recently MTH11 (Auchincloss et al., 2002; Schwarz et al., 2007; Loiselay et al., 2008; Eberhard et al., 2011; Rahire et al., 2012; Schwarz et al., 2012; Ozawa et al., 2020).

Many of these identified factors belong to the family of helical repeat proteins, composed of multiple tandem repeats of variable amino acid number. The three main classes of such proteins are the tetratricopeptide repeat (TPR), pentatricopeptide repeat (PPR) and octotricopeptide repeat (OPR) proteins (reviewed in Hammani et al., 2014). While TPR proteins were shown to be involved mainly in protein-protein interactions, PPR and OPR proteins are involved in the sequence-specific RNA-binding with the aforementioned functions in transcription, translation and most post-transcriptional RNA maturation steps (Hammani et al., 2014; Bohne et al., 2016).

An additional dimension of regulation of gene expression in the chloroplast has been described for *C. reinhardtii*, with the so-called translation zones (T-zones) and the related spatial organization of protein synthesis (Zerges and Rochaix, 1998; Uniacke and Zerges, 2007; Uniacke and Zerges, 2009; Sun et al., 2019). These T-zones were described as specialized regions adjacent to the pyrenoid and are thought to be the location where the expression of plastid-encoded PSII subunits is concerted with their assembly with nucleus-encoded subunits for the efficient *de novo* biogenesis of PSII. It was shown that these T-zones are characterized by a high accumulation of plastid ribosomes, transcripts coding for the PSII subunits *psbC* and *psbA* as well as of RBP40 (RB38), an RNA-binding protein involved in *psbD* expression

(Schwarz et al., 2012; Sun et al., 2019). The advantages of such specialized regions for an organism are numerous as PSII *de novo* assembly is a highly regulated and elaborated process and the misassembly as well as unbound pigments could lead to the generation of reactive oxygen species (ROS) (for a review on PSII assembly see Nickelsen and Rengstl, 2013).

Taken together, with all the nuclear factors characterized it seems obvious that the gross of the complex regulation machinery of chloroplast gene expression occurs at the post-transcriptional level with many nuclear-encoded factors being involved (Figure 4; Maier et al., 2008; Tillich et al., 2010).

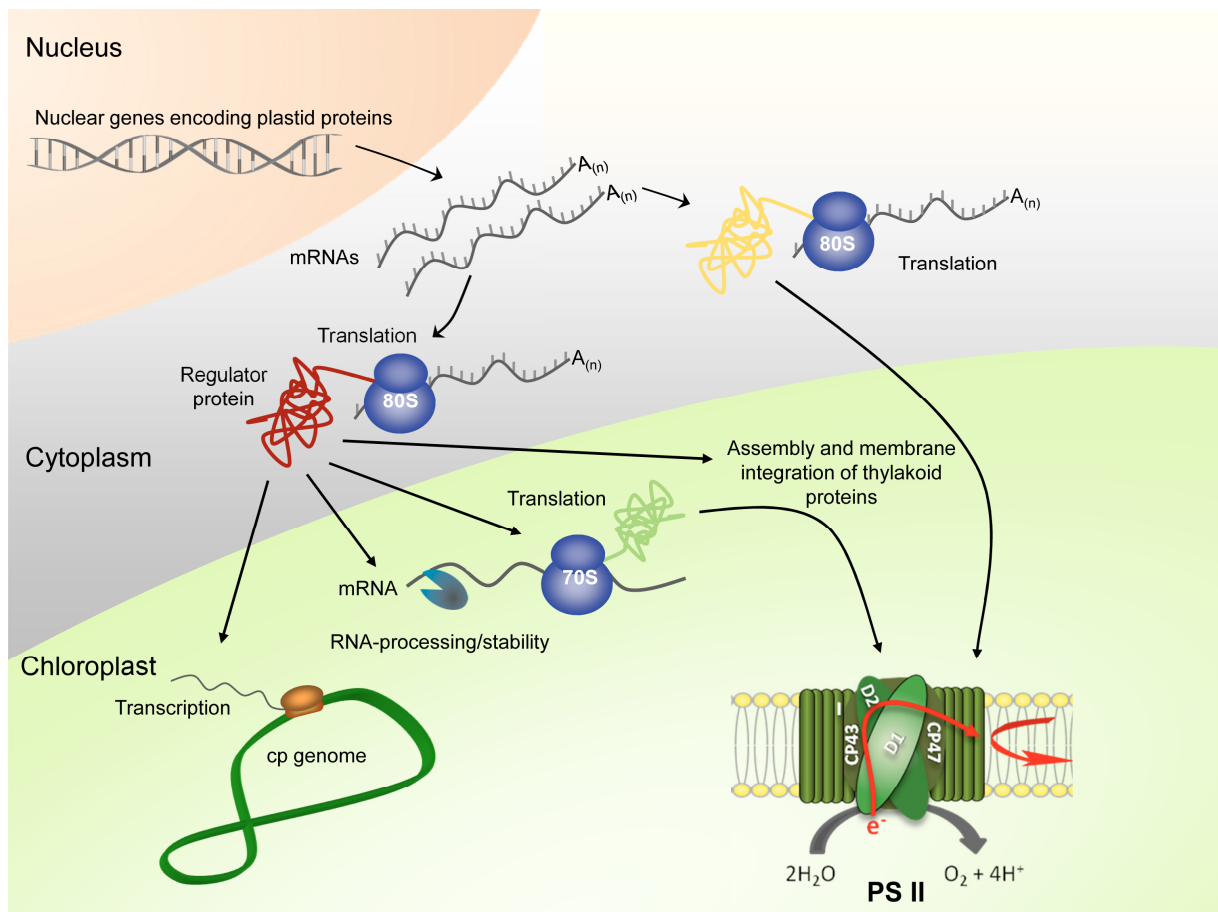


**Figure 4: The role of nuclear encoded proteins in the regulation of chloroplast gene expression.**

Nuclear encoded factors are translated at cytoplasmic ribosomes, are imported to the chloroplast where they are involved in the regulation of various processes, e.g. transcription, RNA-processing, translation, or the assembly of multi-protein complexes. Kindly provided by A. Bohne (adapted from Bohne et al. (2009)).

#### I.4.3. *psbA* gene expression

The most prominent example for this elaborated regulation in *C. reinhardtii* is arguably the regulation of the *psbA* gene expression resulting in the synthesis of the PSII core protein D1. Not only is *psbA* one of the most abundant transcripts in the chloroplast, but it is also

translated in two distinct processes, the PSII *de novo* assembly and the PSII repair (Nickelsen and Rengstl, 2013; Sun et al., 2019).

The main regulation of *psbA* expression was shown to involve at least one multi-protein complex. This complex consists of at least 4 proteins (RB47, RB38, RB60 and RB55) which bind to an SD sequence within a stem-loop structure in the 5' UTR of the *psbA* mRNA (for a review on *psbA* expression see Mulo et al., 2012). Here, RB47, a poly(A)-binding protein, and RB38, a poly(U)-binding protein, were described to bind the *psbA* mRNA with the RNA-binding of RB38 only shown *in vitro*. RB60, a protein disulfide isomerase, as well as an additional factor, TBA1, were postulated to be involved in the redox regulation of the RNA-binding activity of RB47 while the function of RB55 still remains elusive.

Besides this regulation and the aforementioned spatial separation of *psbA* expression postulated by Uniacke and Zerges (2007), the *de novo* synthesis of D1 and other PSII subunits is even controlled on additional levels. To ensure the coordinated accumulation of certain subunits of photosynthetic complexes, plastid proteases degrade subunits which are not assembled with their respective partners (Wollman et al., 1999). Moreover, a mechanism called control by epistasy of synthesis (CES), described by Choquet and Vallon (2000), involves a negative feedback regulation of unassembled D1 protein on the expression of its own corresponding mRNA and the mRNA of subsequent subunits in assembly (Minai et al., 2006). This results in a sort of hierarchy where D1 is only expressed when D2 is accumulating, CP47 is only expressed when D1 is accumulating and so on (D2 for D1 or D1 for CP47). A series of autoregulation of subunits was also described for PSI and the cytochrome *b6/f* complex (Choquet et al., 2001; Wostrikoff et al., 2004; reviewed in Sun and Zerges, 2015).

A feature that distinguishes the D1 protein from other PSII subunits is its high vulnerability to light induced damage. Thus, organisms have developed an elaborated mechanism called the PSII repair cycle to efficiently cope with photodamage (reviewed in Theis and Schroda, 2016). In short, this cycle involves the lateral migration of photodamaged PSII complexes from the grana stacks to stromal thylakoids, the degradation of photodamaged D1 by two proteases (Deg and FtsH proteases), and the subsequent co-translational insertion of the newly synthesized D1 protein. As D1 translation for PSII repair is distributed over stromal thylakoids in the chloroplast, it is distinctly separated from D1 translation for PSII *de novo* biogenesis at the T-zones described by Uniacke and Zerges (2007).

Furthermore, an additional factor has been described to be involved in the regulation of *psbA* expression in *C. reinhardtii*, namely DLA2 (Ossenbühl et al., 2002; Bohne et al., 2013). Interestingly, DLA2 is also the E2 subunit of the plastid pyruvate dehydrogenase complex. This

new characterized RNA-binding function of DLA2 makes it not only a protein being involved in the above described complex mechanism of *psbA* regulation, but also a member of the highly interesting group of moonlighting enzymes.

## **I.5. Moonlighting enzymes**

Moonlighting enzymes are a class of multifunctional proteins in which a single polypeptide chain performs multiple, often completely separated functions (reviewed in Jeffery, 2018). They are thought to have started from unifunctional proteins whose second function evolved over time but there is also evidence for cases where the dual function resulted from the fusion of two genes that initially encoded proteins with single functions (Jeffery, 2003; Brill and Fani, 2004; Gancedo and Flores, 2008). In either case these enzymes are favorable to the synthesis of two separate proteins concerning consumption of energy and resources like amino acids (Jeffery, 1999). The first moonlighting enzyme described was a crystallin in the lens of vertebrates which also had an argininosuccinate lyase activity (Piatigorsky, 1998). Soon, the characterization of many more moonlighting enzymes followed and even a database for the collection of such proteins was implemented (Mani et al., 2015). The first moonlighting enzyme which was identified in chloroplasts was a sulfite reductase which possesses a DNA-binding capacity and is involved in regulation of plastid transcription in addition to its enzymatic function (Sekine et al., 2002). Despite the large number of characterized moonlighting enzymes in mammals, yeast and bacteria, there are still only a few reported proteins in chloroplasts to date (Cohen et al., 2006; Bross et al., 2017; Abolhassani Rad et al., 2018; Schreier et al., 2018; Schmid et al., 2019). One of these moonlighting proteins identified in the chloroplast is the aforementioned DLA2, a subunit of the PDC (Bohne et al., 2013).

### **I.5.1 The pyruvate dehydrogenase complex**

The PDC is a ubiquitous enzyme complex among organisms which is in eukaryotes located within mitochondria. In the last 10 years the research on the mitochondrial pyruvate dehydrogenase complex (mtPDC) is flourishing again as it was shown to be involved in some forms of cancer, type 2 diabetes and obesity (Imbard et al., 2011; Patel et al., 2012; Jeoung et al., 2014; reviewed in Byron and Lindsay, 2017). Photosynthetic eukaryotes additionally possess a second form of the PDC which is located in the chloroplast. Like its mitochondrial counterpart, the plastid pyruvate dehydrogenase complex (cpPDC) is a multi-enzyme complex which is catalyzing the reaction from pyruvate to acetyl-CoA (Thompson et al., 1977). It consists of many copies of three different subunits. The E1 subunit is the pyruvate

dehydrogenase and is catalyzing the decarboxylation of pyruvate and the associated reductive acetylation of the lipoyl group covalently bound to the E2 subunit which is the dihydrolipoyl acetyltransferase (DLA2 in *C. reinhardtii*). Subsequently, the E2 subunit catalyzes the transfer of the acetyl moiety to coenzyme A (CoA) resulting in the formation of acetyl-CoA. In the last step, the E3 subunit, which is the dihydrolipoamide dehydrogenase (DLD2 in *C. reinhardtii*), performs the oxidative regeneration of the lipoyl residue and thereby produces NADH.

In many organisms e.g. *Chlamydomonas*, the E1 subunit is composed of heterotetramers of two proteins, E1 $\alpha$  and E1 $\beta$  (PDC2 and PDH2 in *C. reinhardtii*). A schematic overview of the reaction catalyzed by the PDC is depicted in Figure 5.

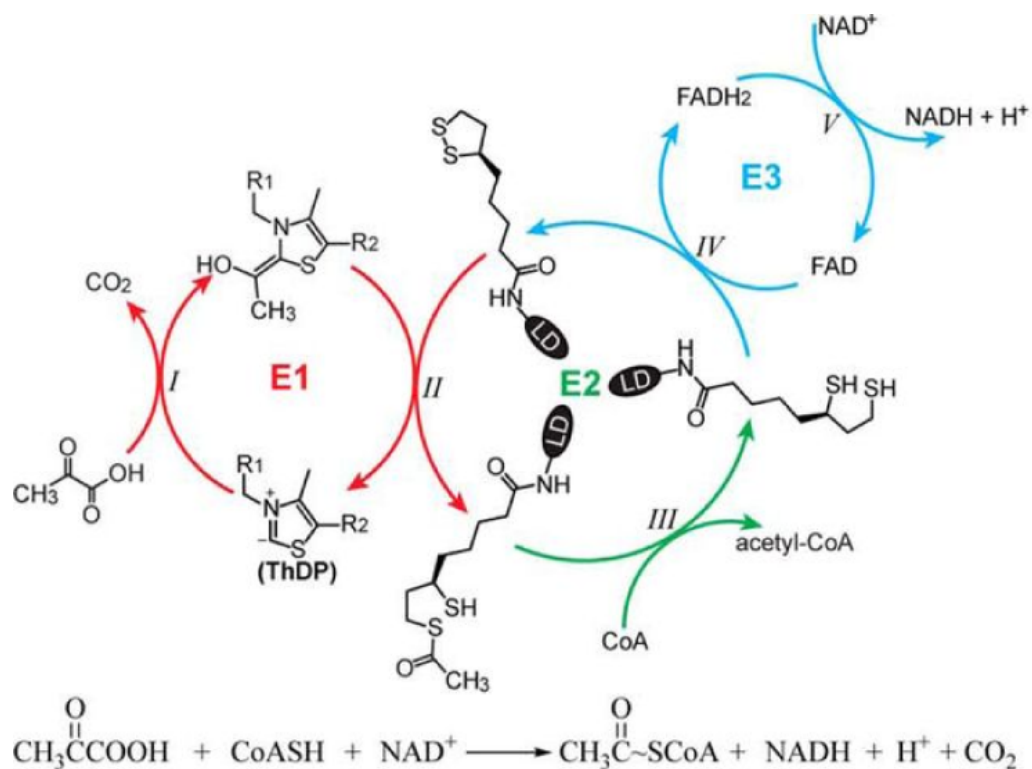


**Figure 5: Mechanism of the reaction from pyruvate to acetyl-CoA catalyzed by the PDC (Patel et al., 2014).** The by the E1 subunit catalyzed reactions, involving a thiamin diphosphate (ThDP) cofactor, are depicted in red. The reactions catalyzed by E2 and E3, which involve a dihydrolipoyl moiety bound to the lipoyl-binding domain (LD) of E2, are shown in green and blue, respectively.

The general organization of the enzymatic complex in different organisms can be grouped into two classes. The prokaryotic type which is present in *Escherichia coli* and many gram-negative bacteria is the simplest form of this assembly with about 12 copies of E1, 24 copies of E2 and 6 copies of E3 (Chandrasekhar et al., 2013). The eukaryotic type which is present in mitochondria of most eukaryotes and in some gram-positive bacteria is more elaborated as it usually contains more copies (about 60 copies of E2) and by this comprising

one of the largest multienzyme complexes known (Zhou et al., 2001). Additionally, higher eukaryotic PDCs usually have two associated regulatory enzymes, pyruvate dehydrogenase kinase (PDK) and pyruvate dehydrogenase phosphatase (PDP), which regulate the PDC activity via reversible phosphorylation at the E1 subunit (Gudi et al., 1995; Huang et al., 1998). Some eukaryotes like yeast, nematodes and mammals even have an additional structural component, the E3-binding protein (E3BP). This E3BP probably substitutes for E2 subunits in the core to mediate the E2-E3 binding (Vijayakrishnan et al., 2010). Little is known about the structure of the PDC in the chloroplast of plants and algae but the absence of E3BPs, PDKs and PDPs in the so far analyzed organisms suggests that it resembles the prokaryotic type (Johnston et al., 1997; Mooney et al., 2002).

Although the number of subunit copies and with that the size of the two complex types can vary immensely (4.5 MDa in *E. coli*, 9 MDa in *H. sapiens*), the general structure is very similar with a dodecahedral or cubic inner core of E2 subunits serving as a scaffold with the other components organized around it (Figure 6; for an overview on PDC structures, see Patel et al., 2014). This scaffold consists of trimers of E2 subunits with the C-terminal half building the 3-dimensional structure and the N-terminal part with the lipoyl moiety being very flexible (Yang et al., 1997; Zhou et al., 2001).

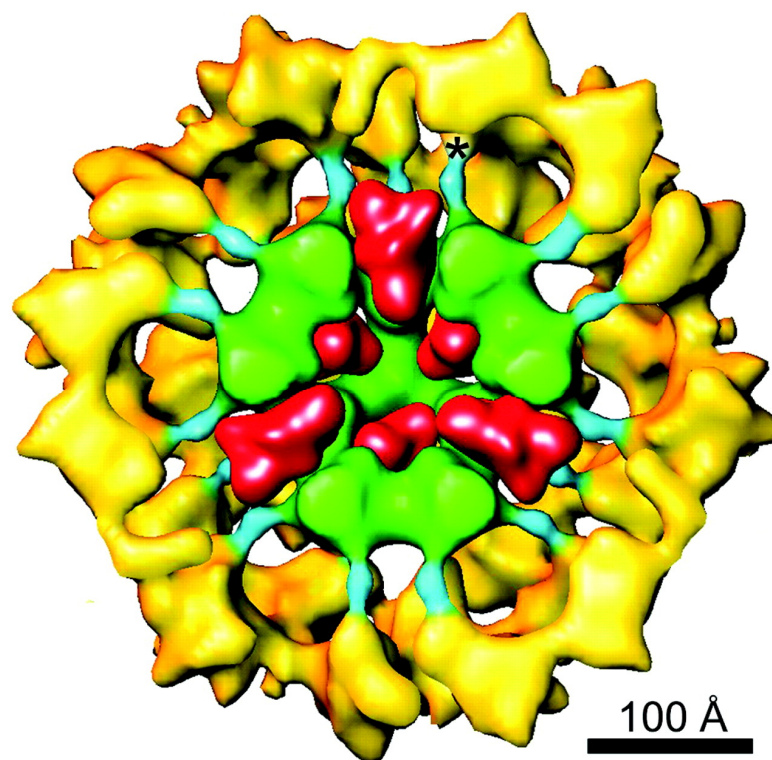


**Figure 6: Cut-away model of the fully assembled PDC (Zhou et al., 2001).**

Zhou et al. (2001) used the X-ray structure of the E3-homodimer (red) of *Azotobacter vinelandii* and docked it into the E2-core structure of *Saccharomyces cerevisiae* (green). The E1 subunits are shown in yellow.

While the activity of the cpPDC is not regulated by phosphorylation, both the cpPDC and the mtPDC are sensitive to product inhibition (Camp et al., 1988). Furthermore, the cpPDC activity is regulated by the pH and  $Mg^{2+}$  concentration in the chloroplast which change when plants are shifted to the light (Camp and Randall, 1985; reviewed in Tovar-Mendez et al., 2003).

The acetyl-CoA which is produced by the cpPDC is crucial for fatty acid synthesis in the chloroplast, especially under photoautotrophic conditions (Camp and Randall, 1985; Mooney et al., 2002; Lin and Oliver, 2008). The ability of *C. reinhardtii* to use acetate from the medium to produce acetyl-CoA makes PDC activity redundant under conditions where acetate is available. This likely enables DLA2 to fulfill a second distinct function in RNA binding and regulation of *psbA* expression.

### I.5.2. DLA2, a moonlighting enzyme

The RNA-binding activity of DLA2 was first identified by Ossenbühl et al. (2002) who were screening for RNA-binding proteins in the chloroplast of *C. reinhardtii* and named the protein RBP63. It was shown to bind to a poly(A)-stretch in the 5' UTR of the *psbA* mRNA and was thylakoid associated. Later on, Bohne et al. (2013) identified the RBP63 as the dihydrolipoyl acetyltransferase subunit (DLA2) of the cpPDC by mass spectrometry (Mooney et al., 1999). According to their postulated model, under photoautotrophic and heterotrophic growth conditions DLA2 is performing its primary function in the cpPDC, producing acetyl-CoA which is mainly used for the essential synthesis of fatty acids in the chloroplast (Figure 7). Under favorable conditions when light and acetate are available, DLA2 is also part of a high-molecular-weight (HMW) complex binding to the *psbA* mRNA thereby localizing it to the T-zones for translation of D1 and the efficient *de novo* biogenesis of PSII. Under these conditions, acetate from the medium can be used for the synthesis of acetyl-CoA by two cpPDC-independent systems, the acetate synthetase (ACS) and the acetyl-kinase/phosphate acetyltransferase (ACK/PAT) system (Spalding, 2009). Furthermore, the presence of light seemed to be crucial for the formation of the HMW complex as no RNase-sensitive DLA2 complex could be detected under heterotrophic conditions. This would make DLA2 an integrator of light signals and carbon availability for the coordination of two of the most essential cell functions, gene expression and carbon metabolism.

Additional data generated by Kleinknecht (2018) indicated that the accumulation of DLA2 does not increase under mixotrophic compared to photoautotrophic growth conditions and that the other cpPDC subunits are not part of the ribonucleoprotein (RNP) complex. This indicates that part of the DLA2 pool must leave the cpPDC for RNA-binding. However, the

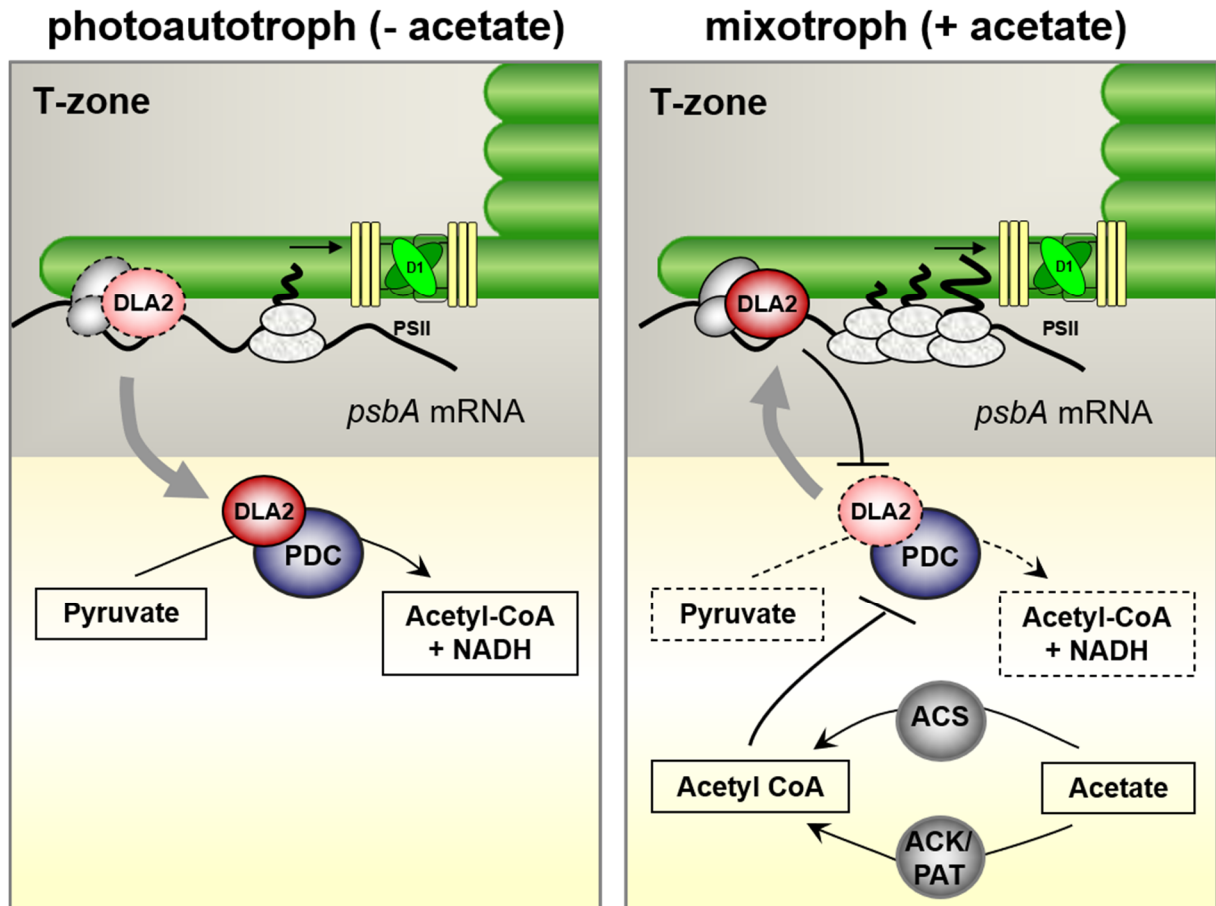


**Figure 7: Acetate-dependent regulation of *psbA* gene expression by DLA2 in *C. reinhardtii*.**

Under photoautotrophic conditions, DLA2 is part of the cpPDC catalyzing the reaction of pyruvate to acetyl-CoA. Under mixotrophic conditions, a part of the DLA2 pool is binding the *psbA* mRNA and localizing it to the T-zones. Figure was kindly provided by A. Bohne (adapted from Bohne et al. (2013)).

mode how DLA2 senses the growth conditions and how it is leaving the cpPDC remains to be analyzed. As the RNA-binding activity of DLA2 is acetate-dependent and the E2 subunit of the mtPDC in Arabidopsis was found to be acetylated, lysine acetylation might be involved in this regulation (König et al., 2014). However, as light was also essential for the moonlighting function of DLA2, a second light-dependent regulatory mechanism might be involved as well.

## I.6. Lysine acetylation, an advancing regulatory mechanism

Initially characterized as a histone modification by Phillips (1963), it took more than 20 years to find the first cytoplasmic protein to be acetylated (Piperno and Fuller, 1985). After this finding it quickly became clear that this mechanism is much more than just a histone modification. In the following decades, protein lysine-N<sup>ε</sup>-acetylation was extensively investigated in mammalian and microbial cells with its importance becoming more obvious (Choudhary et al., 2009; Rao et al., 2014). It is a post-transcriptional modification (PTM) ubiquitously found from archaea over bacteria to eukaryotes and its abundance and complexity

does not seem to lag behind O-phosphorylation (Rao et al., 2014). PTMs in general are important regulation mechanisms in all organisms as they allow a much more rapid response to cellular signals than transcriptional or translational regulation (Soppa, 2010; Xing and Poirier, 2012). There are several types of protein acetylation, e.g. O-acetylation of serine/threonine residues or non-reversible N<sup>α</sup>-acetylation of protein N-termini, but reversible lysine-N<sup>ε</sup>-acetylation is thought to be the most common type. Therefore, this type will be addressed as lysine acetylation in the course of this work (Martinez et al., 2008).

Protein lysine acetylation is performed by protein Lys-N<sup>ε</sup>-acetyltransferases (KATs) while the deacetylation reaction is catalyzed by protein Lys-N<sup>ε</sup>-deacetylases (KDACs), analogue to kinases and phosphatases in protein O-phosphorylation. The KATs are a diverse group with three of four families being widespread in eukaryotes, eubacteria and archaea (Pandey et al., 2002; reviewed in Rao et al., 2014). Despite various differences between the four families, all of them contain large, complex and multidomain proteins (Röttig and Steinbüchel, 2013). Similar to the KATs, the KDACs are a widespread and diverse group and usually have a complex domain organization (Hollender and Liu, 2008; reviewed in Rao et al., 2014). Despite this diverse repertoire of enzymes, there is also evidence for enzyme-independent and autoacetylation events (Yang et al., 2012; Wagner and Payne, 2013). Another group of proteins involved in this regulation process are the bromodomain (BRD) proteins which recognize and bind to acetylated lysine residues. They are also a widespread group but their predicted number varies significantly in plants from 57 in *Glycine max* to nine in the red alga *Cyanidioschyzon merolae* (Rao et al., 2014). The exact function and the relationship of these BRD proteins to the acetylated proteins is still elusive but is thought to be similar to the recognition and binding of O-phosphorylated proteins by 14-3-3 proteins (de Boer et al., 2013).

The research on protein acetylation in mammals showed how important and extensive this regulation mechanism is, with almost every enzyme in glycolysis, gluconeogenesis, the tricarboxylic acid (TCA) cycle, the urea cycle, fatty acid and glycogen metabolism being acetylated in human liver tissue (Zhao et al., 2010). But still, the knowledge about protein acetylation in plants and algae and especially in chloroplasts is extremely limited (Finkemeier et al., 2011; König et al., 2014; Salvato et al., 2014; Smith-Hammond et al., 2014; Mo et al., 2015; Chen et al., 2018; Yan et al., 2020).

## I.7. Aims of this study

Regulation of essential cellular functions like the synthesis of proteins, fatty acids or sugars is performed on various levels in all living organisms. But the coregulation of these processes is as important, especially for the appropriate adaptation of the cell or organism to changing growth conditions. Factors involved in these kinds of adaptation processes are called integrator or regulator proteins. DLA2 is thought to be such a protein in *C. reinhardtii*, integrating environmental stimuli for the coordination of gene expression and carbon metabolism for the efficient biogenesis of thylakoid membranes (Bohne et al., 2013; for a review on biogenesis of thylakoid membranes, see Rast et al., 2015). Here, DLA2 is usually part of the cpPDC to catalyze the synthesis of acetyl-CoA for fatty acid synthesis in the chloroplast. Under favorable conditions (availability of light and acetate), DLA2 dissociates from the cpPDC to fulfill an RNA-binding function, thereby localizing the *psbA* mRNA to the T-zones for the efficient biogenesis of PSII.

Despite all the data generated by Bohne et al. (2013) and Kleinknecht (2018), the regulation mechanism of DLA2 function remains elusive. Additionally, the mode of RNA-binding of DLA2 is still not completely understood. To address these points, state-of-the-art techniques were used to analyze the RNA-binding function by microscale thermophoresis and the involvement of lysine acetylation in the regulation of DLA2's function performing a proteome wide acetylome analysis in *C. reinhardtii* (Moon et al., 2018). Furthermore, a *dla2* mutant was generated using the CRISPR/Cas9 system recently established for *C. reinhardtii* (Greiner et al., 2017). This allowed complementation of the *dla2* mutant with various *dla2* versions, to analyze the lysine residues identified in the preceding acetylome analysis *in vivo*. Furthermore, the, to my knowledge, first analysis of protein-RNA interaction by Förster resonance energy transfer (FRET) microscopy in *C. reinhardtii* was performed, to investigate the formation of the RNP complex *in vivo* (Huranová et al., 2009; Lorenz, 2009). Taking all these data together, this study aims to substantially enhance the understanding of the RNA-binding mode of DLA2 and the regulation of its function.

## II. MATERIAL & METHODS

### II.1. Material

#### II.1.1. Chemicals

All chemicals used in this study were purchased from Carl-Roth, Sigma-Aldrich or AppliChem, if not indicated otherwise. A list of the suppliers can be found in Table 1.

**Table 1: List of suppliers for chemicals, enzymes, and equipment.**

| <b>Supplier</b>             | <b>Address</b>                                       |
|-----------------------------|--|
| Agilent Technologies        | Agilent Technologies Inc., Santa Clara, USA          |
| Agrisera                    | Agrisera AB, Vännäs, Sweden                          |
| AppliChem                   | AppliChem GmbH, Darmstadt, Germany                   |
| Biogenes                    | BioGenes GmbH, Berlin, Germany                       |
| Bio-Rad                     | Bio-Rad Laboratories GmbH, Feldkirchen, Germany      |
| Biozym Scientific           | Biozym Scientific GmbH, Hessisch Oldendorf, Germany  |
| Bruker Daltonik             | Bruker Corporation, Billerica, USA                   |
| Carl Roth                   | Carl Roth GmbH + Co. KG, Karlsruhe, Germany          |
| DWK Life Sciences           | DWK Life Sciences GmbH, Wertheim, Germany            |
| Eppendorf                   | Eppendorf AG, Hamburg, Germany                       |
| GE Healthcare               | GE Healthcare GmbH, Munich, Germany                  |
| Genaxxon bioscience         | Genaxxon bioscience GmbH, Ulm, Germany               |
| Implen                      | Implen GmbH, Munich, Germany                         |
| Integrated DNA Technologies | Integrated DNA Technologies Inc., Coralville, USA    |
| Macherey-Nagel              | MACHEREY-NAGEL GmbH & Co. KG, Düren, Germany         |
| Merck Millipore             | Merck KGaA, Darmstadt, Germany                       |
| Metabion                    | Metabion International AG, Munich, Germany           |
| NanoTemper                  | NanoTemper Technologies GmbH, Munich, Germany        |
| Nepa Gene                   | Nepa Gene Co. Ltd., Chiba, Japan                     |
| New England Biolabs         | New England Biolabs GmbH, Frankfurt am Main, Germany |
| NIPPON Genetics             | NIPPON Genetics EUROPE GmbH, Düren, Germany          |
| Olympus Deutschland         | Olympus Deutschland GmbH, Hamburg, Germany           |
| Paul Marienfeld             | Paul Marienfeld GmbH, Lauda Königshofen, Germany     |
| Photometrik                 | Photometrik GmbH, Eppertshausen, Germany             |
| Photon Systems Instruments  | PSI spol. s r.o., Drasov, Czech Republic             |
| Pineda                      | Pineda Antikörper-Service, Berlin, Germany           |
| Promega                     | Promega GmbH, Walldorf, Germany                      |
| QIAGEN                      | QIAGEN GmbH, Hilden, Germany                         |
| Restek                      | Restek Corporation, Bellefonte, USA                  |
| Roche                       | Roche Diagnostics GmbH, Mannheim, Germany            |
| SERVA                       | SERVA Electrophoresis GmbH, Heidelberg, Germany      |
| Sigma-Aldrich               | Sigma-Aldrich Chemie GmbH, Munich, Germany           |
| Stratagene                  | Stratagene California, San Diego, USA                |
| Thermo Fisher Scientific    | Thermo Fisher Scientific Inc., Waltham, USA          |

VWR

VWR International GmbH, Darmstadt, Germany

### II.1.2. Oligonucleotides

All oligonucleotides were ordered from Sigma-Aldrich, resuspended in ddH<sub>2</sub>O to a concentration of 100  $\mu$ M and stored at -20°C. Sequences of the oligonucleotides used in this research work are denoted in the appendix in Supplemental Table S1.

### II.1.3. Plasmids

All plasmids created and/or used in this work are listed including a short description in the appendix in Supplemental Table S2.

### II.1.4. Enzymes

All enzymes used in this study are presented in Table 2.

**Table 2: List of enzymes used in this study.**

| Enzyme                           | Company                  | Application  |
|----------------------------------|--------------------------|--------------|
| Restriction enzymes              | Thermo Fisher Scientific | cloning      |
| RiboLock RNase Inhibitor         | Thermo Fisher Scientific | SEC analysis |
| RNase A                          | Genaxxon bioscience      | SEC analysis |
| RNase One                        | Promega                  | SEC analysis |
| Q5® High-Fidelity DNA Polymerase | New England Biolabs      | PCR          |
| T4 DNA-Ligase                    | Thermo Fisher Scientific | cloning      |

### II.1.5. Kits

All kits used in this study are listed in Table 3. All kits were used according to the manufacturer's protocol.

**Table 3: List of kits used in this study.**

| Kit   | Company                  | Application                                |
|---|--------------------------|--|
| CloneJET PCR Cloning Kit                    | Thermo Fisher Scientific | cloning                                    |
| NucleoSpin® Plasmid EasyPure                | Macherey-Nagel           | cloning                                    |
| NucleoSpin Gel and PCR Clean-up             | Macherey-Nagel           | cloning                                    |
| Phire™ Plant Direct PCR Kit                 | Thermo Fisher Scientific | Colony PCR from <i>C. reinhardtii</i>      |
| DNeasy Plant Mini Kit                       | QIAGEN                   | cloning                                    |
| QuikChange XL Site-Directed Mutagenesis Kit | Agilent Technologies     | Mutagenesis of the constructs used for MST |

### II.1.6. *Escherichia coli* strains

Recombinant plasmids were amplified in *Escherichia coli* (*E. coli*) strain XL1-Blue [endA1 gyrA96(nalR) thi-1 recA1 relA1 lac glnV44 F' Tn10 proAB+ lacIq  $\Delta$ (lacZ)M15

hsdR17(rK- mK+)] (Stratagene). Overexpression of recombinant proteins was performed using the BL21-DE3 [F-, dcm, ompT, hsdS(rB- mB-), gal, [malB+]K-12( $\lambda$ S)] strain (Stratagene).

### II.1.7. *Chlamydomonas reinhardtii* strains

The *C. reinhardtii* strains used and/or created in this research work are stated in the following table (Table 4).

**Table 4: List of *C. reinhardtii* strains used in this work.**

| Strain                                       | Description  | Reference                  |
|--|--|----------------------------|
| cc-3403 (RU-387)                             | nit1 arg7-8 cw15 mt-   | Greiner et al. (2017)      |
| FuD7   | Deletion mutation spanning the <i>psbA</i> gene in CC-741  | Bennoun et al. (1980)      |
| <i>dla2</i>                                  | Insertion mutant, knock out of the <i>DLA2</i> gene in cc-3403 background, transformed with pARG7 for complementation of arginine auxotrophy | Generated during this work |
| <i>dla2:DLA2</i> (denoted as DLA2-HA)        | <i>dla2</i> mutant complemented with a HA-tagged version of the <i>DLA2</i> gene   | Generated during this work |
| <i>dla2:DLA2 K197Q</i> (denoted as K197Q-HA) | <i>dla2</i> mutant complemented with a HA-tagged and mutated (K197 $\rightarrow$ Q) version of the <i>DLA2</i> gene                          | Generated during this work |
| <i>dla2:DLA2 K197R</i> (denoted as K197R-HA) | <i>dla2</i> mutant complemented with a HA-tagged and mutated (K197 $\rightarrow$ R) version of the <i>DLA2</i> gene                          | Generated during this work |
| <i>dla2:DLA2 K193Q</i> (denoted as K193Q-HA) | <i>dla2</i> mutant complemented with a HA-tagged and mutated (K193 $\rightarrow$ Q) version of the <i>DLA2</i> gene                          | Generated during this work |
| <i>dla2:DLA2 K200Q</i> (denoted as K200Q-HA) | <i>dla2</i> mutant complemented with a HA-tagged and mutated (K200 $\rightarrow$ Q) version of the <i>DLA2</i> gene                          | Generated during this work |

### II.1.8. Antibodies

All antibodies used in this work are listed together with the titer of the working solution in Table 5.

**Table 5: Antibodies used in this study.**

| Antibody    | Titer   | Reference   |
|-------------|---------|---|
| Anti-DLA2   | 1:1000  | Bohne et al. (2013)                                 |
| Anti-PDC2   | 1:10000 | Provided by Peter Nixon (Imperial College London)   |
| Anti-PDH2   | 1:2000  | Pineda  |
| Anti-DLD2   | 1:5000  | Pineda  |
| Anti-D1     | 1:1000  | Agrisera  |
| Anti-D2     | 1:1000  | Biogenes  |
| Anti-RbcL   | 1:5000  | provided by G. F. Wildner (Ruhr Universität Bochum) |
| Anti-PsaA   | 1:1000  | Agrisera  |
| Anti-AtpB   | 1:5000  | Agrisera  |
| Anti-HSP70B | 1:10000 | Provided by Michael Schroda (TU Kaiserslautern)     |

|  |         |                          |
|--|---------|--------------------------|
| Anti-DYKDDDDK (HA) Tag Monoclonal Antibody (FG4R), DyLight 550                 | 1:100   | Thermo Fisher Scientific |
| Anti-Rabbit IgG (whole molecule)– Peroxidase antibody produced in goat         | 1:10000 | Sigma-Aldrich            |
| Anti-Chicken IgY (IgG) (whole molecule)–Peroxidase antibody produced in rabbit | 1:10000 | Sigma-Aldrich            |

### II.1.9. Software and online tools

This work was performed using the following software and online tools (Table 6).

**Table 6: List of software and online tools used in this study.**

| Name  | Manufacturer/Website  | Reference               | Application  |
|---|---|-------------------------|--|
| CLC Main Workbench                                | QIAGEN  |                         | <i>In silico</i> cloning and sequence analysis     |
| Microsoft office                                  | Microsoft Corporation   |                         | Data analysis and generation of figures            |
| MO.Affinity Analysis software                     | NanoTemper  | Wienken et al. (2010)   | Analysis of MST data                               |
| ImageJ  | <a href="https://imagej.nih.gov/ij/index.html">https://imagej.nih.gov/ij/index.html</a>   | Schneider et al. (2012) | Quantification of protein signals                  |
| PredAlgo  | <a href="https://giavap-genomes.ibpc.fr/cgi-bin/predalgotdb.perl?page=main">https://giavap-genomes.ibpc.fr/cgi-bin/predalgotdb.perl?page=main</a> | Tardif et al. (2012)    | Prediction of subcellular localization of proteins |
| Protein Homology/analogY Recognition Engine V 2.0 | <a href="http://www.sbg.bio.ic.ac.uk/~phyr/e2/html/page.cgi?id=index">http://www.sbg.bio.ic.ac.uk/~phyr/e2/html/page.cgi?id=index</a>             | Kelley et al. (2015)    | Generation of protein structure models             |
| JAVA Codon Adaption Tool (jcat)                   | <a href="http://www.jcat.de/">http://www.jcat.de/</a>   | Grote et al. (2005)     | Codon adaptation to <i>E. coli</i>                 |
| CRISPR-P v2.0                                     | <a href="http://crispr.hzau.edu.cn/cgi-bin/CRISPR2/CRISPR">http://crispr.hzau.edu.cn/cgi-bin/CRISPR2/CRISPR</a>                                   | Lei et al. (2014)       | gRNA Design for CRISPR/Cas9-System                 |

## II.2. Methods

### II.2.1. Growth and harvesting of bacterial strains

Liquid cultures of *E. coli* were grown in LB-medium (1 % peptone, 0.5 % yeast extract, 1 % NaCl, pH 7) at 37°C and shaking at 180 rpm (Bertani, 1951). For the generation of selection plates, 1.5 % agar was added to the LB-medium and the respective selection antibiotics were supplemented after autoclaving. Liquid cultures were harvested by centrifuging the cells at 5000 g for 10 min.

### II.2.2. Growth and harvesting of *C. reinhardtii* strains

*C. reinhardtii* strains were maintained at 23°C under continuous light (30  $\mu\text{E m}^{-2}\text{s}^{-1}$ ) on Tris-acetate-phosphate media (TAP) agar plates (Harris, 1989). If not indicated otherwise, all experiments were performed with liquid cultures grown under the same temperature and light

conditions in TAP medium supplemented with 1 % sorbitol (TAPS) to a density of  $\approx 2 \times 10^6$  cells/mL. For photoautotrophic growth cells were grown in high salt medium (HSM) (Sager and Granick, 1953). For growth of the cc3403 ARG<sup>-</sup> strain the medium was supplemented with 100  $\mu\text{g}/\text{mL}$  arginine. Liquid cultures were harvested at 1200 g for 10 min.

### II.2.3. Chlorophyll fluorescence analysis of *C. reinhardtii* strains

For the initial characterization of *C. reinhardtii* strains the maximum PSII quantum yield ( $F_v/F_m$ ) was determined. For this, strains were streaked out on TAP plates and grown in low light ( $\approx 8 \mu\text{E m}^{-2}\text{s}^{-1}$ ) for 48 h. Afterwards, plates were dark adapted for 5 min and maximum PSII quantum yield was measured using a FluorCam 800MF (Photon Systems Instruments).

### II.2.4. Drop plating test

Liquid cultures of the cc-3403, the *dla2* knock out mutant and the DLA2-HA strain were grown in TAPS + arginine to a cell density of about  $2 \times 10^6$  cells/mL. After harvesting, cells were resuspended to a cell density of  $1 \times 10^7$  cells/mL. Using 1.5 mL reaction tubes and TAPS + arginine medium a serial dilution was performed with a dilution factor of 10 resulting in 5 tubes with different cell density per strain, starting from  $10^7$  to  $10^3$  cells/mL. For each strain, a 10  $\mu\text{l}$  drop from each dilution was spotted onto a TAP + arginine plate, starting with the highest cell density on top to the lowest cell density at the bottom of the plate. Cell drops were dried for 5 min before plates were closed and incubated at the various temperature and light conditions ( $23^\circ\text{C}$ ,  $30 \mu\text{E m}^{-2}\text{s}^{-1}$ ;  $23^\circ\text{C}$ ,  $100 \mu\text{E m}^{-2}\text{s}^{-1}$ ;  $23^\circ\text{C}$ ,  $0 \mu\text{E m}^{-2}\text{s}^{-1}$ ;  $15^\circ\text{C}$ ,  $30 \mu\text{E m}^{-2}\text{s}^{-1}$ ;  $30^\circ\text{C}$ ,  $30 \mu\text{E m}^{-2}\text{s}^{-1}$ ). After incubation for five to seven days cell growth was documented by scanning of the plates.

### II.2.5. Nucleic acid methods

#### II.2.5.1. Isolation of plasmid DNA from *E. coli*

Isolation of plasmids from 5 mL of liquid *E. coli* XL1-blue cultures was performed using the NucleoSpin® Plasmid EasyPure kit (Macherey-Nagel) according to the manufacturer's instructions.

#### II.2.5.2. Isolation of genomic DNA from *C. reinhardtii*

50 mL of a cc3403 liquid culture was harvested and genomic DNA was isolated using the DNeasy Plant Mini Kit (QIAGEN) according to the manufacturer's instructions.

#### II.2.5.3. Determination of nucleic acid concentrations

Concentration of double stranded DNA fragments or plasmids was determined using a Nanophotometer P330 (Implen).

#### II.2.5.4. Agarose electrophoresis of DNA

The size-separation of DNA fragments was performed using tris-acetate-EDTA (TAE) agarose gels in horizontal gel apparatus (Mupid-One, NIPPON Genetics). Agarose gels were prepared with 1:10000 (v/v) Midori Green Advance (NIPPON Genetics) and 1-3 % of agarose, depending on the size of the DNA fragments. Samples were supplemented with 6x DNA loading dye (Thermo Fisher Scientific) and loaded onto the gel. As a size standard 3  $\mu$ L of the GeneRuler™ 1 kb Plus ladder (Thermo Fisher Scientific) were loaded onto the gel as well and electrophoretically separated at 100V for 30 min. Afterwards, DNA fragments were visualized and documented using a Bio-1000F fluorescence gel scanner (SERVA Electrophoresis).

#### II.2.5.5. Cloning

DNA restriction digest, dephosphorylation and ligation were performed using the respective kits and enzymes by Thermo Fisher Scientific according to the manufacturer's instructions.

#### II.2.5.6. Polymerase chain reaction (PCR)

Amplification of DNA fragments was performed using Q5® High-Fidelity DNA Polymerase (New England Biolabs) according to the manufacturer's instructions. PCRs had a volume of 50  $\mu$ L and were operated using a Master Cycler (Eppendorf). The amount of template DNA was 10 ng of plasmid or 200 ng of genomic DNA. A typical PCR protocol is shown in Table 7 in which the annealing temperature depends on the primers and the elongation time depends on the length of the desired fragment.

**Table 7: Example of a typical PCR protocol.**

|                      |         |          |
|----------------------|---------|----------|
| Initial Denaturation | 95°C    | 2 min    |
| Denaturation         | 95°C    | 30       |
| Annealing            | 55-70°C | 30 s     |
| Elongation           | 72°C    | 2 kb/min |
| Final Elongation     | 72°C    | 10 min   |

#### II.2.5.7. Sequencing

For the sequencing of plasmids, 100 ng (pET-Sumo) or 500 ng (pBC1) of sample DNA was mixed with 10 pmol of the respective primer (see Supplemental Table S1), 1  $\mu$ L of

sequencing buffer (30 % (v/v) DMSO in 70 mM Tris/Cl, pH 8.5) and filled up with H<sub>2</sub>O to a volume of 7 µL. The sequencing reaction was performed by the sequencing service of the faculty of biology using the BigDye® Terminator v3.1 Cycle Sequencing protocol (Thermo Fisher Scientific).

#### II.2.5.8. Transformation of *Escherichia coli*

For heat-shock transformation of *E. coli* cells, plasmid DNA or ligation products were pipetted to 50µL aliquots of cells, shortly mixed and kept on ice for 30 min. After a heat shock at 42°C for 1 min, 200 µL of LB medium was added and the cell mixture was incubated at 37°C for 30 min with moderate shaking (600 rpm). After the recovering phase the cells were transferred to an LB plate with the respective selection antibiotics and incubated at 37°C for 15 – 20 h.

#### II.2.5.9. Transformation of *C. reinhardtii*

For transformation of the *dla2* knock out mutant with the various DLA2 complementation constructs, a liquid culture of 100 mL was grown in TAPS to a cell density of  $\approx 1 \times 10^6$  cells/mL. Cells were harvested and resuspended in MAX Efficiency Transformation Reagent for Algae (Thermo Fisher Scientific) supplemented with 40 µM sucrose to a cell density of  $1 \times 10^8$  cells/mL. 250 µL of the cell suspension were transferred to an electroporation cuvette (4 mm gap width, Biozym Scientific) and mixed with 50 µg of denatured salmon sperm and 10 µg of the respective plasmid DNA. The cuvette was incubated for 20 min at 16°C followed by the electroporation which was performed using a Gene Pulser II (Bio-Rad Laboratories) with standard settings (resistance = high range; capacity = 10 µF). One pulse with a voltage of 0.8 kV and two additional pulses with a voltage of 0.2 kV were applied followed by an additional incubation at 16°C for 20 min. Subsequently cells were recovered in 20 mL of TAPS medium supplemented with 100 µg/mL ampicillin for 24 h. After the recovery cells were centrifuged at 1000 g for 10 min and resuspended in 500 µL of HSM medium. The cell suspension was transferred to HSM plates supplemented with 200 µg/mL of ampicillin and incubated at 23°C for 14-21 days for selection of restored photoautotrophic growth.

#### II.2.5.10. Generation of a *dla2* knock out mutant using the CRISPR/Cas9 system

The generation of a *dla2* mutant using the CRISPR/Cas9 system was performed in the lab of Prof. Dr. Peter Hegemann (Humboldt University of Berlin) with the kind help of Dr. Simon Kelterborn according to their published work (Greiner et al., 2017). The used cc-3403 strain has an arginine auxotrophy, which was used for transformation selection by including the

pARG7 plasmid containing the ARG7 gene in the transformation mix. A short double stranded DNA fragment (Mutation oligo) containing of two annealed reverse complement oligonucleotides (EMX1-1-FLAGv3 insert and EMX1-1-FLAGv3 insert RC) was also added to the transformation mix. This mutation oligo contained an additional Cas9 restriction site (EMX1), a FLAG-tag sequence for PCR screening and three stop codons in each frame to increase the knock-out efficiency. The DLA2 KO gRNA was designed using the CRISPR-P v2.0 online tool. The gRNA showed a relatively high on-target efficiency score (0.7471), a low number of off-target hits (15) and targeted the Cas9 enzyme to a restriction site at the beginning of the first exon of *dla2* (+94 bp relative to the ATG). The corresponding DLA2 KO crRNA (gRNA + 16 bp complementary to the tracrRNA) together with the tracrRNA were purchased from Integrated DNA Technologies. The recombinant Cas9 enzyme from *Streptococcus pyogenes* was provided by the AG Hegemann and was incubated together with the tracrRNA and the DLA2 KO crRNA to form the active Cas9/gRNA-RNP complex prior to the addition to the transformation mix. The electroporation was performed using a NEPA21 electroporator (Nepa Gene) using the published settings and conditions for the cc-3403 strain (Greiner et al., 2017). After selection and picking of clones, the screening process was performed in 96-well plates using the Phire™ Plant Direct PCR Kit (Thermo Fisher Scientific) for *C. reinhardtii* colony PCR with the primers DLA2 short locus fw and DLA2 short locus rev. Afterwards, the amplified DNA fragments were separated on a 2 % agarose gel to check for insertion of the mutation oligo and/or the ARG7 cassette. The sequence of the oligonucleotides used in the generation of the *dla2* mutant can be found in Supplemental Table S1. For an overview on the generation of the *dla2* mutant see Figure 16.

## II.2.6. Protein methods

### II.2.6.1 Determination of protein concentrations

Protein concentrations were measured according to Bradford (1976) using the ROTI®Quant reagent (Carl Roth) according to the manufacturer's instructions.

### II.2.6.2. SDS polyacrylamide gel electrophoresis

Proteins were separated on discontinuous polyacrylamide gels according to their molecular weight as described by Laemmli (1970). The Mighty Small™ II Mini Vertical Electrophoresis System (SERVA Electrophoresis) was used to prepare and run the gels. Sample preparation was performed by mixing the appropriate amount of protein with ROTI®Load 1 (Carl Roth) and denaturing the samples at 50°C for 15 min. Afterwards, the samples were

loaded onto the gel together with a BlueStar Prestained Protein Marker (NIPPON Genetics) and were separated as described by Schagger and von Jagow (1987). The running buffer used for electrophoresis consisted of 25 mM Tris, 192 mM glycine and 0.1 % sodium dodecyl sulfate (SDS). After electrophoresis proteins were detected by using immunoblot analysis.

#### *II.2.6.3. Immunoblotting*

For immunoblotting, proteins were separated by SDS-PAGE and subsequently transferred to a nitrocellulose membrane (pore size 0.45  $\mu\text{m}$ , AppliChem) using a three-buffer system. For this, one layer of Whatman paper soaked in anode buffer I (0.3 M Tris pH 10.4, 20 % methanol) was applied to the anode of a semi dry blot transfer apparatus (VWR), followed by two layers of Whatman paper soaked in anode buffer II (0.025 M Tris pH 10.4, 20 % methanol). Next, the nitrocellulose membrane soaked in anode buffer II and the protein gel soaked in cathode buffer (0.04 M 6-aminohexanoic acid, 0.025 M Tris pH 9.4, 20 % methanol) were applied before three layers of Whatman paper soaked in cathode buffer were positioned on top of the gel. The transfer was performed for 75 min at 0.8 mA/cm<sup>2</sup>. After the transfer, the proteins on the membrane were visualized and documented using a Ponceau S solution (0.2 % Ponceau S, 1 % acetic acid). Subsequently, the membrane was incubated in 5 % (w/v) milk powder solution in 1x TBS-T (150 mM NaCl, 10 mM Tris/HCL pH 7.5, 0.05 % (v/v) Tween 20) for 1 h at room temperature (RT) followed by an incubation in primary antibody in TBS-T at 4°C overnight. The titer of the respective antibody solutions can be found in Table 5. On the next day, membranes were washed three times for 10 min at RT with TBS-T before incubation with the respective secondary antibody for at least 1 h at RT. Afterwards, the membrane was washed four times for 10 min at RT with TBS-T followed by the detection of the HRP conjugated secondary antibodies using enhanced chemiluminescence (ECL) solution (0.4 mM p-coumaric acid, 2.5 mM luminol, 0.7 % DMSO, 0.01 % H<sub>2</sub>O<sub>2</sub>, 100 mM Tris pH 8.5) and an ImageQuant™ LAS 500 (GE Healthcare). Quantification of the detected protein signals was performed using the ImageJ software.

#### *II.2.6.4. Generation of constructs for the expression of recombinant proteins*

All constructs employed for the expression of the recombinant proteins used in MST were generated by the same procedure. Fragments coding for each amino-acid sequence were amplified by PCR using primers listed in Supplemental Table S1. To increase overexpression, a synthetic version of the DLA2 cDNA (Metabion) that conformed to the codon usage of *Escherichia coli* was used as a template for PCRs. The PCR product was cloned into the vector pET-28b-Sumo (Bepperling et al., 2012) using *Bam*HI and *Sal*I restriction sites, and the

resulting construct was transformed into *Escherichia coli* BL21 (DE3) cells for overexpression. For the pSUMO: DLA2  $\Delta$ E3B construct expressing the  $\Delta$ E3B protein, the 5' region of the cDNA was amplified using the primers DLA2 cDNA fw 2 *Bam*HI and DLA2 -E3B rev *Sal*I and cloned into pET-28b-Sumo. The 3' region was amplified using the primers DLA2-E3B fw *Sal*I and DLA2 cDNA rev *Sal*I and cloned downstream of the 5' region via the restriction site *Sal*I.

To generate the constructs expressing the acetylation mimicking proteins (DLA2 K193R, DLA2 K193Q, DLA2 K197R, DLA2 K197Q, DLA2 K200R and DLA2 K200Q), the construct pSUMO:DLA2 WT was mutagenized using the QuikChange XL Site-Directed Mutagenesis Kit (Agilent Technologies) to obtain the respective amino acid change.

For the generation of the pBC1:DLA2-HA construct, a fragment covering the entire *DLA2* cDNA was amplified using the primers DLA2 fw *Nde*I and DLA2-3xHA rev *Eco*RI thereby adding a triple HA-tag sequence to the 3' end of the cDNA. As a template, a cDNA clone (MXL069g06) covering the whole *DLA2* cDNA was purchased from the Kazusa DNA Research Institute, Japan (Asamizu et al., 2004). The resulting fragment was cloned into the pBC1-CrGFP vector using *Nde*I and *Eco*RI restriction sites. Afterwards, a fragment covering the *DLA2* genomic DNA from the 5'UTR until the third exon was amplified using the primers DLA2 5' UTR fw *Bam*HI and DLA2 Exon 3 rev *Sfi*I and isolated genomic DNA from the cc-3403 strain as template. Subsequently, the fragment was cloned into the pBC1:DLA2 cDNA-HA plasmid using the restriction sites *Bam*HI and *Sfi*I to replace the *PsaD* promoter and parts of the *DLA2* cDNA with the 5'UTR and genomic DNA of the *DLA2* gene. The resulting pBC1:DLA2-HA construct was used for complementation of the *dla2* mutant and as template for the generation of the mutated constructs (pBC1:DLA2 K197R-HA, pBC1:DLA2 K197Q-HA, pBC1:DLA2 K193Q-HA and pBC1:DLA2 K200Q-HA) using the QuikChange XL Site-Directed Mutagenesis Kit. All primer sequences used for the generation of the constructs as well as amino acid coverage of resulting proteins for the overexpression constructs are listed in Supplemental Table S1. The pET-Sumo:PratA construct for the expression of the recombinant PratA protein was generated by Dr. Steffen Heinz according to Heinz et al. (manuscript in preparation).

#### II.2.6.5. Expression and purification of recombinant proteins

Overexpression of all recombinant proteins used for MST was performed in BL21 *E. coli* cells. Four 1 L cultures were inoculated and grown at 37°C in LB medium supplemented with 50  $\mu$ M kanamycin. At an OD600 of 0.6, overexpression was induced by the addition of 1 mM IPTG and performed at 12°C overnight. His-Sumo-tagged proteins were purified with

Protino® Ni-NTA agarose beads (Macherey-Nagel) according to the manufacturer's instructions, followed by the removal of the His-Sumo-tag by proteolytic digestion with Sumo protease at 4°C overnight and 1 h at 30°C. After digestion, the Sumo protease as well as the His-Sumo-tag were removed using Protino® Ni-NTA agarose beads and the recombinant protein solution was dialyzed to MST buffer (50 mM Tris/HCl pH 7.8, 60 mM KCl, 10 mM MgCl<sub>2</sub>, 0.05 % Tween 20) to get rid of the imidazole.

#### II.2.6.6. Microscale thermophoresis

Microscale thermophoresis (MST) was used to quantify the binding affinities of Cy5-labeled *psbA* 5'UTR probes for wild-type and mutant DLA2 proteins. Synthetic RNAs were purchased from Metabion. To guarantee high comparability between different samples, all recombinant proteins of an experiment were overexpressed, purified and measured at the same time. The concentration of purified recombinant proteins was adjusted to 44 µM using MST buffer. Subsequently, the fluorescently labeled RNA probe was diluted to 20 nM in MST buffer and decreasing amounts of the respective proteins were incubated with the RNA. Afterwards, samples were loaded into MST NT.115 premium glass capillaries (NanoTemper) and ran at 40 % LED power and 20 % MST power at RT in a Monolith NT.115 instrument (NanoTemper) at the Bioanalytic Service Unit of the Biocenter of the Ludwig-Maximilians-Universität, Munich.  $K_D$  values were calculated using the MO.Affinity Analysis software (NanoTemper) by evaluating the MST-curves at the earliest time point as long as the signal to noise ratio of all samples of an experiment was at least 12.

#### II.2.6.7. Isolation of total protein extracts from *C. reinhardtii*

Total cell protein lysates were extracted from 25 mL of cultures having a cell density of  $\approx 1\text{-}2 \times 10^6$  cells/mL. Cells were harvested and resuspended in 700 µL lysis buffer (120 mM KCl, 20 mM tricine pH 7.8, 0.4 mM EDTA) supplemented with 0.5 % Triton X-100. Breakage of the cells was achieved by sonication (3 x 5 pulses) on ice followed by a 10 min incubation for solubilization of membranes. Afterwards, the protein concentration was determined and equal amounts of proteins were loaded onto an SDS-PAGE gel.

#### II.2.6.8. Isolation of membrane proteins from *C. reinhardtii*

To isolate membrane proteins, 150 mL of a *C. reinhardtii* culture was harvested and resuspended in 700 µL of lysis buffer without Triton X-100. The cell suspension was added to a screw lid tube filled with  $\approx 200$  µL of glass beads (0.5 mm diameter, Carl Roth) and cells were broken by shaking the tubes 5 times for 40 s at 400 rpm using a BeadBug Homogenizer

(Biozym Scientific). Subsequently, the lysate was centrifuged for 5 min at 3000 g and 4°C to pellet whole cells and the supernatant was transferred to another tube and centrifuged for 20 min at 20,000 g and 4°C to spin down the membrane fraction. After centrifugation, the supernatant was discarded and the membrane fraction was washed twice with lysis buffer before resuspended in 150 µL lysis buffer supplemented with 0.5 % Triton X-100 followed by incubation for 10 min at 4°C for solubilization of the membranes. The lysate was centrifuged again for 10 min at 20,000 g and 4°C to spin down insoluble particles before the supernatant was transferred to a new tube and the protein concentration was determined.

#### *II.2.6.9. Chloroplast and thylakoid isolation from C. reinhardtii*

Chloroplasts from cw15 strains of *C. reinhardtii* were isolated according to Zerges and Rochaix (1998). Subsequently, they were lysed by resuspension in hypotonic solution (10 mM tricine pH 7.8, 10 mM EDTA) and incubation for 20 min at 4°C. Crude thylakoids were separated from stromal proteins by centrifugation on a 1 M sucrose cushion in hypotonic solution. The supernatant was taken as stromal proteins and the thylakoid membrane pellet was solubilized by resuspension in lysis buffer with 0.2 % Triton X-100 and incubation for 20 min at 4°C. Afterwards, insoluble particles were removed by an additional sucrose cushion step (in lysis buffer) and the supernatant was subjected to size exclusion chromatography.

#### *II.2.6.10. Size exclusion chromatography analysis of thylakoid membrane proteins*

Thylakoid protein lysates were split in half and either treated with 400 U RNase One (Promega) and 1 mg RNase A (Genaxxon bioscience) /mg protein for 60 min at 4 °C (+RNase) or with 1 mg yeast tRNA (Sigma-Aldrich) and 300 U RiboLock RNase Inhibitor (Thermo Fisher Scientific) /mg protein (-RNase). Afterwards, samples were loaded to a Sephacryl S-500 HR column (GE Healthcare) and size exclusion chromatography was performed at 4°C with gel filtration buffer (50 mM KCl, 5 mM e-aminocaproic acid, 2.5 mM EDTA, 20 mM tricine-KOH pH 7.8 and 0.1 % Triton X-100) at a flow rate of 0.3 mL/min and using an ÄKTApurifier 10 system (GE Healthcare). Proteins in the resulting 1 mL fractions were precipitated by the addition of 200 µL trichloroacetic acid and an incubation for 1 h on ice. Afterwards, precipitated proteins were pelleted by centrifugation at 20000g for 20 min and 4°C and washed twice with 80 % cold acetone. Subsequently, the protein pellet was dried at 95°C, resuspended in 1 x ROTI®Load 1 and loaded onto an SDS-PAGE gel (see chapter II.2.6.2).

#### II.2.6.11. Co-immunoprecipitation

*C. reinhardtii* cultures were harvested and resuspended in 700  $\mu$ L IP buffer (20 mM Tris-HCl pH 7.8, 150 mM NaCl, 1 mM EDTA, 5 % glycerol and cComplete™ protease inhibitor cocktail (Roche)). Cells were broken using glass beads and a Bead Bug Homogenizer (5 x 40 s at 400 rpm) and centrifuged for 20 min at 20,000 g and 4°C. The supernatant with the soluble proteins was transferred to a new tube and the protein concentration was determined. Subsequently, 2 mg of the soluble cell extract was incubated with 50  $\mu$ L of Pierce™ Anti-HA Magnetic Beads (Thermo Fisher Scientific) for 2 h at 4°C on an overhead shaker. Afterwards, beads were washed three times with IP buffer and proteins were eluted with 50  $\mu$ L 1x non-reducing Roti®-Load 2 (Carl Roth) at 50°C for 30 min. Beads were removed and eluates were supplemented with 20mM DTT and separated via SDS-PAGE (see chapter II.2.6.2).

#### II.2.6.12. cpPDC activity assay

cpPDC activity assay was basically performed as described by Bohne et al. (2013). 150 mL of mixotrophically grown *C. reinhardtii* cultures were harvested and resuspended in 700  $\mu$ L PDC lysis buffer (100 mM Tricine pH 8.0, 25 mM MgCl<sub>2</sub>, 5 % (v/v) Glycerol). Cells were broken using glass beads and a Bead Bug Homogenizer (5 x 40 s at 400 rpm). Afterwards insoluble particles were separated by centrifugation at 20000 g for 20 min at 4°C and the supernatant containing the soluble protein fraction was transferred to a new tube. Subsequently, the protein concentration was determined and adjusted to 1 mg/mL with PDC lysis buffer. The reaction mix contained 0.1 mM thiamine pyrophosphate (TPP), 5 mM MgCl<sub>2</sub>, 2 mM NAD<sup>+</sup>, 0.1 mM acetyl-CoA, 3 mM cysteine, 0.1 M tricine pH8.0 and 200  $\mu$ g of protein lysate in a volume of 999  $\mu$ L. The reaction was started by the addition of 1 mM pyruvate and the change in absorbance at 340 nm caused by NADH production was analyzed for 2 min using a Ultrospec™ 2100 spectrophotometer (GE Healthcare). The PDC activity in the *dla2* mutant was determined as well and defined as background and consequently subtracted from the PDC activity in the other lines.

#### II.2.6.13. Förster resonance energy transfer microscopy

Förster resonance energy transfer was used to visualize DLA2-*psbA* mRNA interactions in various strains. *C. reinhardtii* cell preparation was done on a borosilicate glass slide (DWK Life Sciences). To prevent dehydration each step was done in a humid box. First, fluorescence *in situ* hybridization (FISH) staining was performed which was adapted from Uniacke et al. (2011). After adherence of the cells on the microscope slide, cells were permeabilized in 1 x PBS supplemented with 0.5 % Tween 20 for 10 min followed by a wash with 1 x PBS. To fixate

the cells, they were incubated with 3.7 % formaldehyde in 1 x PBS for 10 min followed by two washing steps to remove residual formaldehyde. Subsequently, cells were incubated with hybridization solution (1.6 x SSC buffer, 25 µg salmon sperm, 50 % formamide, 10 ng of each of the four oligonucleotide) over night at 37°C. DNA oligonucleotides (four for each of the target mRNAs, *psbA* and *psaA*) were purchased from Sigma-Aldrich and were modified with an Atto 488 fluorescent label on the 5' end. On the next day, samples were washed five times: First wash with 50 % formamide in 1 x SSC for 30 min at 37 °C, second wash with with 1 x SSC for 20 min at RT, third wash with 0.5 x SSC for 10 min, and another two washes with 1 x PBS for 10 min.

For immunofluorescence (IF) staining, samples were incubated in blocking solution (5 % BSA in 1 x PBS) for 1 h followed by an incubation with an HA Tag Monoclonal Antibody coupled to a DyLight 550 fluorophore (Thermo Fisher Scientific). Subsequently samples were washed three times with 1 x PBS for 10 min. After samples were dried for several hours, they were incubated over night with a drop of Calbiochem FluorSave™ Reagent (Merck Millipore) and a high precision coverslip (Paul Marienfeld). On the next day, samples were sealed with nail polish and visualized on an IX71 inverted microscope (Olympus Deutschland) combined with a Delta Vision Elite Filter Set (GE Healthcare) and a CoolSNAP HQ2 camera (Photometrik). Quantification of the fluorescence signal intensities was performed using ImageJ.

#### II.2.6.14. <sup>35</sup>S Pulse labeling of proteins

<sup>35</sup>S Pulse labeling of proteins was adapted from Bohne et al. (2013) and performed by Jing-Tsong Teh (AG Nickelsen, LMU Munich). Chlamydomonas liquid cultures were grown in TAPS at 23°C and 30 µE of light to a density of 1 x 10<sup>6</sup> cells/mL. After 16 h of growth in TAPS-sulfur, the pulse was performed using 100 mCi H<sub>2</sub><sup>35</sup>SO<sub>4</sub> and incubation for 15 min at the same light conditions. After centrifugation, the sedimented cells were frozen in liquid nitrogen and resuspended in 100 µL of 1 x ROTI®Load 1 (Carl Roth) sample buffer. After short sonication (5 s, RT) and incubation for 30 min at RT, 10 µL of each sample was loaded onto an SDS-PAGE gel. After electrophoresis, proteins were blotted onto a nitrocellulose membrane (AppliChem) and radioactive signal was detected using phosphorimaging.

#### II.2.6.15. D1 repair experiment

Duplicates of liquid cultures of the DLA2-HA strain, the *dla2* mutant and the DLA2 acetylation strains K197Q-HA and K197R-HA, were grown under mixotrophic growth conditions at a light intensity of 30 µE to a cell density of about 2 x 10<sup>6</sup> cells/mL. One of the

cultures was supplemented with 500 µg/mL lincomycin and 100 µg/mL chloramphenicol for inhibition of plastidic protein synthesis before both cultures were shifted to a Multi-Cultivator MC 1000-OD (Photon Systems Instruments) and illuminated with about 800 µE for 1.5 h. Whole cell proteins of the samples were separated via SDS-PAGE and objected to immunoblotting.

#### *II.2.6.16. Sulfur starvation experiment*

Sulfur starvation experiments for analysis of *psbA de novo* synthesis was performed according to Muranaka et al. (2016) and Malnoë et al. (2014). Cells were grown in 200 mL of TAPS and 30 µE of light to a cell density of  $5 \times 10^5$  cells/mL. Subsequently, the cells were centrifuged, washed twice and resuspended in 200 mL of TAPS-sulfur. After 48 h, cells were centrifuged again, resuspended in TAPS and grown for another 24 h. Whole cell proteins of the samples were separated via SDS-PAGE and objected to immunoblotting.

#### *II.2.6.17. Lipid and fatty acid analysis*

Liquid cultures (1 L) of *C. reinhardtii* strains cc-3403 and the *dla2* knock out mutant were grown heterotrophically in TAPS supplemented with 100 µg/mL arginine. At a cell density of about  $5 \times 10^5$  a sample was taken by vacuum filtrating 40 mL of culture onto a glass fiber filter and snap freezing the sample in liquid nitrogen. Afterwards, the cultures were shifted to 30 µE of light and another sample was taken after 24 h. The frozen sample were processed and mass spectrometry data were analyzed by Dr. Martin Lehmann of the service unit Mass Spectrometry of Biomolecules at LMU (MSBioLMU).

## III. RESULTS

### III.1. Mode of RNA-binding of DLA2

#### III.1.1. Protein structure of DLA2

DLA2 consists of three domains connected by two intrinsically disordered linker regions. The N-terminal domain is the lipoyl-binding domain, where the lipoyl moiety is attached. This domain consists in many organisms of up to three lipoyl domains, but DLA2 contains only one, which has been reported for the homologous protein from *A. thaliana* mitochondria to be sufficient for the catalytic function (Mooney et al., 1999; Broz et al., 2014; Patel et al., 2014). The middle domain shows strong homology to the peripheral E3-binding domain (E3BD) and is therefore supposed to be the binding site for the E3 and the E1 subunits. Mutagenesis analysis performed on the E3BD of the *E. coli* protein suggests that the two subunits bind to overlapping but not identical loci within the E3BD (Park et al., 2004). Modelling of the DLA2 protein structure suggests that the E3BD forms an exposed helix-loop-helix motif which is found in many E2 subunits analyzed (Figure 8; Mande et al., 1996; Frank et al., 2005; Arjunan et al., 2014). The large C-terminal catalytic domain comprises almost half of the protein and is responsible for synthesis of acetyl-CoA and the formation of the 3-dimensional inner core structure of the cpPDC. To guarantee the protein's flexibility, the functional domains are interconnected by the two intrinsically disordered linkers which are highly enriched in proline and alanine residues.

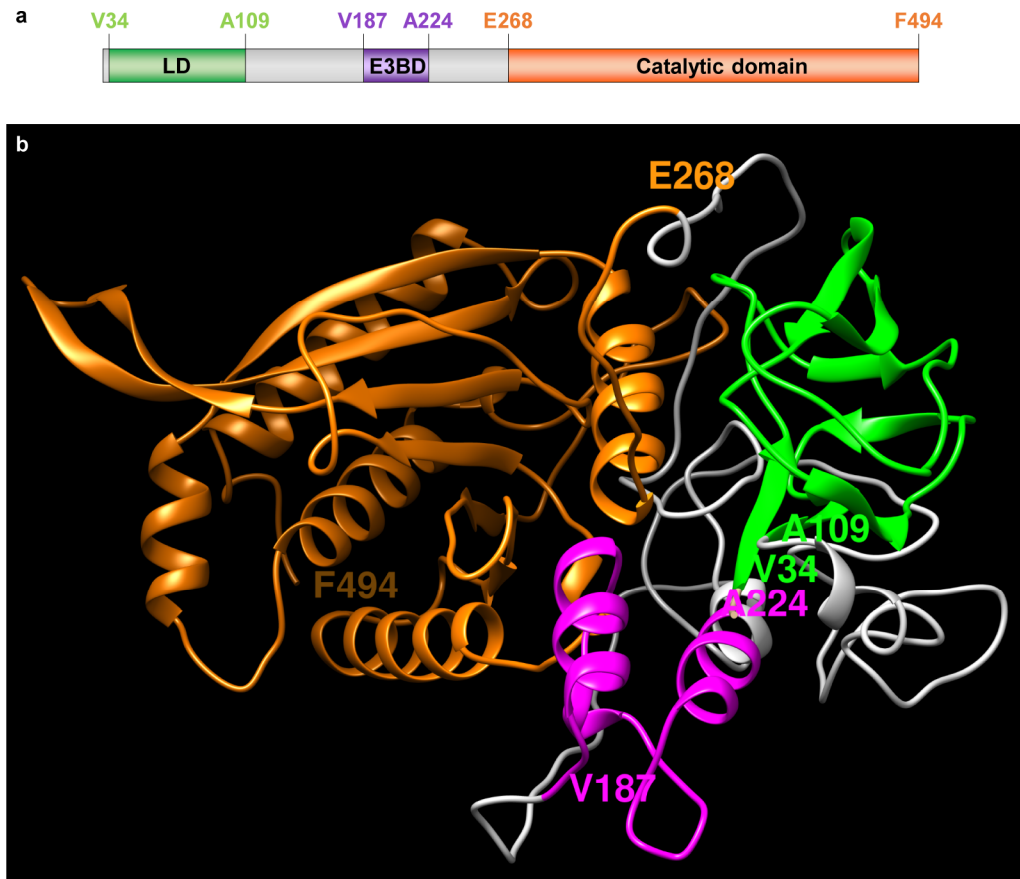


**Figure 8: Domain structure of DLA2 from *C. reinhardtii*.**

Protein sequence (Cre03.g158900) was obtained from Phytozome v5.5. Amino acids 32 – 494 which correspond to the full-length protein without the predicted transit peptide used. Transit peptide prediction was performed using the PredAlgo web tool. Domain annotations were obtained from InterPro and inferred from homology to E2 domains from other organisms. The lipoyl-binding domain (V34 - A109) is depicted in green while the E3-binding region (V187 – A224) and the catalytic domain (E268 – F494) are depicted in purple and orange, respectively. Intrinsically disordered linker regions are depicted in grey. **a**, Schematic overview of the protein domains of DLA2. **b**, Protein structural model of DLA2 generated using the Phyre2 web portal for protein modeling, prediction, and analysis (Kelley LA et al., 2015). Modelling was performed using the intensive modelling mode.

### III.1.2. Multiple domains are involved in RNA-binding of DLA2

*In vitro* experiments by Bohne et al. (2013) showed an intrinsic RNA-binding activity of DLA2 with a dissociation constant ( $K_d$ ) of about 51 nM. They also performed *in silico* predictions of RNA-binding probability which suggested that the E3BD might be involved in RNA-binding as most amino acids predicted to bind to RNA were located within the E3BD (Figure 9). Furthermore, the E3BD contains a predicted Rossmann fold (Rao and Rossmann, 1973). These structural motifs typically bind to cofactors like  $\text{NAD}^+$  or FAD, but were also shown to be involved in RNA-binding of proteins (Nagy et al., 2000; Barbas et al., 2013).

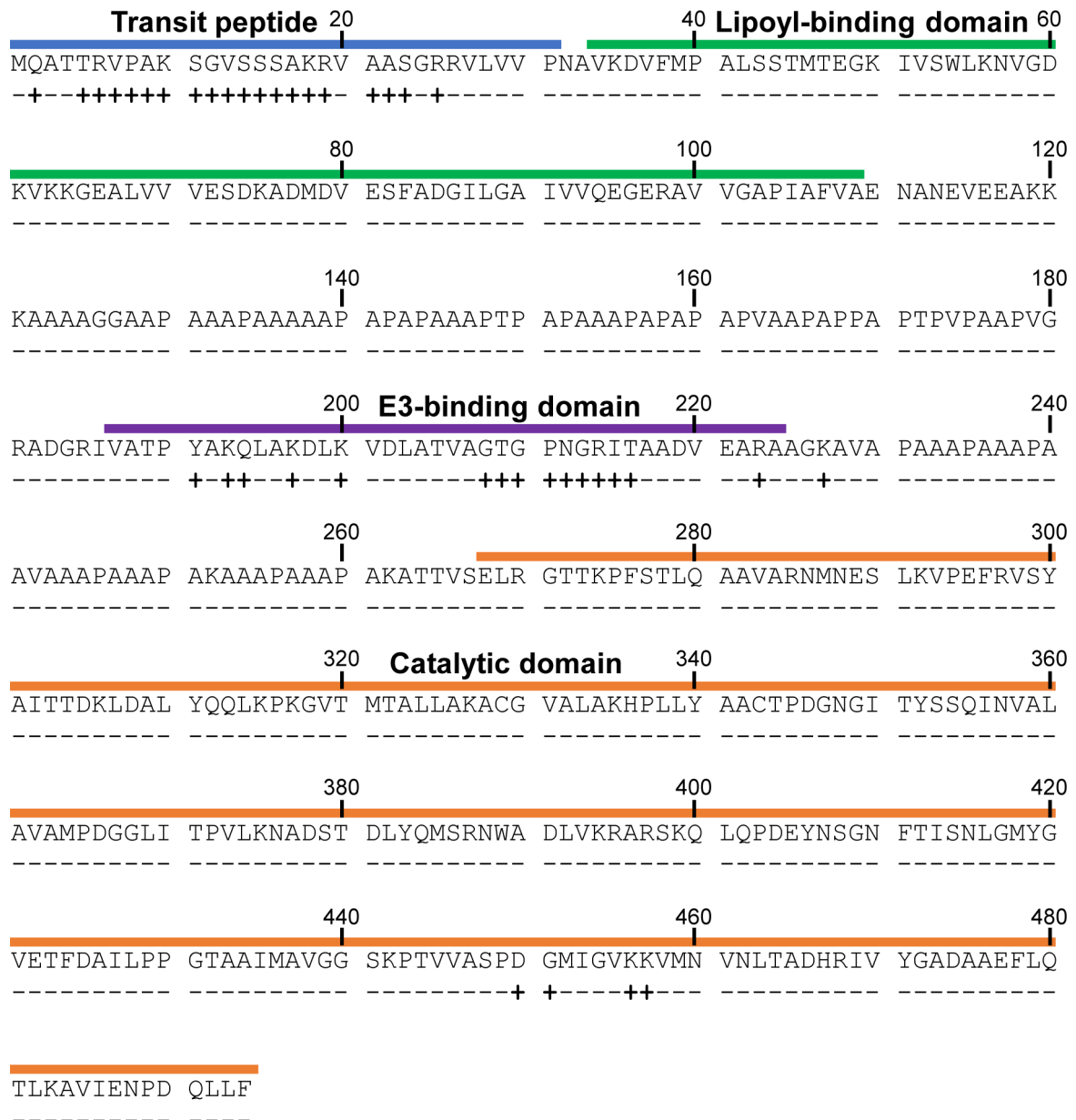


**Figure 9: Prediction of RNA-binding residues in the DLA2 protein from *C. reinhardtii*.**

Possible RNA binding residues were previously predicted by using the RNABindR tool (<http://ailab-projects1.ist.psu.edu:8080/FastRNABindR/>). Plus signs below the amino acid sequence indicate the predicted RNA-binding residues, whereas minus signs indicate a low probability of RNA binding. The conserved domains for lipoyl-binding domain, E3-binding domain, and the 2-oxo acid dehydrogenase catalytic domain are marked above the sequence by green, purple, and orange bars, respectively. The transit peptide is marked in blue. Adapted from Bohne et al. (2013).

Data from UV-crosslinking experiments by Kleinknecht (2018) supported the hypothesis of a E3BD-dependent RNA-binding of DLA2, as they could show that the E3 subunit and the *psbA* mRNA compete for binding to DLA2 *in vitro*. However, a detailed analysis of the domains involved in RNA-binding is still lacking.

To further narrow down the RNA-binding region in DLA2, microscale thermophoresis (MST) was used to analyze the binding affinity of various DLA2 mutant proteins to a

Cy5-labeled *psbA* 5' UTR mRNA probe. This probe covered 49 nucleotides of the *psbA* mRNA from position -36 to +13 relative to the AUG start codon thereby containing the A-rich sequence essential for DLA2-binding identified by Ossenbühl et al. (2002) (compare Figure 12a).

As a proof of principle, first, the RNA-binding affinity of the wild-type DLA2 protein in comparison to a protein without RNA binding capacity, PrataA, was determined (Figure 10). PrataA is a periplasmic TPR protein involved in manganese delivery for biogenesis of PSII in *Synechocystis* sp. PCC 6803 (Klinkert et al., 2004; Schottkowski et al., 2009; Stengel et al., 2012). All proteins used for MST analysis were overexpressed in *E. coli* as fusion proteins containing a His-Sumo-tag. Affinity purification of His-tagged proteins under native conditions was performed using Ni<sup>2+</sup>-NTA resin followed by removal of the His-Sumo-tag by proteolytic digestion and a second purification step. Before objecting the proteins to MST analysis, protein concentration was determined and adjusted to 44µM.

For DLA2, a protein concentration-dependent shift of MST traces could be observed indicating binding of the *psbA* mRNA probe (Figure 10a). Analyzing of this shift resulted in a typical saturation curve and a  $K_d$  of 106 nM (Figure 10b). In contrast, there was no protein concentration-dependent shift of MST curves for the PrataA protein indicating that the shift seen for the DLA2 protein is indeed because of its interaction with the *psbA* mRNA probe.

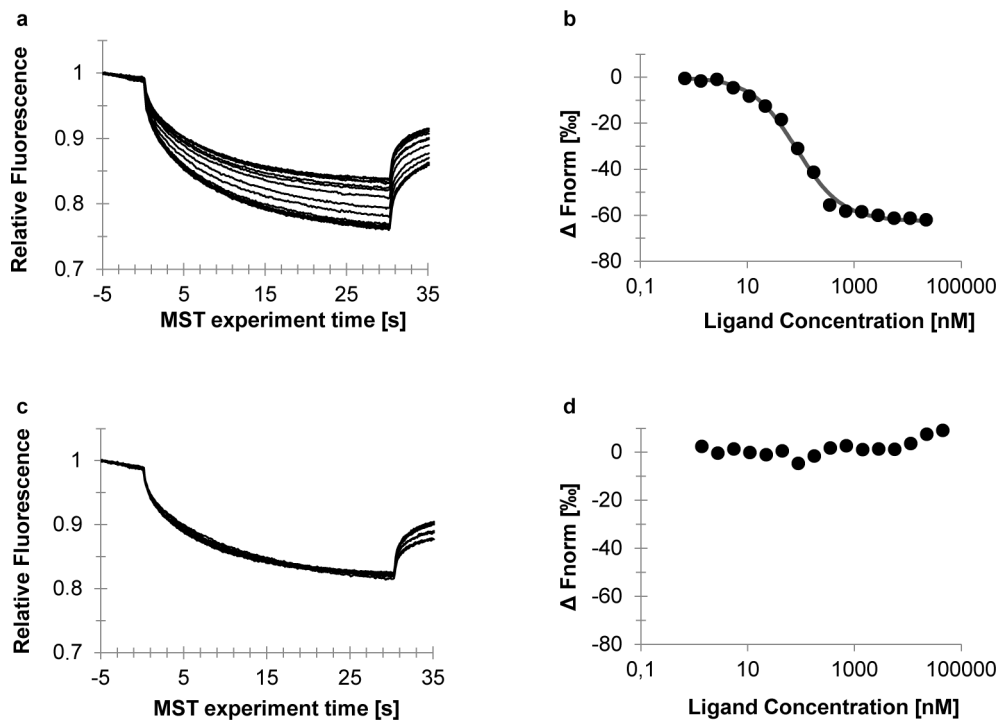


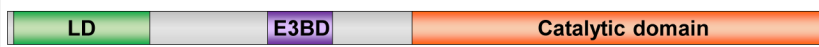
**Figure 10: Microscale thermophoresis (MST) traces and RNA-binding curves of the recombinant DLA2 protein (a, b) and the *Synechocystis* protein PrataA as a negative control (c, d).**

**a, c,** MST traces obtained with increasing amounts of recombinant protein are shown as black lines. **b, d,** The difference in fluorescence between the MST traces after 15 sec was evaluated and is depicted as black dots. The best fit generated by the NanoTemper software (NanoTemper, Munich) is depicted as a dark grey line.

The obtained  $K_d$  value of 106 nM was slightly higher than the value (51 nM) previously reported by Bohne et al. (2013) using filter binding assay and a radioactively labeled RNA probe. This deviation might simply be due to the use of a different methodical approach or due to the shorter RNA probe used here. While the one used here covered 49 nucleotides of the *psbA* mRNA, the one used by Bohne et al. (2013) covered 124 nucleotides from position -111 to +13 relative to the AUG start codon. The additional 75 nucleotides of the *psbA* 5' UTR in the probe used by Bohne et al. (2013) might contain further features to stabilize or enhance the binding to DLA2.

Next, the RNA-binding affinity of various DLA2 mutant proteins was determined to identify regions which are important for binding of the *psbA* mRNA probe. The results obtained are summarized in Figure 11.

Upon deletion of the N-terminal lipoyl-binding domain no change in RNA-binding affinity was detected in comparison to the full-length protein, showing that this domain is not needed for RNA-binding (Figure 11,  $\Delta$ Lip). With a deletion of the E3BD the RNA-binding

| Protein  | Name             | $K_D$ [nM] | Relative Affinity [%] |
|--|------------------|------------|-----------------------|
|  | DLA2             | 106 ± 24   | 100                   |
|  | $\Delta$ Lip     | 107 ± 20   | 99,1                  |
|  | $\Delta$ E3B     | 241 ± 21*  | 44,0                  |
|   | $\Delta$ Cat 462 | 427 ± 55*  | 24,8                  |
|   | $\Delta$ Cat 450 | 466 ± 65*  | 22,7                  |
|   | $\Delta$ Cat 394 | 558 ± 77*  | 19,0                  |
|   | $\Delta$ Cat 315 | 607 ± 82*  | 17,5                  |
|   | $\Delta$ Cat     | 911 ± 60*  | 11,6                  |

**Figure 11: RNA-binding affinities of various mutant DLA2 proteins.**

The binding affinity of different DLA2 mutant proteins for a Cy5-labelled 5'UTR *psbA* probe was measured using MST. A schematic representation showing the domain structure of the analyzed recombinant proteins is displayed in the left column. The lipoyl-binding domain (LD) is depicted in green while the E3BD and the catalytic domain are depicted in purple and orange, respectively. Intrinsically disordered linker regions are shown in grey.  $K_d$  values are displayed as mean ± standard deviation of three independent experiments. For better comparability, the binding affinity relative to the WT protein is shown at the right. The amino acid numbers given in protein names refer to the first deleted amino acid in the respective protein. If no amino acid number is indicated the respective domain was deleted completely. Differences in MST traces were evaluated after 15 sec. The respective MST curves can be seen in Supplemental Figure S1. An asterisk indicates that a mean is significantly different from the mean of the WT DLA2 protein determined by a two-sample *t*-test ( $p < 0.05$ ). For Coomassie blue stained SDS-PAGE gels of the recombinant proteins used for MST analysis, see Supplemental Figure S2.

affinity decreased to 44 % compared to the wild-type DLA2 protein (Figure 11,  $\Delta E3B$ ). A deletion of the catalytic domain even resulted in a decrease of the RNA-binding affinity to 11.6 % (Figure 11,  $\Delta Cat$ ). This indicates that the E3BD of DLA2 and especially the catalytic domain is involved in *psbA* mRNA-binding.

To narrow down the region important for RNA-binding within the catalytic domain, truncated DLA2 versions with progressively deleted portions of the catalytic domain, starting from the C-terminus, were analyzed for their RNA-binding affinity. Interestingly, the DLA2 version with the smallest deletion of only 32 amino acids showed already a dramatic reduction of RNA-binding to about 25 % (Figure 11,  $\Delta Cat$  462). This suggests a crucial role for the C-terminal part of the catalytic domain in *psbA* mRNA-binding. With increasing truncation of the catalytic domain, the RNA-binding affinity decreased progressively to 22.7, 19.0 and 17.5 % of the wild-type affinity, respectively (Figure 10,  $\Delta Cat$  450,  $\Delta Cat$  394,  $\Delta Cat$  315). Taken together, this suggests that beside the E3BD the whole catalytic domain, but especially the very C-terminal part, is crucial for the RNA-binding ability of DLA2.

### III.1.3. E3BD is crucial for RNA recognition

The existence of two separated domains important for RNA-binding raised the question if both are recognizing the *psbA* mRNA with the same specificity. Therefore, the A-stretch within the *psbA* 5' UTR mRNA probe was mutated to a C-stretch and the RNA-binding affinity of selected DLA2 versions to the mutated probe was determined to elucidate if they are still able to recognize this probe (Figure 12a).

First, the binding affinity of the wild-type DLA2 protein to the C-stretch probe was determined. The measured  $K_d$  value of about 248 nM represents a reduction in binding affinity to about 42.7 % compared to the native *psbA* mRNA probe (Figure 12b, DLA2). This reinforces the importance of the A-stretch in the *psbA* 5' UTR for binding of DLA2 previously described by Ossenbühl et al. (2002). When the RNA-binding affinity of the DLA2 version with deleted E3BD was determined, a reduction of binding affinity to the C-stretch probe compared to the native *psbA* mRNA probe could not be detected (Figure 12b,  $\Delta E3B$ ). This indicates that by deleting the E3BD, this DLA2 version lost its ability to recognize the A-stretch within the 5' UTR of the *psbA* mRNA. Interestingly, when analyzing the DLA2 version with the very C-terminal deletion, there was still a significant C-stretch-dependent reduction of RNA-binding affinity (Figure 12b,  $\Delta Cat$  462). While the determined RNA-binding affinity of the  $\Delta Cat$  462 protein to the native *psbA* mRNA probe was about 427 nM, the  $K_d$  value for binding to the C-stretch probe was 625 nM. This reduction of the binding affinity indicates that despite its

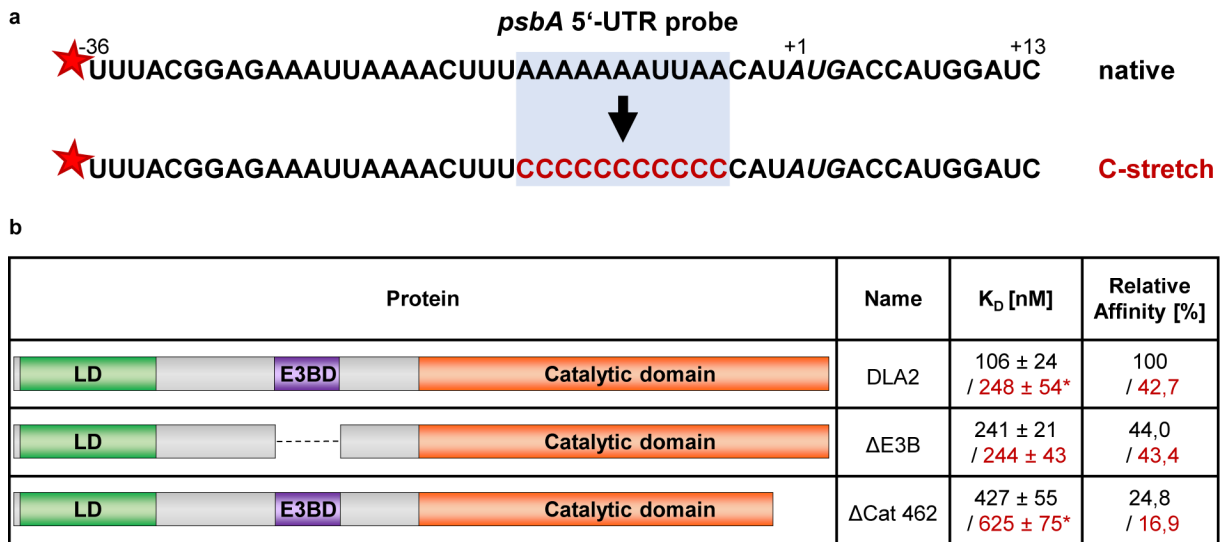


**Figure 12: Specificity of RNA recognition by recombinant DLA2 proteins.**

**a**, Sequences of the native *psbA* 5'-UTR probe and the mutated probe with the C-stretch. Mutated nucleotides are depicted in red and positions relative to the AUG start codon (italics) are marked above the sequence. **b**, Comparison of the binding affinities of different DLA2 mutant proteins for the native Cy5-labeled 5'UTR *psbA* probe and the mutated C-stretch probe. Differences in MST traces were evaluated after 15 sec. The respective MST-curves can be seen in Supplemental Figure S3. The means ± standard deviations (n=3) of the binding affinities to the native *psbA* probe are shown in black, while the values for the mutated C-stretch probe are shown in red. All affinity values indicated in the right column are relative to the binding affinity of the WT protein to the native *psbA* probe. An asterisk indicates that the mean binding affinity of the protein to the C-stretch probe is significantly different from the mean binding affinity of the respective protein to the native *psbA* probe determined by a two-sample *t*-test ( $p < 0.05$ ).

already low RNA-binding affinity, the ΔCat 462 protein still has the ability to recognize the A-stretch in the 5' UTR of the *psbA* mRNA.

Taken together, these data suggest that both the E3BD as well as the catalytic domain are crucial for RNA-binding. However, the DLA2 version lacking the E3BD could not discriminate between the native and the C-stretch probe, indicating that this domain is conferring the sequence specific *psbA* mRNA recognition while the catalytic domain is important for RNA binding in general.

## III.2. Is reversible lysine acetylation regulating DLA2 function?

### III.2.1. Differential acetylation of DLA2 *in vivo*

Although MST analysis elucidated the mode of RNA-binding of DLA2, the regulation mechanism of DLA2 function is still unknown. The fact that the RNA-binding function of DLA2 is strictly acetate-dependent together with *in vitro* experiments from Kleinknecht (2018), which showed that autoacetylation of DLA2 can influence RNA-binding, suggested that lysine-acetylation may provide the molecular switch searched for.

To address this, the acetylome of *C. reinhardtii* under different growth conditions was analyzed together with the group of Prof. Dr. Iris Finkemeier (Westfälische Wilhelms Universität Münster; König et al., manuscript in preparation). The DLA2-specific analysis of the generated data revealed acetylation of four lysine residues (Figure 13). K61 within the lipoyl domain, K197 within the E3BD and K315 and K394 within the catalytic domain. Interestingly, while K61, K315 and K394 showed no significant changes in acetylation between the growth conditions, acetylation at K197 was dramatically increased under mixotrophic (4-fold) and heterotrophic (3-fold) conditions compared to photoautotrophic growth conditions. This acetate-dependent acetylation and the localization within the E3BD which is important for *psbA* mRNA recognition, makes K197 a high potential candidate for the regulation of DLA2's function. However, the fold changes of the two acetylation sites within the catalytic domain of DLA2, although not significant ( $0.1 > p\text{-values} > 0.05$ ), indicate an acetylation pattern specifically downregulated under mixotrophic growth conditions. In the presence of light and acetate acetylation at K315 and K394 was decreased to about 60 % compared to hetero- or photoautotrophic growth conditions. As acetylation neutralizes the positive charge of lysine residues, the increase of positive charges within the catalytic domain, which was shown to be important for RNA-binding (compare Figure 11), might increase DLA2's affinity to the negatively charged RNA molecule under mixotrophic growth conditions. Nevertheless, due to the heterogeneity of the replicates concerning the acetylation at K315 and K394 mean values were not significant. Therefore, future work would be needed to confirm the putative differential acetylation at these positions and the associated hypothesis of an influence on RNA-affinity. Another interesting observation was that the DLA2 protein abundance was significantly decreased to about 70 % under heterotrophic compared to mixo- or photoautotrophic growth conditions. This would be in line with the thought of cpPDC activity being essential under photoautotrophic conditions and DLA2's RNA-binding function being restricted to mixotrophic conditions.

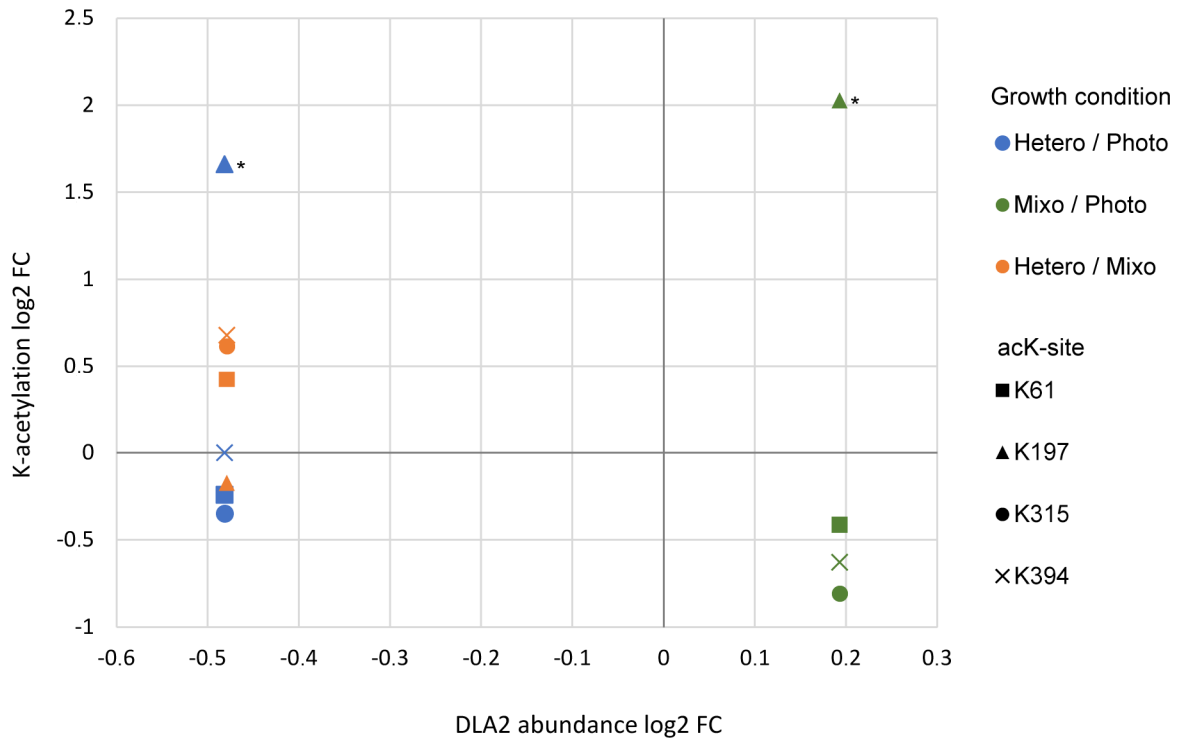


**Figure 13: Acetylation at K197 of DLA2 is increased under hetero- and mixotrophic growth conditions.**

Scatter plot comparing log2 fold change of acetylation at the identified lysine residues of DLA2 (Y-axis) and the log2 fold change of DLA2 abundance (x-axis) between the tested growth conditions. The log2 fold change between hetero- and photoautotrophic growth conditions (Hetero / Photo) is depicted in blue. The log2 fold change between mixo- and photoautotrophic growth conditions (Mixo / Photo) is depicted in green and the log2 fold change between hetero- and mixotrophic growth conditions (Hetero / Mixo) is depicted in orange. Values are means of three biological replicates. An asterisk indicates that acetylation at the respective lysine residue is significantly changing between the two compared growth conditions using a LIMMA statistical analysis ( $p < 0.05$ ). Generation of acetylome raw data was performed by Dr. Ann-Christine König and analysis of mass spectrometry data and LIMMA statistical analysis was performed by Dr. Jürgen Eirich (AG Finkemeier, Westfälische Wilhelms Universität Münster). Values of the log2 fold changes and the corresponding  $p$ -values can be seen in Supplemental Table 3 and 4.

### III.2.2. Evolutionary conservation of K197 might enable lysine acetylation-dependent regulation in photosynthetic organisms

*In vitro* data from Bohne et al. (2013) indicated that the RNA-binding activity of DLA2 might be a conserved trait of E2 subunits of various organisms. Thus, the conservation of the identified acetylation site K197 was analyzed in E2 subunits from mitochondria, chloroplasts and prokaryotic organisms (Figure 14). Interestingly, the generated alignment of various E3BDs showed that the lysine residue at position 197 of DLA2 is rather conserved in E2 subunits from plastids or photosynthetic prokaryotes. In contrast, most of the analyzed E2 subunits from mitochondria or non-photosynthetic prokaryotes did not have a lysine residue at the corresponding position.

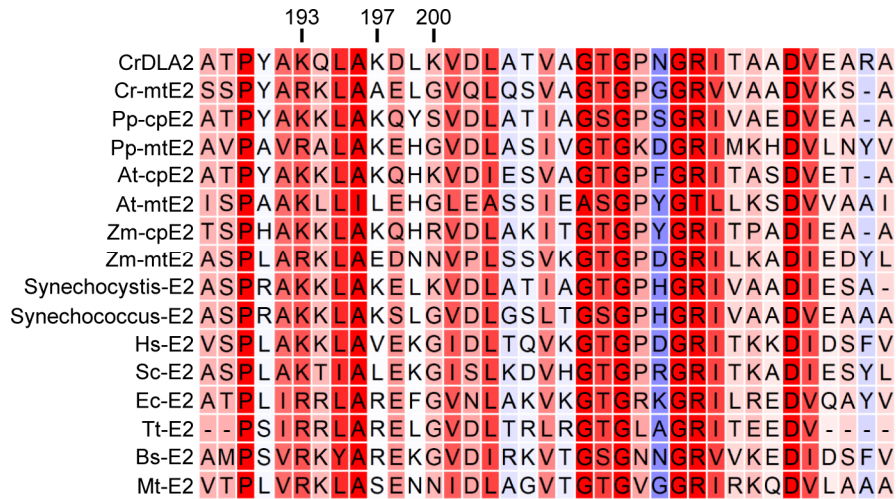


**Figure 14: Conservation of K197 in the E3BD of the plastidic E2 subunit of *C. reinhardtii* in various organisms.**

Alignment of the E3-binding domain of the E2 subunits of various organisms. For photosynthetic eukaryotic organisms, sequences of plastidic (cp) and mitochondrial (mt) isoforms are given. High conservation is depicted in red while low conservation is depicted in blue. The position of the three lysine residues in the E3BD of DLA2 is marked above. Sequences were obtained from Uniprot and alignment was created using CLC main workbench. Accession numbers are as follows: *C. reinhardtii* CrDLA2 (DLA2, A0A2K3DW88), *C. reinhardtii* Cr-mtE2 (DLA1, A8J1V5), *P. patens* Pp-cpE2 (A0A2K1KW62), Pp-mtE2 (A0A2K1K9P5), *A. thaliana* At-cpE2 (LTA2, NP\_189215), At-mtE2 (LTA3, NP\_190788), *Zea mays* Zm-cpE2 (A0A1D6Q1G1), Zm-mtE2 (DLA1, Q9SWR9), *Synechocystis* sp. 6803 *Synechocystis*-E2 (sll1841, NP\_441936), *Synechococcus* sp. 6301 *Synechococcus*-E2 (pdhC, NC\_006576), *H. sapiens* HS-E2 (DLAT, NM\_001931), *S. cerevisiae* Sc-E2 (Lat1, NP\_014328), *E. coli* Ec-E2 (AceF, NP\_414657), *T. thermophilus* Tt-E2 (NC\_006461), *B. subtilis* Bc-E2 (pdhC, NP\_389343), *M. tuberculosis* Mt-E2 (SucB, WP\_003411450).

Furthermore, acetylome data from various organisms were analyzed in respect to acetylation within the respective E2 subunits (Zhao et al., 2010; Finkemeier et al., 2011; Henriksen et al., 2012; Kim et al., 2013; Wagner and Payne, 2013; Zhang et al., 2013; König et al., 2014; Liu et al., 2014; Smith-Hammond et al., 2014; Mo et al., 2015; Chen et al., 2018; Wang et al., 2019; Yan et al., 2020). In line with the ubiquity of this PTM through organisms, all the E2 subunits were found to be acetylated with most of them having one or two acetylated lysine residues and all of them within the catalytic domain. Only the E2 subunit from *S. cerevisiae*, LAT1, showed a distinct acetylation pattern with 11 acetylated lysine residues distributed all over the protein and three of them in the E3BD. However, all the acetylome data published except for the *Synechocystis* acetylome, were generated from mitochondria or non-photosynthetic prokaryotes. Additionally, the mitochondrial E2 subunits, DLA1 and DLA3 were identified in our acetylome analysis from *C. reinhardtii* but no acetylation sites could be detected.

Taken together, these data suggest that the lysine residue at position 197 in DLA2 might be evolutionary conserved from E2 subunits of cyanobacteria to the ones from chloroplasts of higher plants. Acetylation within the E3BD, as it has been seen for DLA2, could not be detected

for mitochondrial and prokaryotic E2 subunits published. This still leaves room for an acetylation-dependent regulation exclusively attributed to photosynthetic organisms, but to clarify this more acetylome data regarding chloroplast proteins are needed.

### III.2.3. Acetylation at K197 of DLA2 does not influence RNA-binding affinity *in vitro*

To elucidate if the differential acetylation at K197 of DLA2 influences the RNA-binding affinity, additional MST experiments with mutated recombinant DLA2 proteins were performed. Therefore, K197 was mutated to glutamine (K197Q) or to arginine (K197R). While glutamine mimics a constitutive acetylation because it does not have a positive charge compared to lysine, arginine mimics the non-acetylated state, as it preserves the positive charge and cannot be acetylated (Figure 15). This method was first described by Ren and Gorovsky (2001) and is an often used tool in the analysis of protein acetylation sites (Aljaberi et al., 2015; Min et al., 2015; Wang et al., 2016). The E3BD of DLA2 contains two more lysine residues available for acetylation site analysis, K193 and K200. The positive charge at position 193 seems to be essential for the protein as it is conserved in all E2 subunits analyzed before, while K200 was only found in *Synechocystis* spp. (compare Figure 14). Because of the conservation of K193 and the close proximity to K197, the lysine residues K193 and K200 were also mutated as controls for site specificity of acetylation-dependent effects.

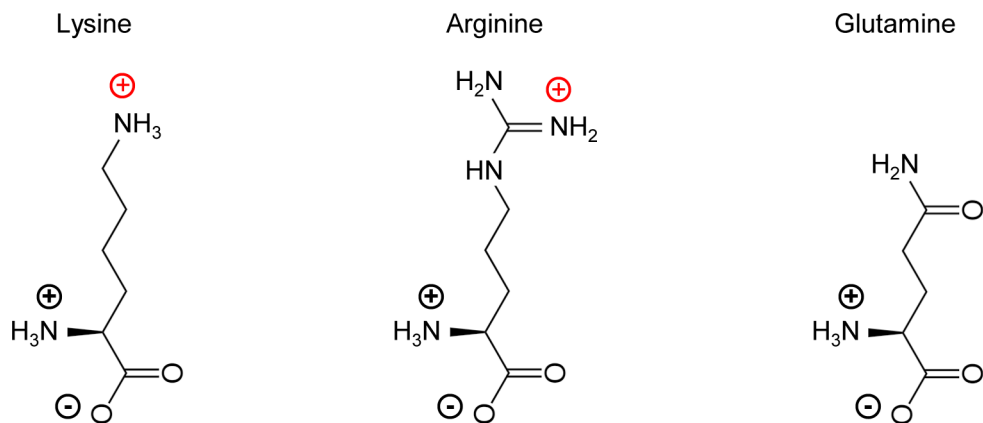


**Figure 15: Amino acid structures of lysine, arginine and glutamine.**

Structure of lysine and the amino acids used for substitution in the recombinant proteins used for MST analysis. Substitution of lysine to arginine preserves the positive charge at the side chain thereby mimicking the constitutively deacetylated state. Substitution to glutamine results in no positive charge at the side chain thereby mimicking constitutive acetylation. Negative and positive charges are marked as minus (-) and plus (+) signs, respectively. The critical charges at the amino groups of the respective side chains are depicted in red.

The determination of the binding affinity using recombinant protein and the former used Cy5-labeled *psbA* 5' UTR mRNA probe, showed no significant differences when mutating K197 to arginine or glutamine (Figure 16, DLA2 K197R and DLA2 K197Q). Mutation of K200 resulted in a slight but not significant reduction of the binding affinity for both mutations (Q and R) indicating that acetylation at this position does not influence RNA-binding (Figure 16, DLA2 K200R and DLA2 K200Q). This suggests that both K197 and K200 are not involved in RNA-binding. Interestingly, upon mutation of the K193 to glutamine mimicking acetylation, the RNA-binding affinity decreased dramatically to 48 % compared to the wild-type DLA2, while mutation to arginine had no effect on RNA-binding (Figure 16, DLA2 K193R and DLA2 K193Q).

Taken together, these data suggest that only K193 is involved in RNA-binding and that the acetylation of K197 detected *in vivo*, is not changing the RNA-binding affinity of recombinant DLA2.

| Protein  | Name       | $K_D$ [nM] | Relative Affinity [%] |
|--|------------|------------|-----------------------|
|  | DLA2 K193R | 104 ± 23   | 102,0                 |
|  | DLA2 K193Q | 221 ± 60*  | 48,0                  |
|  | DLA2 K197R | 93 ± 30    | 114,0                 |
|  | DLA2 K197Q | 114 ± 21   | 93,0                  |
|  | DLA2 K200R | 132 ± 45   | 80,3                  |
|  | DLA2 K200Q | 151 ± 35   | 70,2                  |

**Figure 16: RNA-binding affinities of various acetylation mutant DLA2 versions.**

The binding affinity of different DLA2 mutant proteins for a Cy5-labelled 5'UTR *psbA* probe was measured using MST. A schematic representation showing the domain structure of the analyzed recombinant proteins is displayed in the left column. The red arrowhead indicates the position of the mutated lysine residue. Differences in MST traces were evaluated after 5 sec. The respective MST-curves can be seen in Supplemental Figure S4.  $K_D$  values are displayed as mean ± standard deviation of three independent experiments. For better comparability, the binding affinity relative to the WT protein (compare Figure 9) is shown. An asterisk indicates that a mean is significantly different from the mean of the WT DLA2 protein in Figure 9 determined by a two-sample *t*-test ( $p < 0.05$ ). For Coomassie blue stained SDS-PAGE gels of the recombinant proteins used for MST analysis, see Supplemental Figure S5.

### III.3. Generation of a *dla2* mutant using the CRISPR/Cas9 system

The *in vitro* data showed that acetylation of K197 does not influence RNA-binding affinity of DLA2 suggesting that it might instead influence the binding of the other cpPDC subunits and complex stability. As all of the cpPDC subunits are known to aggregate and build homooligomers it was not feasible to perform *in vitro* binding assays with multiple cpPDC subunits (Johnston et al., 1997; Mooney et al., 1999; Broz et al., 2014). A *dla2* knock out mutant, which could be used for complementation with the acetylation mimicking constructs to analyze the influence of the acetylation *in vivo*, was not available. Therefore, the CRISPR/Cas9 system which was recently established for *C. reinhardtii* (Greiner et al., 2017), was used to generate a *dla2* knock out mutant in collaboration with the group of Prof. Dr. Peter Hegemann (Humboldt University, Berlin). A schematic overview of the process of generation of the *dla2* knock out mutant is depicted in Figure 17a. The arginine auxotrophic strain cc-3403 was used as recipient strain and the *ARG7* gene coding for the argininosuccinate lyase was used for selection. A short double-stranded DNA sequence called mutation oligo which contained stop-codons in every frame was included in the transformation to increase the knock-out efficiency (Figure 17b; Ran et al., 2015). Moreover, the mutation oligo contained a short human sequence from the *EMX1* gene including a restriction site for the RNA-guided DNA endonuclease Cas9 which would allow CRISPR/Cas9-mediated integration of external DNA at the insertion site of the mutation oligo in future experiments. Besides the *ARG7* gene and the mutation oligo, the recombinant Cas9 protein of *Streptococcus pyogenes* together with an associated guide RNA were included in the transformation mix. This guide RNA was targeting the Cas9 endonuclease to a restriction site within the first exon of the *DLA2* gene (Figure 17c).

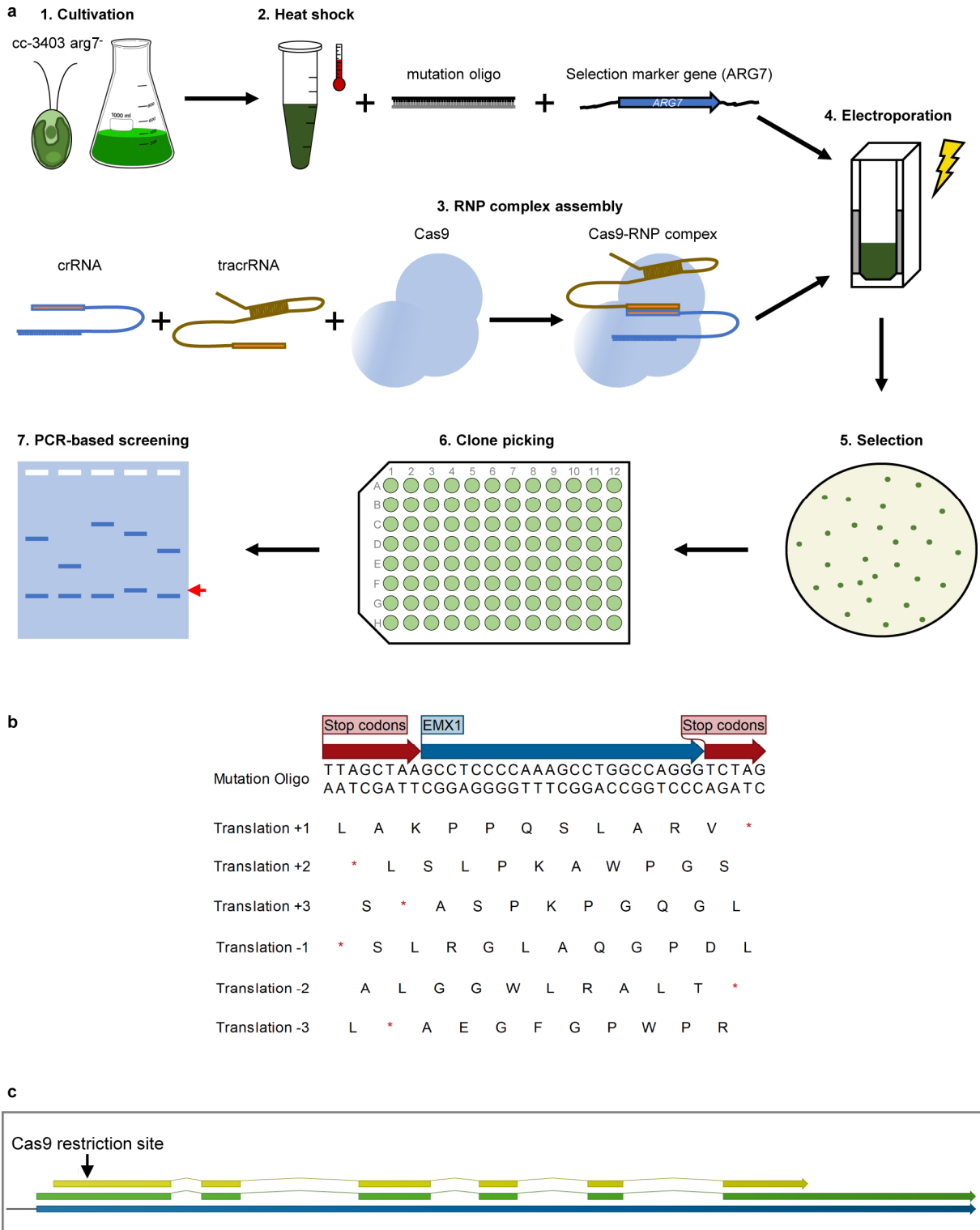


**Figure 17: Generation of a *dla2* knock out mutant.**

**a**, Working scheme for the generation of a *dla2* knock out mutant using the CRISPR/Cas9 system. **b**, Sequence of the mutation oligo used for the generation of the mutant. Stop codons at the 5' and 3' end are represented by a red arrow. The EMX1 genomic sequence is represented by a blue arrow. The different translation frames are displayed below. **c**, Gene model of the *DLA2* gene located on the third chromosome of *C. reinhardtii* (Cre03.158900, Phytozome version 5.5). The *DLA2* gene is depicted in blue while the mRNA and the cDNA are depicted in green and yellow, respectively. The black arrow marks the position of the Cas9 restriction site within the first exon used for the generation of the *dla2* mutant.

After transformation, PCR-based screening for insertions was performed using primers binding 90 bp up- and downstream of the restriction site. This resulted in a clear size shift of the fragment size of one clone (Figure 18a). This clone was diluted and plated for isolation of a single cell colony to exclude possible wild-type contamination. After the isolated clone showed the same fragment size shift as in the first screening round, the fragment was sequenced and showed an insertion of the mutation oligo at the Cas9 restriction site in exon 1 of the *DLA2* gene resulting in a translation stop after 31 amino acids. As the transit peptide is predicted to have a length of 31 amino acids, the inserted stop codon should result in the absence of the *DLA2* protein. To analyze this, Western blot analysis was performed and could confirm that there is no *DLA2* accumulation in the newly generated *dla2* mutant (Figure 18b). To ensure that there is no residual *DLA2* accumulating and that there is no wild-type contamination left, the *dla2* knock out mutant was tested for an acetate-requiring phenotype on minimal medium (HSM) supplemented with arginine. While the cc-3403 strain showed rapid growth on these plates, no growth could be detected for the *dla2* mutant, confirming the *DLA2* knock-out, as PDC activity is thought to be essential under photoautotrophic conditions (Figure 18c).

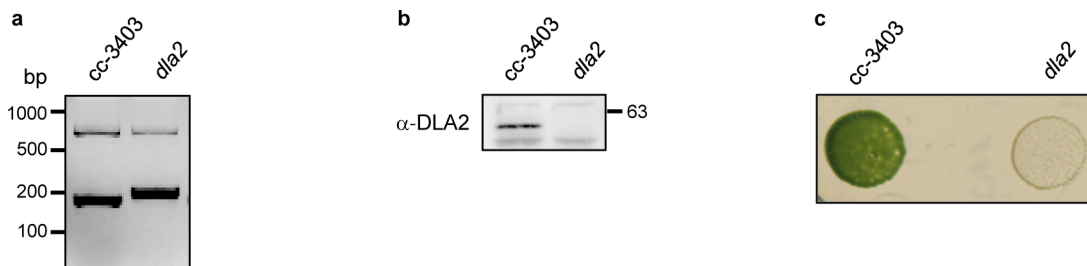


**Figure 18: Identification of a *dla2* knock out mutant.**

**a**, PCR products obtained by using cc-3403 or *dla2* genomic DNA as a template and primers which bind 90 bp upstream and downstream of the Cas9 restriction site, were separated on an agarose gel. **b**, Western blot analysis of 15 µg of whole cell protein lysates of the cc-3403 strain and the *dla2* knock out mutant (*dla2*) using a *DLA2* antibody. **c**, Drop plating test of the cc-3403 strain and the *dla2* mutant on HSM plates supplemented with arginine. Cells were grown in liquid culture in the presence of acetate to a density of about  $10^6$  cells/mL before 10 µl of each strain were spotted onto the plate. After incubation for 7-10 days plates were documented.

### III.3.1. Complementation of the *dla2* mutant with a construct encoding an HA-tagged *DLA2* version restores growth on minimal medium

To confirm that the failure of the *dla2* mutant to grow under photoautotrophic conditions is a result of missing acetyl-CoA synthesis because of the knock-out of *DLA2* and not caused by a second site mutation, the mutant was complemented with the pBC1:*DLA2*-HA construct for expression of the native *DLA2* protein fused with a triple hemagglutinin (HA) tag. When analyzing the expression of the *DLA2*-HA fusion protein in the complemented strain by

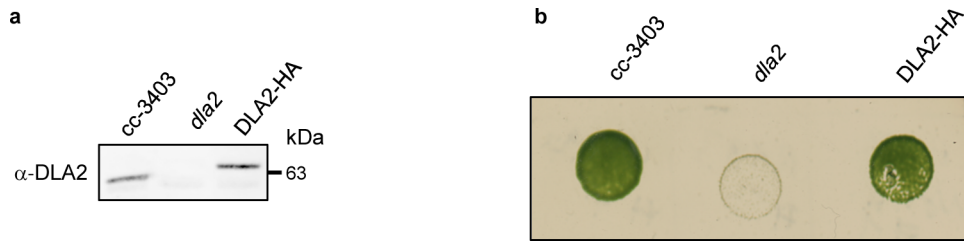


**Figure 19: Complementation of the *dla2* knock out mutant rescues the photoautotrophic growth phenotype.**

**a**, Western blot analysis of the DLA2 accumulation in the cc-3403 strain, the *dla2* mutant and the complemented DLA2-HA strain. **b**, Growth of the cc-3403, the *dla2* mutant and the DLA2-HA complemented strain on HSM plates supplemented with arginine.

Western blot analysis, DLA2 accumulation at least to wild-type level could be detected. The detected protein revealed a slightly slower migration in the gel as the wild-type protein indicating the presence of the fused HA-tag (Figure 19a). With accumulation of DLA2 in the complemented strain the growth under photoautotrophic conditions could be restored (Figure 19b). This shows that DLA2 is missing in the *dla2* mutant and that cpPDC activity is indeed essential in the absence of acetate.

To analyze the growth of the *dla2* knock out mutant and the DLA2-HA strain in more detail, growth curves were performed and doubling times under mixotrophic and photoautotrophic conditions were calculated. There were no significant differences of doubling times between the strains under mixotrophic conditions (Table 8). In line with the plate spotting tests, there was no photoautotrophic growth for the *dla2* mutant and complementation with the DLA2-HA construct led to restored photoautotrophic growth to wild-type level.

**Table 8: Doubling times of the cc-3403 strain, the *dla2* knock out mutant as well as the complemented DLA2-HA strain.** Values are means from at least 3 biological replicates.

| strain      | mixotroph [h] | photoautotroph [h] |
|-------------|---------------|--------------------|
| cc-3403     | 10.2 ± 0.9    | 36.1 ± 5.9         |
| <i>dla2</i> | 10.0 ± 0.5    | -                  |
| DLA2-HA     | 9.5 ± 0.3     | 38.8 ± 4.9         |

Next,  $F_v/F_m$  values were determined using a FluorCam 800MF for analysis of strains on plates. The  $F_v/F_m$  value is a common parameter in the analysis of photosynthetic organisms as it describes the efficiency of light absorption at PSII which often allows conclusions regarding PSII functionality (Kitajima and Butler, 1975; for a review on chlorophyll fluorescence measurements, see Rungrat et al., 2016). Both the *dla2* knock out mutant as well as the

DLA2-HA strain showed wild-type-like  $F_v/F_m$  values between 0.80 and 0.82 indicating there are no PSII specific defects under these conditions.

To examine if the *dla2* knock out mutant shows any growth defects under other conditions, drop plating tests were performed. Therefore, decreasing cell numbers of the three strains were used and dropped onto TAP plates supplemented with arginine. After incubation of the plates for several days under various conditions, growth was documented and analyzed (Figure 20).

The plates were subjected to dark, moderate and higher light intensities (0, 30 and  $100 \mu\text{E m}^{-2}\text{s}^{-1}$ ) as well as to lower, optimal and higher temperature (15, 23 and  $30^\circ\text{C}$ ). Both dark ( $23^\circ\text{C}$ ,  $0 \mu\text{E m}^{-2}\text{s}^{-1}$ ) and cold ( $15^\circ\text{C}$ ,  $30 \mu\text{E m}^{-2}\text{s}^{-1}$ ) conditions resulted in limited growth of all strains but no conditions led to a DLA2-specific retardation of growth.

Taken together, the knock-out of DLA2 led to inhibited growth under photoautotrophic conditions which could be restored by complementation with a DLA2-HA fusion protein. Besides the acetate requiring phenotype of the *dla2* knock out mutant, no other effects resulting from the CRISPR/Cas9 treatment were observed under the -growth conditions tested.

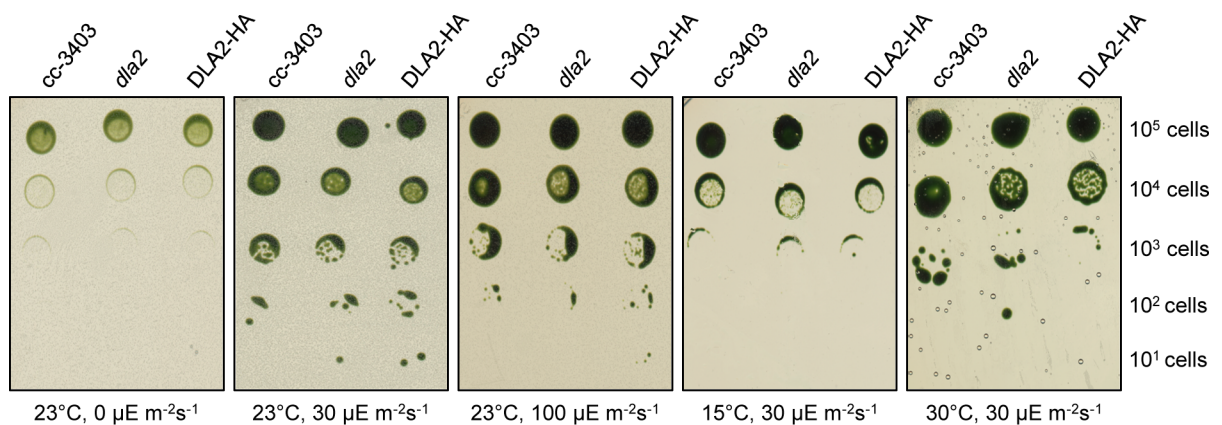


**Figure 20: Growth analysis of the *dla2* knock out mutant under different light and temperature conditions.** Drop plating tests of the cc-3403 strain, the *dla2* knock out mutant and the complemented DLA2-HA strain. Different amounts of cells were spotted onto TAP-arginine plates and incubated for 5-7 days under the indicated light and temperature conditions. The starting number of cells which were spotted is displayed on the right.

### III.3.2. Loss of DLA2 does not lead to severe changes in lipid and fatty acid accumulation in the presence of acetate

The DLA2 containing cpPDC is responsible for acetyl-CoA production and with that directly linked to fatty acid and lipid synthesis in the chloroplast. Hence, a comprehensive analysis of the lipid composition in the *dla2* knock out mutant was undertaken. As the *dla2* mutant was not able to grow photoautotrophically, the analysis was performed under hetero- and mixotrophic conditions. Therefore, the *dla2* mutant and the cc-3403 strain were grown in the dark for 36 h. After collection of the sample under heterotrophic conditions, cultures were shifted to the light and after 24 h the sample under mixotrophic conditions was collected. After mass spectrometry and data analysis the fold change of lipid accumulation upon the shift to mixotrophic conditions was calculated and is depicted in Figure 21a.

The influence of the growth condition shift on the lipid abundancy seems to be similar in cc-3403 and the *dla2* mutant. Diacylglycerols (DAG) and triacylglycerols (TAG) decrease upon the shift to mixotrophic conditions. Especially TAG accumulation was decreased by 97 % and 96 % respectively. It is known that algae accumulate neutral lipids like TAGs and DAGs under heterotrophic conditions, as TAG is the most important storage lipid and DAG is involved in a plethora of metabolic pathways and a building block for many lipids (Liu et al., 2011; Singh et al., 2014)

The chloroplast lipids MGDG and DGDG as well as the extraplastidic membrane lipid classes of diacylglyceryl-3-O-4'-(N,N,N-trimethyl)-homoserine (DGTS) and phosphatidylethanolamine (PE) were in most cases slightly reduced. This might be a result of cells starting to rapidly divide upon the shift to mixotrophic conditions resulting in a decreased amount of lipids per cell. Despite the absence of DLA2 in the *dla2* mutant there were only very slight differences in lipid accumulation compared to the cc-3403 strain under both growth conditions. Heterotrophic conditions resulted in only six lipids significantly altered in their accumulation (Figure 21b). Interestingly, three of those lipids potentially belonged to the same class based on their elution pattern but could not be assigned to a common lipid class and were named “unknown apolar compound” (UAC). They might belong to a compound class specifically upregulated in the *dla2* mutant under heterotrophic conditions. Mixotrophic conditions lead only to four lipids with significantly but very slightly altered accumulation (Figure 21c). This indicates that the supply of external acetate can fully complement the loss of DLA2 and with that missing cpPDC activity with respect to lipid synthesis under the growth conditions tested.

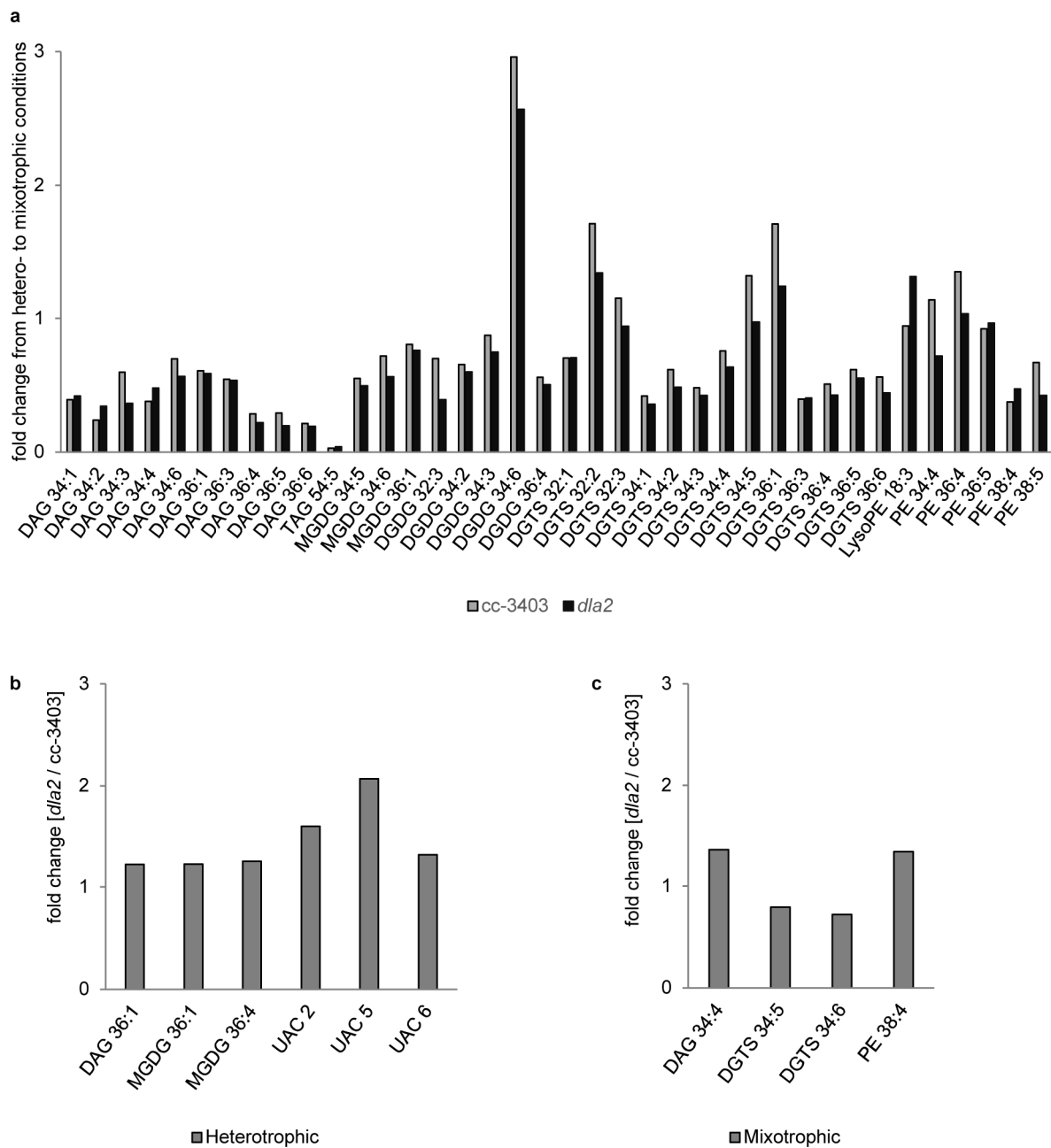


**Figure 21: Absence of DLA2 results only in minor changes of lipid accumulation in response to changing growth conditions.**

Liquid cultures of the cc-3403 strain and the *dla2* knock out mutant were grown in TAPS + arginine in the dark for 36 h to a cell density of  $\sim 1 \times 10^6$  cells/mL. Cells were shifted from heterotrophic growth in the dark to mixotrophic conditions by applying light of about  $30 \mu\text{E m}^{-2}\text{s}^{-1}$ . Samples were taken right before (heterotrophic) and 24 h after (mixotrophic) the shift. **a**, Fold change of accumulation of indicated lipids is depicted for both strains. Values were calculated from three biological replicates. For a better overview only the lipids which change significantly in at least one of the strains are depicted here. A list with all identified lipids can be found in supplemental Table S5. **b**, **c**, Lipids accumulating to significantly different amounts between the *dla2* knock out mutant and the cc-3403 strain (**b**) under heterotrophic conditions before illumination and (**c**) under mixotrophic conditions after 24 h of illumination. Significance was determined using a two-sample *t*-test ( $p < 0.05$ ). Mass spectrometry was performed by Dr. Martin Lehmann of the mass spec service unit of the LMU (MSBioLMU).

### III.4. Analysis of mutants mimicking the acetylation state of K197 of DLA2 *in vivo*

#### III.4.1. Modification of the acetylation state of K197 leads to altered growth under photoautotrophic conditions

To analyze the influence of the K197 acetylation *in vivo*, the *dla2* knock out mutant was complemented by nuclear transformation with mutated DLA2-HA versions where K197 was substituted by a glutamine (K197Q-HA) or by an arginine (K197R-HA). As described above for the *in vitro* analysis of the recombinant DLA2 protein by MST (compare Fig 14), these substitutions should mimic the acetylated (K197Q-HA) and the non-acetylated (K197R-HA) state, respectively.

All experiments including the cc-3403 strain had to be performed with media supplemented with arginine because of its arginine auxotrophy. Therefore, the DLA2-HA strain was used as reference strain for the subsequent experiments. As no differences could be detected between the DLA2-HA and the cc-3403 strain in our initial characterization (compare Fig. 18) and all complemented strains possessed the same insertion of the *ARG7* gene as the *dla2* knock out mutant, arginine-dependent phenotypical effects caused by different insertion and expression of this gene could be eliminated. To exclude a potential impact of the C-terminally fused triple HA-tag on DLA2's function and/or stability the generated acetylation mutants were compared to the identically tagged DLA2-HA strain in the following experiments.

The determined doubling time of the generated acetylation mutants revealed no significant differences of mixotrophic growth compared to the DLA2-HA strain (Table 9). In contrast, photoautotrophic growth was slightly decreased in the K197Q-HA strain, while it was slightly increased for the K197R-HA strain.

**Table 9: Doubling times of the complemented strains under different growth conditions.**

Values are means from at least 3 biological replicates. An asterisk indicates that a mean is significantly different from the mean of the DLA2-HA strain determined by a two-sample *t*-test ( $p < 0.05$ ).

| strain   | mixotroph [h] | photoautotroph [h] |
|----------|---------------|--------------------|
| DLA2-HA  | 9.5 ± 0.3     | 38.8 ± 4.9         |
| K197Q-HA | 9.9 ± 0.2     | 45.3 ± 6.3 *       |
| K197R-HA | 9.8 ± 0.2     | 34.4 ± 3.6 *       |

To elucidate if this growth effect is just reflecting different DLA2 accumulation levels in the respective strains, protein abundance of all cpPDC subunits and selected photosynthetic proteins was analyzed (Figure 22).

Intriguingly, the retarded growth of the K197Q-HA strain under photoautotrophic growth conditions cannot be explained by diminished DLA2 accumulation as its DLA2 level was 20 % increased compared to the DLA2-HA strain. The K197R-HA strain showed a wild-type like accumulation of DLA2. This indicates that neither in the strain K197Q-HA nor in K197R-HA a reduced DLA2 abundance is responsible for the detected growth phenotype.

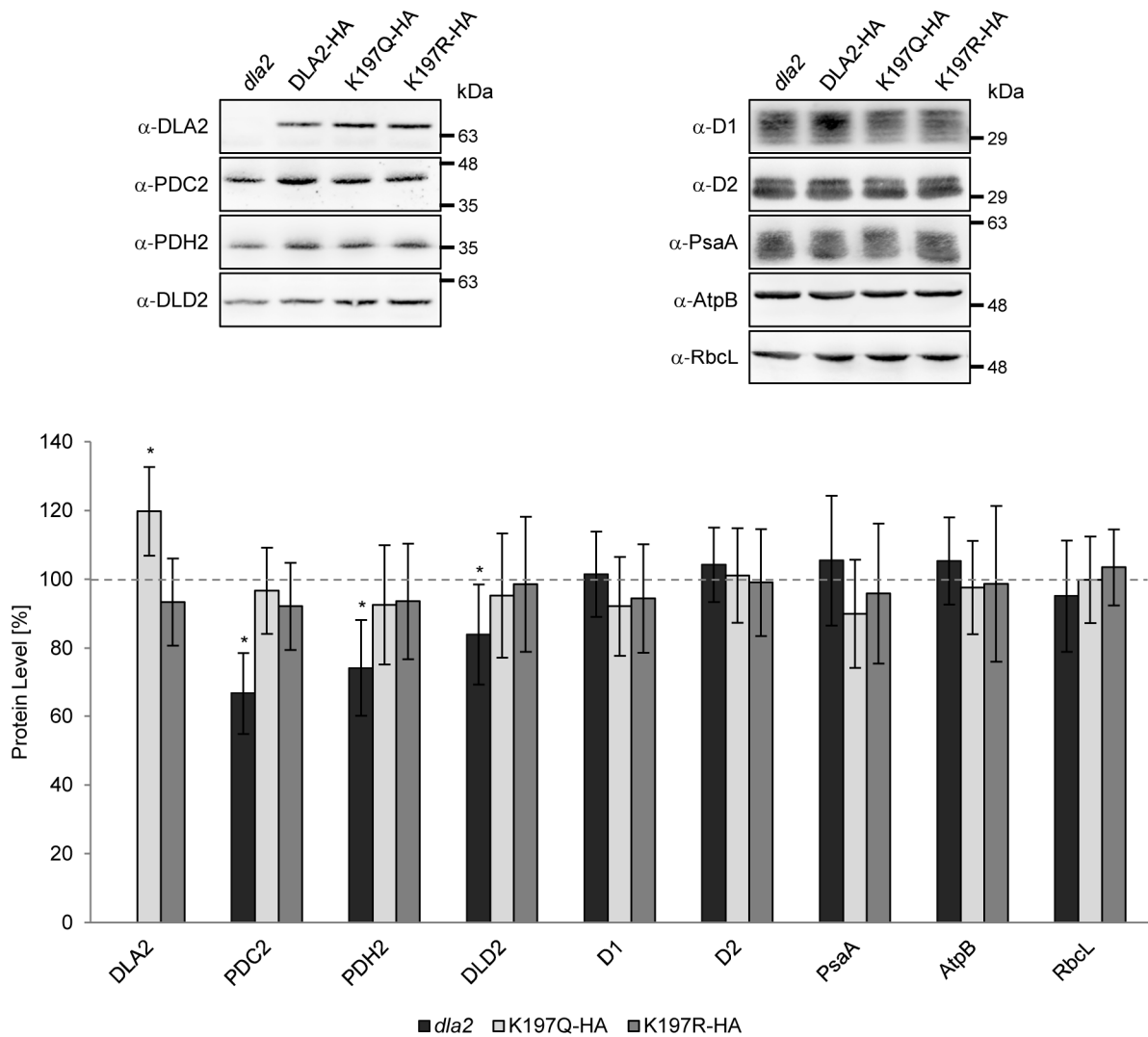


**Figure 22: Western blot analysis of the accumulation of cpPDC subunits and various photosynthetic proteins in the DLA2 acetylation mutants.**

15  $\mu$ g of total cell lysates of each strain were separated via SDS-PAGE and objected to immunoblotting (top). Protein signals of at least five independent experiments were quantified using ImageJ. The signal of the DLA2-HA strain was set to 100 % and the mean and standard deviation of the *dla2* knock out mutant and the two DLA2 acetylation mutants were calculated and shown in the bottom diagram. An asterisk indicates that the mean protein accumulation is significantly different from the mean accumulation of the respective protein in the DLA2-HA strain determined by a one-sample *t*-test ( $p < 0.05$ ).

When analyzing the accumulation of the other cpPDC subunits in the *dla2* knock out mutant, a significant decrease of the three remaining cpPDC subunits, PDC2 (E1 $\alpha$ ), PDH2 (E1 $\beta$ ) and DLD2 (E3), was detected. This decrease was stronger for the E1 subunits, and especially PDC2, than for DLD2. This might be due to lower stability of the unassembled E1 subunits. However, the observed decrease is most likely caused by the lack of DLA2 as all complemented strains (DLA2-HA, K197Q-HA and K197R-HA) showed a restored accumulation of the cpPDC subunits. This is supported by Kleinknecht (2018) reporting that the *iDLA2* line generated by Bohne et al. (2013) had lower accumulation of the other cpPDC subunits as well. The abundance of D2, PsaA, AtpB, RbcL and even D1 was not significantly affected in any of the analyzed lines.

To analyze the acetylation-dependent growth phenotype in more detail, additional DLA2 acetylation lines were generated in accordance with the recombinant DLA2 mutant versions used for MST analysis (compare Figure 16). Therefore, the *dla2* knock out mutant was complemented with a DLA2 version mimicking an acetylation at lysine 193 (K193Q-HA) and with a DLA2 version mimicking an acetylation at lysine 200 (K200Q-HA). The complementation with the versions containing an arginine residue at these positions was not carried out as our acetylome study revealed that these lysine residues are not acetylated *in vivo*.

Similar to the K197Q-HA strain, growth analysis of the K193Q-HA line showed a slightly decreased photoautotrophic growth while the mixotrophic growth was wild-type-like (Table 10). The doubling time of the K200Q-HA strain was not significantly different from the reference strain regarding both growth conditions.

**Table 10: Doubling times of the K193Q-HA and K200Q-HA acetylation strains.**

Values are means from at least 3 biological replicates. An asterisk indicates that a mean is significantly different from the mean of the DLA2-HA strain determined by a two-sample *t*-test ( $p < 0.05$ ).

| strain   | mixotroph [h] | photoautotroph [h] |
|----------|---------------|--------------------|
| DLA2-HA  | 9.5 $\pm$ 0.3 | 38.8 $\pm$ 4.9     |
| K193Q-HA | 9.3 $\pm$ 0.3 | 44.2 $\pm$ 5.4 *   |
| K200Q-HA | 9.7 $\pm$ 0.3 | 35.6 $\pm$ 4.3     |

In line with the results from K197 acetylation strains, complementation of the *dla2* knock out mutant with K193Q-HA and K200Q-HA versions could restore the accumulation of the cpPDC subunits to wild-type levels (Figure 23). With K193Q-HA accumulating wild-type levels of DLA2 and K200Q-HA even accumulating about 130 % of the DLA2 levels detected

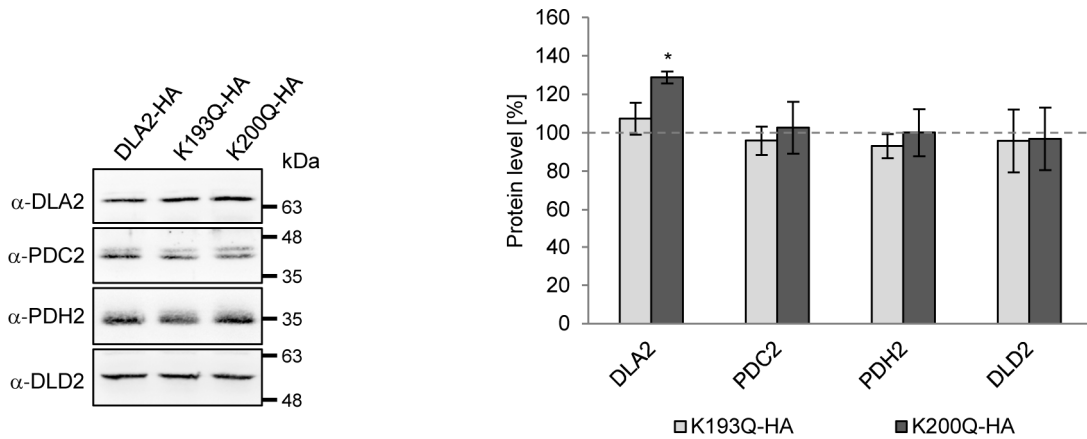


**Figure 23: Western blot analysis of the accumulation of the cpPDC subunits in K193Q-HA and K200Q-HA acetylation strains.**

15  $\mu$ g of total cell lysates were separated via SDS-PAGE and objected to immunoblotting. Protein signals of at least three independent experiments were quantified and shown on the right. The signal of the DLA2-HA strain was set to 100 % and is depicted as a grey dotted line. Mean and standard deviation of the two DLA2 acetylation mutants are shown. An asterisk indicates that the mean protein accumulation is significantly different from the mean accumulation of the respective protein in the DLA2-HA strain determined by a one-sample *t*-test ( $p < 0.05$ ).

in the DLA2-HA strain, any growth phenotype seen for the acetylation mutants was not the result of a decreased accumulation of DLA2 or any other cpPDC subunit.

#### III.4.2. The acetylation state of K197 influences cpPDC activity

The acetylation-dependent growth phenotype of three of the DLA2 acetylation mutants (compare Tables 9 and 10) is most likely connected to one of the two DLA2 functions, binding of the *psbA* mRNA or the catalytic function as part of the cpPDC. As the growth phenotype was restricted to photoautotrophic conditions where the cpPDC function is essential and no modified RNA-binding affinity was detected for the K197Q and K197R mutations *in vitro*, it was rather likely that differential acetylation might influence cpPDC activity, i.e. complex assembly and/or stability. Therefore, *in vitro* PDC activity assays were performed using soluble protein lysates of the various strains and photometrical detection of the conversion from  $\text{NAD}^+$  to NADH (Figure 24). As there is also a mitochondrial PDC and other enzymes converting  $\text{NAD}^+$ , buffer conditions promoting cpPDC activity were used and the residual cpPDC activity in the *dla2* mutant was defined as background and subtracted from the cpPDC activity measured for the other strains. Interestingly, the cpPDC activity in the K193Q-HA and the K197Q-HA strain was dramatically reduced. While K197Q-HA showed only 50 % of cpPDC activity compared to the DLA2-HA reference strain, the cpPDC activity of the K193Q-HA strain was even reduced to about 30 % which might cause their retarded growth under photoautotrophic conditions. In contrast, the K197R exhibits an increased cpPDC activity to 140 %. In line with

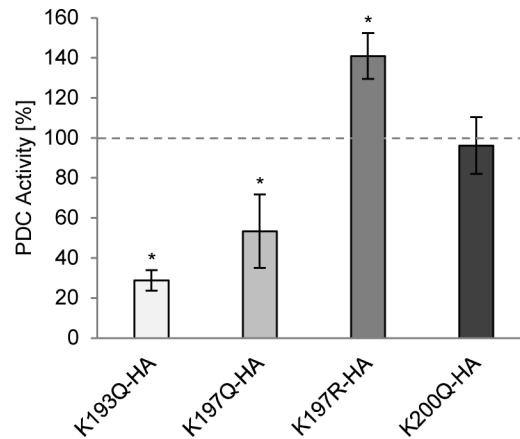


**Figure 24: Acetylation state of lysine residues within the E3BD influences cpPDC activity.**

cpPDC activity tests were basically performed as described in the Material & Methods section. The cpPDC activity measured in the DLA2-HA strain was set to 100 % and is depicted as a grey dotted line. Mean values and standard deviations from at least three independent experiments are shown. An asterisk indicates that the mean cpPDC activity of this strain is significantly different from the mean cpPDC activity of the DLA2-HA strain determined by a one-sample *t*-test ( $p < 0.05$ ).

the wild-type-like growth behavior, the K200Q-HA strain had no altered cpPDC activity compared to the DLA2-HA strain (compare Table 10).

Taken together, this shows that the simulation of constitutive acetylation at K193 or K197 leads to a drastic reduction of cpPDC activity while the same had no effect at K200. The increase of cpPDC activity in the constitutively non-acetylated K197R-HA strain suggests that the native DLA2 pool in the DLA2-HA line is partially acetylated as its cpPDC activity is intermediate between the activity observed in the K197R-HA and the K197Q-HA line.

### III.4.3. cpPDC complex stability is influenced by acetylation of K197 within the E3BD

cpPDC activity assays showed that simulated acetylation at K193 and K197 decreases cpPDC activity, but the molecular mechanism is still unclear. As both lysine residues are located within the E3BD, which is important for binding of the other cpPDC subunits, it is likely that acetylation affects complex assembly. Thus, co-immunoprecipitation experiments were performed, precipitating DLA2 with an antibody binding to the C-terminally fused HA-tag and determining the amount of co-precipitated PDC2, PDH2 and DLD2 protein in the various lines (Figure 25). As in contrast to the DLA2 containing RNP complex, the cpPDC is expected to mainly reside in the chloroplast stroma, soluble extracts were used for co-immunoprecipitation. Interestingly, under mixotrophic conditions K197Q-HA co-precipitated dramatically less cpPDC subunits compared to the DLA2-HA reference strain (Figure 25a). While the amount of DLD2 and PDH2 were reduced to 60 % and 40 % respectively, co-precipitated PDC2 was even reduced to 20 %. This indicates that mimicked acetylation of K197

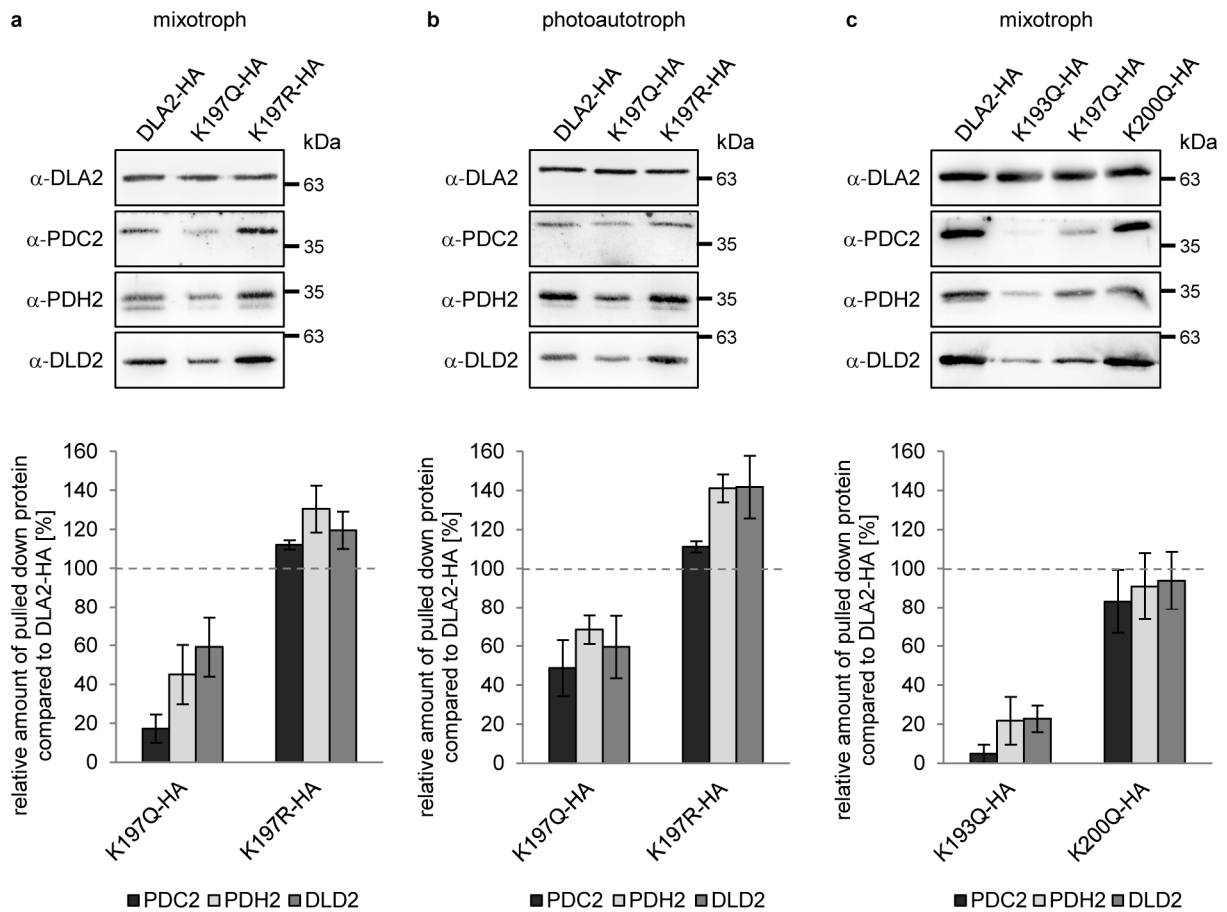


**Figure 25: Acetylation state of lysine residues within the E3BD influences complex stability.**

Co-immunoprecipitation with soluble extracts of the DLA2-HA and various acetylation strains using bead-coupled HA antibodies. The obtained pellets were separated via SDS-PAGE and the accumulation of the PDC subunits was detected using Western blot analysis. The protein signals of three independent experiments were quantified and the respective signal in the DLA2-HA strain was set to 100 %. Mean and standard deviation of the different protein signals in the acetylation mutants was calculated and depicted in the bottom diagrams. **a**, K197 acetylation mutants grown under mixotrophic conditions. **b**, K197 acetylation mutants grown under photoautotrophic conditions. **c**, K193, K197 and K200 acetylation mutants grown under mixotrophic conditions. For better comparability K197Q-HA is shown here again on Western blot level. For quantification of K197Q-HA, see **a**. An asterisk indicates that the mean co-precipitation of the protein in this strain is significantly different from the mean co-precipitation of the respective protein in the DLA2-HA strain determined by a one-sample *t*-test ( $p < 0.05$ ).

decreases cpPDC stability immensely. In contrast, missing acetylation in the K197R-HA line led to significantly increased co-precipitation of all subunits, indicating an increased complex stability *in vivo*. Under photoautotrophic growth conditions, the results were similar to the ones obtained for mixotrophic conditions (Figure 25b). Dramatically less cpPDC subunits were co-precipitated in the K197Q-HA strain while significantly more of these subunits were co-precipitated in the K197R-HA strain. This suggests that there is still some acetylation at K197 in the DLA2-HA strain under photoautotrophic conditions, although it is about 4 times less than under mixotrophic conditions according to our acetylome study. Analysis of the K193Q-HA and K200Q-HA lines under mixotrophic conditions revealed that acetylation at K193 results in a drastically reduced complex stability (Figure 25c). When immunoprecipitating DLA2 in the

K193Q-HA line, only 5 % of PDC2, and 20 % of PDH2 and DLD2 respectively, could be co-precipitated compared to the DLA2-HA line. In contrast, simulated acetylation at K200 in the K200Q-HA line led to no significant differences of co-precipitated cpPDC subunits. Interestingly, complex stability was even more reduced upon simulated acetylation at K193 than at K197 (compare K197Q-HA, Figure 25a). These findings explain the results obtained from the cpPDC activity assay. The reduced cpPDC activity in the K193Q-HA and K197Q-HA strains is a result of lower complex stability and thereby less fully assembled complex in these lines caused by the mimicked acetylation in the E3BD. On the other hand, the non-acetylated arginine substitution in the K197R-HA strain leads to higher complex stability compared to the DLA2-HA line resulting in higher cpPDC activity.

Taken together, the acetylation-dependent complex assembly/stability as simulated in the K193Q-HA, K197Q-HA and K197R-HA strains alters cpPDC activity which in turn contributes to the observed growth phenotype (compare Figure 24 and Tables 9, 10).

#### III.4.4. Lysine acetylation leads to membrane attachment of DLA2

Acetylation at K197 detected *in vivo* resulted in less complex stability and by this a larger pool of DLA2 not assembled in the cpPDC (compare Figure 25). Next, it was elucidated if this increased availability of unbound DLA2 leads automatically to increased amounts of DLA2 involved in RNA-binding and RNP complex formation at thylakoid membranes. Thus, the amount of DLA2 within the membrane fraction of the DLA2-HA, K197Q-HA and K197R-HA strain under mixotrophic and photoautotrophic growth conditions was determined. First, it was analyzed if the increased amount of naturally occurring acetylation at K197 under mixotrophic conditions results in an increased amount of DLA2-HA at membranes in the DLA2-HA line (Figure 26a).

Indeed, there was a 50 % increase of membrane bound DLA2 under mixotrophic compared to photoautotrophic conditions when normalizing the respective DLA2 signal to the AtpB signal in the membrane fraction. As the mass spectrometry data from the acetylome analysis did not show elevated levels of DLA2 under mixotrophic conditions, the increased accumulation at membrane fractions is probably due to a shift of stromal DLA2 to membranes. However, a concomitant decrease of DLA2 in soluble extracts could not be detected (Supplemental Figure S6). As the vast majority of DLA2 is assembled in the stromal cpPDC, the substantial changes observed in the membrane fraction might just lead to relatively minor changes of the DLA2 accumulation in soluble extracts.

Analysis of the DLA2 acetylation strains revealed that mimicking complete acetylation of the DLA2 pool in the K197Q-HA strain as well as non-acetylation in the K197R-HA strain

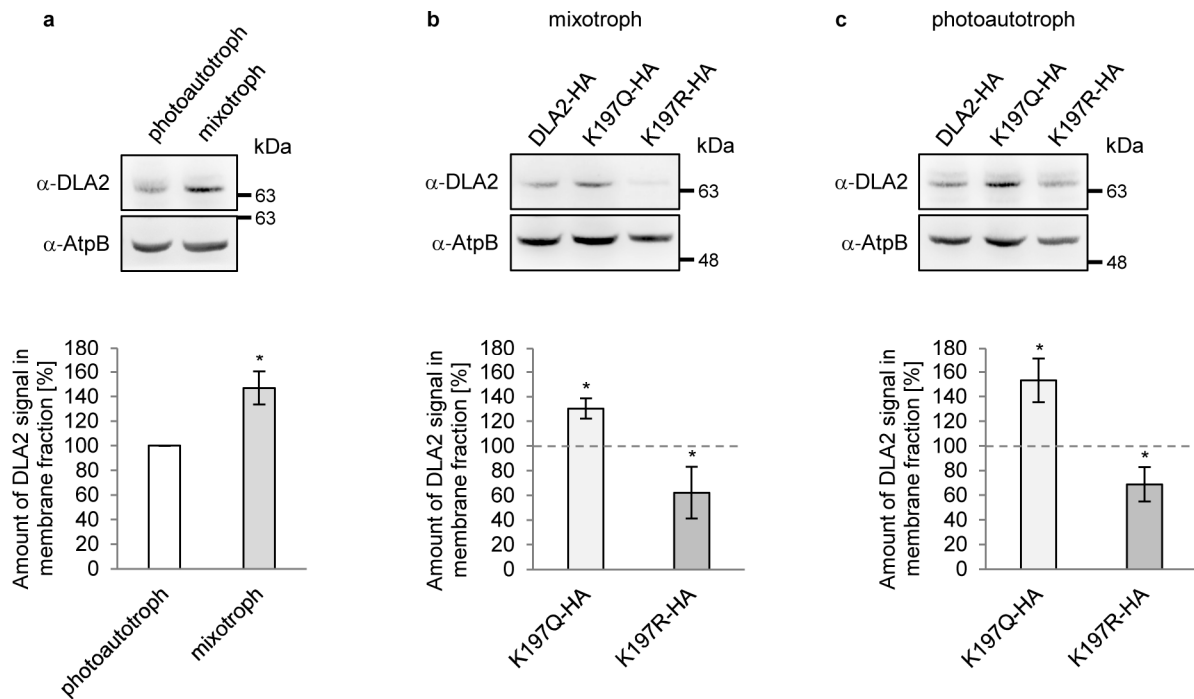


**Figure 26: Acetylation of K197 influences membrane localization of DLA2.**

40  $\mu$ g of Triton X-100 - solubilized membranes were separated via SDS-PAGE and subjected to Western blot analysis to obtain the DLA2 accumulation which was afterwards normalized to the AtpB accumulation in the membrane fraction. **a**, DLA2-HA line under photoautotrophic or mixotrophic conditions. The accumulation under photoautotrophic conditions was set to 100 %. **b**, DLA2-HA line and the K197 acetylation mutants under photoautotrophic conditions. **c**, DLA2-HA line and the K197 acetylation mutants under mixotrophic conditions. **b**, **c**, the DLA2 membrane accumulation in the DLA2-HA strain was set to 100 %. All means and standard deviations are calculated from at least 3 independent experiments. An asterisk indicates that the mean DLA2 / AtpB ratio is significantly different from that (**a**) under photoautotrophic conditions or (**b+c**) from that in the DLA2-HA strain determined by a one-sample *t*-test ( $p < 0.05$ ).

could influence the membrane attachment of DLA2 under both growth conditions tested (Figure 26b, c). Under mixotrophic conditions, simulated acetylation in the K197Q-HA line lead to an increased amount of membrane-bound DLA2 to 130 % while the amount in the K197R-HA line was decreased to about 60 % compared to the DLA2-HA line (Figure 26b). Under photoautotrophic conditions, the amount of membrane-bound DLA2 in the K197Q-HA line was even increased to about 160 % compared to the DLA2-HA line (Figure 26c). This larger effect of the acetylation in the K197Q-HA line might reflect the lower amount of membrane-bound DLA2 in the DLA2-HA reference strain under photoautotrophic conditions (compare DLA2-HA, Figure 26a).

Nevertheless, no acetylation in the K197R-HA strain resulted in a decrease of membrane-bound DLA2 to 70 % under photoautotrophic conditions compared to the DLA2-HA strain (Figure 26c). These data indicate that the acetylation-dependent increase of the pool of unbound DLA2 leads directly to an increase in membrane attachment of DLA2 linked to RNP complex formation. The presence of a residual portion of membrane-bound

DLA2 protein in the DLA2-HA strain under photoautotrophic conditions suggests that there is RNP complex formation and/or assembled cpPDC at membranes. The latter is supported by Bohne et al. (2013) who found cpPDC activity in samples of crude thylakoids. However, the reduction of membrane-bound DLA2 together with increased cpPDC stability in the K197R-HA strain compared to the DLA2-HA strain under photoautotrophic conditions, suggests that there is RNP complex formation at thylakoid membranes in the DLA2-HA strain even in the absence of acetate (Figure 26c).

### III.4.5. K197 acetylation results in an increased RNP complex formation *in vivo*

To elucidate if the distinct membrane attachment of DLA2 in the acetylation lines is reflected by a different abundance of the RNP complex, the RNA association of DLA2 was analyzed *in vivo* by gel filtration experiments (Figure 27). As described by Bohne et al. (2013), thylakoid membranes were extracted and solubilized for isolation of the DLA2 containing RNP complex. Samples were split in half and either treated with RNase or not before proteins were

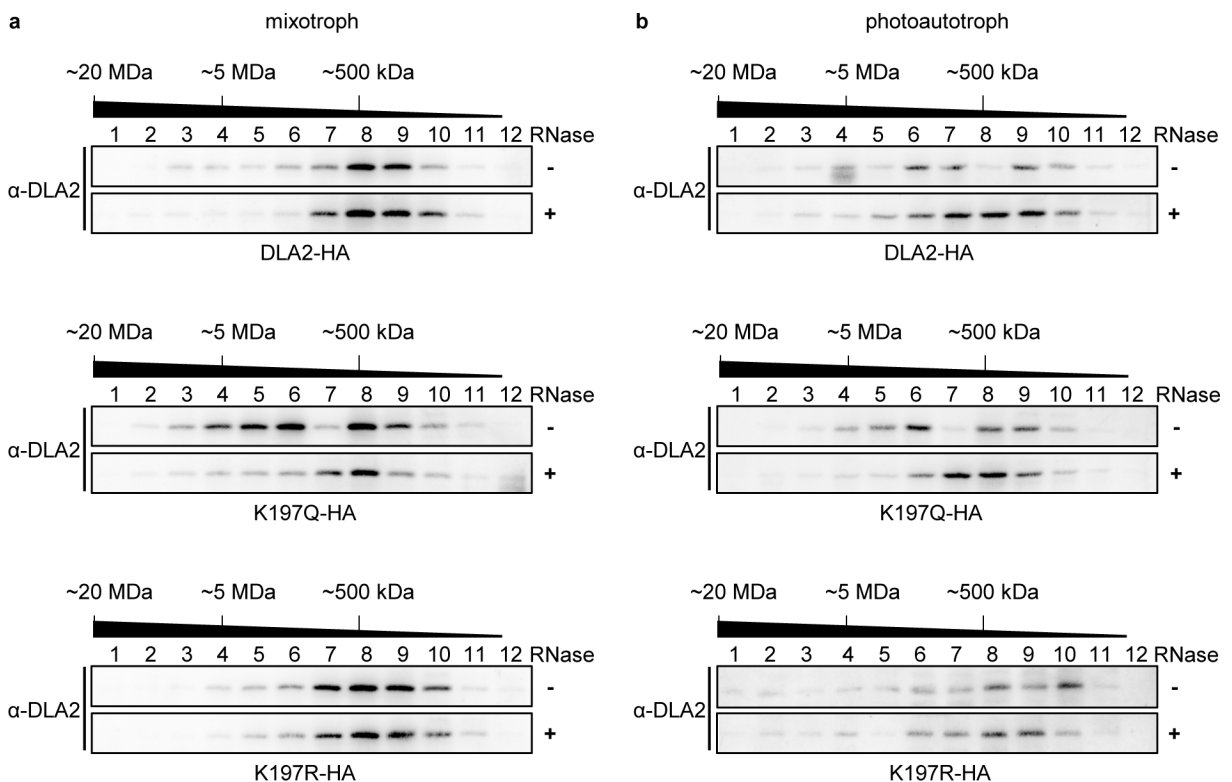


**Figure 27: Acetylation state of K197 influences RNP complex formation.**

Size exclusion chromatography of DLA2 in thylakoid fractions of various strains under (a) mixotrophic and (b) photoautotrophic growth conditions. Strains as indicated below the blots. Triton X-100-solubilized thylakoids from the indicated strains were either treated with (+) RNase or not (-) before loading on the column. Fractions were collected and 1/10th of each fraction was loaded on an SDS gel. cpPDC subunits were detected by immunoblotting using antibodies indicated on the left. Blots shown are representative for at least three independent experiments.

separated by size using size exclusion chromatography. The abundance of the RNP complex was estimated by the amount of DLA2 signal shifting to smaller sizes upon RNA digestion.

When analyzing the RNase-dependent shift in the DLA2-HA strain under mixotrophic growth conditions, only a small shift of the DLA2 signal could be detected, indicated by a slightly stronger signal in fractions 3-6 without RNase treatment (Figure 27a). This shift could not be detected under photoautotrophic conditions, indicating some RNP complex formation under mixotrophic but not under photoautotrophic conditions (Figure 27b). Analysis of the K197Q-HA strain showed a strong shift of the DLA2 signal upon RNase treatment under mixotrophic conditions (Figure 27a). Although total protein amount was higher for the untreated sample, the high DLA2 signal intensities located in fractions 4 to 6 were dramatically decreased upon RNase treatment. Even under photoautotrophic conditions a clear shift of the DLA2 signal intensities from fraction 4 to 6 in the untreated sample to fractions 7 to 9 in the RNase treated sample could be observed (Figure 27b). An RNase-dependent shift of the DLA2 signal in the K197R-HA strain could not be detected neither under mixotrophic nor under photoautotrophic conditions. This suggests that the amount of RNP complex in this line under both growth conditions is too low for detection using this method. The amount of RNase-sensitive complexes detected in all the strains analyzed, especially in the DLA2-HA strain under mixotrophic conditions, seemed to be rather low when comparing it with similar experiments performed by Bohne et al. (2013) or Kleinknecht (2018). This might be due to complex disassembly or degradation during thylakoid membrane isolation or solubilization. Furthermore, an RNP complex destabilizing effect due to the C-terminal triple HA-tag fused to the DLA2 protein in these strains cannot be excluded, especially in regard of the importance of the very C-terminal part of DLA2 on RNA-binding affinity detected in the MST experiments (compare  $\Delta$ Cat 462, Figure 11). Nevertheless, effects of the simulated acetylation states of K197 on RNP complex formation observed in the K197Q-HA and K197R-HA lines are in accordance with our previous data (compare Figures 25, 26). This suggests that acetylation at K197 leads to disassembly of the cpPDC and release of DLA2 which is promoting formation of a DLA2-containing RNP complex attached to thylakoid membranes.

To confirm the hypothesis that the acetylation state at K197 is directly linked to formation of the RNP complex, Förster resonance energy transfer (FRET) microscopy was performed to investigate the acetylation-dependent interaction of DLA2 and *psbA* mRNA *in situ* (Figure 28). As cells are chemically fixed during initial steps of sample preparation, this should inhibit disassembly of RNP complexes during preparation leading to a better visualization of RNP abundance. After fixation, *psbA* mRNA was visualized by fluorescence

*in situ* hybridization (FISH) using chromophore-coupled oligonucleotides and DLA2 was visualized by immunofluorescence using an anti-HA antibody coupled to another chromophore

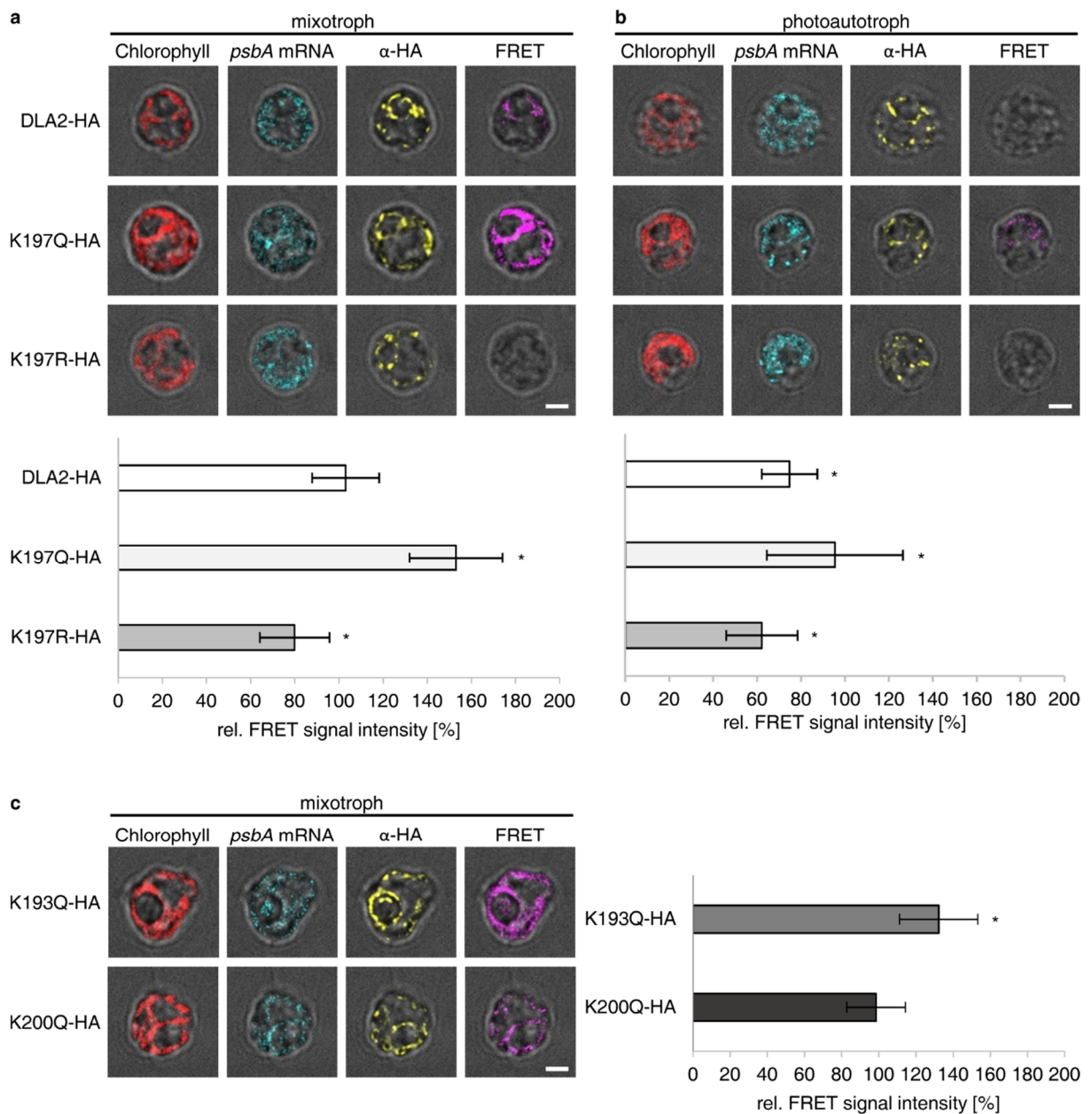


**Figure 28: Interaction of DLA2-HA and the *psbA* mRNA in various strains and growth conditions.**

Fluorescence microscopy pictures of the DLA2-HA strain, as well as the K197Q-HA and K197R-HA acetylation strains under (a) mixotrophic and (b) photoautotrophic conditions. c, Fluorescence microscopy pictures of the K193Q-HA and K200Q-HA acetylation strains under mixotrophic conditions. a-c, Chlorophyll autofluorescence (red), fluorescence *in situ* hybridization (FISH) of the *psbA* mRNA (cyan), immunofluorescence (IF) of the DLA2-HA protein (yellow) and Förster resonance energy transfer signals (FRET), visualizing DLA2-*psbA* interaction (purple), are depicted. Quantification was performed using ImageJ and the ratio of FRET signal / DLA2-HA signal was calculated. Mean value obtained for the DLA2-HA strain under mixotrophic conditions was set to 100 %. Mean values and standard deviations calculated from at least 10 cells are shown. An asterisk indicates that the mean FRET signal / DLA2-HA signal ratio of this strain is significantly different from the mean FRET signal / DLA2-HA signal ratio of the DLA2-HA strain under mixotrophic growth conditions determined by a two-sample *t*-test ( $p < 0.05$ ). Scale bars = 2  $\mu$ m. FRET microscopy was performed by Matthias Ostermeier (AG Nickelsen, LMU Munich). For microscopic pictures of additional cells of each strain, see Supplemental Figures S7 and S8.

as described by Uniacke et al. (2011). The chromophore label of the *psbA* mRNA was excited using a chromophore specific wavelength. When the two different chromophores are in close proximity ( $< 5$  nm), the emission energy of the chromophore labeling the *psbA* mRNA excites the chromophore labeling DLA2. If a fluorescence emitted by the second chromophore can be detected, the close physical proximity of DLA2 and *psbA* mRNA suggests their direct interaction within the RNP complex.

Interestingly, the results from the FRET microscopy were reflecting the results obtained by size exclusion chromatography (compare Fig. 27). Under mixotrophic conditions, an RNP complex formation in the DLA2-HA strain could be visualized (Figure 28a). The mimicking of a complete K197 acetylation in the K197Q-HA strain led to a massive increase of RNP complex formation while no acetylation in the K197R-HA strain revealed no detectable RNP complexes. Quantification of these signals showed that the signal intensity in the K197Q-HA line was 50 % increased while the intensity in the K197R-HA line was reduced to 80 % compared to the DLA2-HA line. Under photoautotrophic growth conditions, FRET signal intensity in the DLA2-HA line was decreased to 75 % compared to mixotrophic conditions (Figure 28b).

Constitutive acetylation in the K197Q-HA line led to a clear RNP complex formation even under photoautotrophic conditions and FRET signal intensity was similar to the one in the DLA2-HA line under mixotrophic conditions. Missing acetylation at K197 in the K197R-HA line under photoautotrophic growth conditions led to a decrease of FRET signal intensity to 60 % compared to the DLA2-HA line under mixotrophic conditions. This shows that there is still RNP complex formation in the K197R-HA line under mixotrophic conditions or in the DLA2-HA line under photoautotrophic conditions as the observed decrease of FRET signal intensity there was smaller. However, the abundance seems to be too low for detection via size exclusion analysis (compare Figure 27). Furthermore, the growth condition-dependent change of RNP complex abundance in the K197Q-HA and K197R-HA lines indicates that besides acetylation of DLA2 at K197 there are other mechanisms or factors involved promoting RNP formation under mixotrophic conditions, as K197 cannot be differentially acetylated in these lines.

Interestingly, the signal distribution seemed to be consistent through the strains and conditions. The *psbA* mRNA seemed to be dispersed all over the chloroplast as it is one of the most abundant transcripts while the DLA2 signal was rather distributed in a punctate pattern. Additionally, part of the DLA2 signal was always concentrated around the pyrenoid which is indicated by a circular structure lacking chlorophyll fluorescence within the chloroplast. As most of the DLA2 pool is thought to be assembled in the cpPDC in the DLA2-HA and

K197R-HA strain, this suggests that also a substantial portion of the cpPDC accumulates at the pyrenoid. This is supported by data from Zhan et al. (2018) identifying DLA2, PDH2 and DLD2 by quantitative mass spectrometry in pyrenoid enriched fractions suggesting that the cpPDC is partially attached to the pyrenoid. However, the FRET signal indicating DLA2-*psbA* mRNA interaction was also concentrated around the pyrenoid suggesting that substantial amounts of both the cpPDC and the RNP complex are located at the pyrenoid. Furthermore, the location of the FRET signal indicates that the RNP complex might be targeted to T-zones around the pyrenoid and is involved in D1 synthesis for *de novo* biogenesis of PSII. Intriguingly, the dramatic increase of FRET signal in the K197Q-HA strain revealed also substantial amounts at chloroplast lobes. This indicates that two factors might be limiting for attachment of functional RNP particles at T-zones around the pyrenoid in the K197Q-HA strain, accessible thylakoid membranes and/or an additional protein which is targeting the RNP complex to T-zones.

The K193Q-HA and the K200Q-HA strains were also analyzed under mixotrophic conditions regarding their RNA-binding *in situ* (Figure 28c). In line with the results from the other experiments, mimicking of acetylation at K200 in the K200Q-HA had no effect on RNA-binding resulting in a FRET signal similar to the one in the DLA2-HA reference strain. Intriguingly, the FRET signal intensity of the K193Q-HA strain was 30 % increased compared to the one in the DLA2-HA strain under these conditions. This probably reflects the decreased cpPDC complex stability in this line resulting in a large pool of unassembled DLA2 and a high potential for RNA-binding. Nevertheless, RNP complex abundance in the K193Q-HA line is still significantly lower than in the K197Q-HA line, probably caused by a decreased RNA-binding affinity upon acetylation at K193 which was detected in the MST analysis (compare Figure 16). This makes K197 the better switch for regulation of DLA2 functions.

Additionally, the *dla2* mutant was analyzed as a control for specificity of the DLA2 signal and the *FuD7* mutant, a *psbA* deletion mutant, for specificity of the *psbA* signal (Supplemental Figure S9). Both mutants did not show a respective signal proving that the DLA2 and *psbA* signals recorded for the DLA2-HA and the acetylation strains were specific for the respective molecule. To verify the binding and specificity of DLA2 to the *psbA* mRNA another abundant mRNA was labeled using oligonucleotides binding to the *psaA* mRNA in the DLA2-HA strain (Supplemental Figure S9). As no visible FRET signal was detected here, the FRET signal detected with oligonucleotides binding to the *psbA* mRNA in the various strains is due to actual binding of DLA2 to the *psbA* mRNA and not just because of abundance of the mRNA. Furthermore, it can be excluded that the *psaA* mRNA is part of the RNP complex involving DLA2 and the *psbA* mRNA suggesting a *psbA* specific complex formation.

Taken together, these data show that DLA2 forms an RNP complex with the *psbA* mRNA which is mainly located around the pyrenoid. Increased acetylation at K197 under mixotrophic growth conditions promotes the formation of this complex although there might be other factors facilitating the formation under these conditions.

### III.4.6. Knockout of *DLA2* results in a reduction of D1 synthesis for PSII *de novo* biogenesis

To test if the altered RNP complex abundance results in altered D1 synthesis rates, <sup>35</sup>S protein pulse labeling assays were performed (Figure 29). Quantification of the D1 signals and normalization on the ATPase signal showed that the constitutive acetylation state in the K197Q-HA and K197R-HA lines and the concomitant altered abundance of the RNP complex did not lead to significantly altered D1 synthesis rates compared to the DLA2-HA strain. The reduced RNP formation in the K197R-HA line might be sufficient to ensure proper D1 synthesis. On the other hand, the unaltered D1 synthesis rate in the K197Q-HA line might be the result of additional factors lacking in the increasingly formed DLA2-*psbA* complex. Nevertheless, the absence of DLA2 in the *dla2* knock out mutant led to a drastic reduction of D1 synthesis rates of about 40 %. The fact that this decreased synthesis rate did not result in

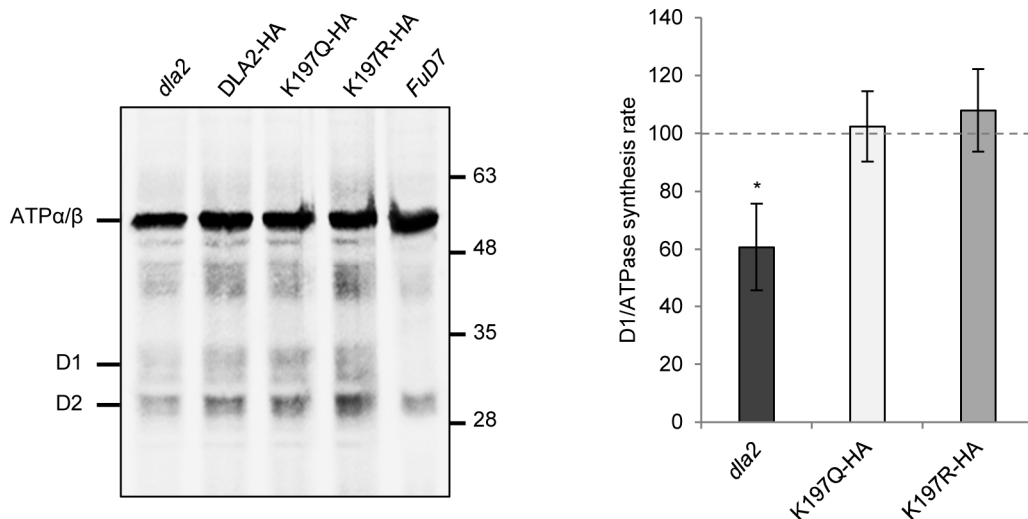


**Figure 29: D1 protein synthesis in the *dla2* knock out mutant and various complemented strains under mixotrophic growth conditions.**

Whole cell proteins were pulse-labeled with <sup>35</sup>S-sulphate prior to separation on an SDS-PAGE gel. Afterwards proteins were blotted onto a nitrocellulose membrane and analyzed by autoradiography. Quantification of the D1 signal was performed using ImageJ software and normalized to the AtpA/B signal. The values obtained for the DLA2-HA line were set to 100 % and is depicted as a dotted line (right panel). Mean and standard deviation from three independent experiments is shown. An asterisk indicates a significant difference ( $p < 0.05$ ) to the DLA2-HA line using a one-sample *t*-test. <sup>35</sup>S pulse-labeling experiments were performed by Jing Tsong Teh (AG Nickelsen, LMU Munich).

lower D1 accumulation might be explained by posttranslational stabilization effects counteracting the reduced synthesis rate.

As *psbA* translation occurs in two fundamentally different PSII assembly pathways, namely PSII repair and PSII *de novo* biogenesis, it was still unclear which pathway is affected by the loss of DLA2 and the concomitant reduced D1 synthesis in the *dla2* mutant. Hence, growth rate analysis under higher light intensities was performed to elucidate if a putative repair deficit in the *dla2* mutant might lead to a growth phenotype under high light intensities (Supplemental Table S6). Under the tested conditions (mixotrophic growth,  $100 \mu\text{E m}^{-2}\text{s}^{-1}$ ), no growth phenotype could be observed for the *dla2* mutant as well as for the DLA2 acetylation lines. To analyze PSII repair in the given lines in more detail, D1 accumulation was analyzed for 1.5 h after a shift of liquid cultures to high light intensities of about  $800 \mu\text{E m}^{-2}\text{s}^{-1}$  (Figure 30, left panel). None of the analyzed strains did show a decrease in D1 accumulation during the time course indicating intact D1 repair synthesis for replacement of photodamaged D1 in all lines. To exclude a stabilization defect of D1, the experiment was repeated in the presence of compounds inhibiting the plastidic protein synthesis and with that D1 repair (Figure 30, right panel). This led to a dramatic decrease of D1 accumulation within 1.5 h in all analyzed strains. Still, no differences between the strains could be detected suggesting that loss of DLA2 does not lead to decreased stability of D1. Together with the location of the DLA2-*psbA* complex signal mainly locating to the T-zones in the FRET microscopy, these results indicate that DLA2 is not involved in D1 synthesis for PSII repair but rather in D1 synthesis for PSII *de novo* biogenesis.

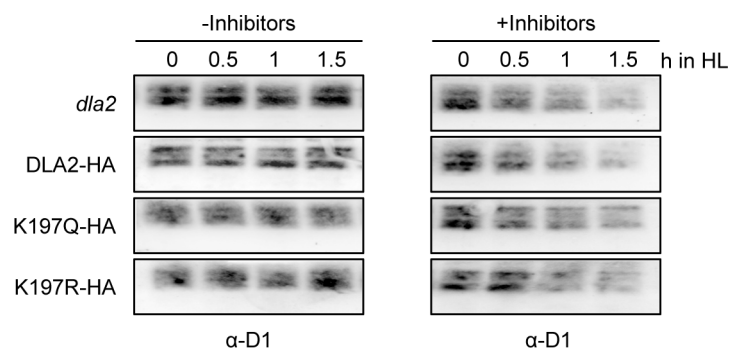


**Figure 30: Loss of DLA2 does not lead to a defect in D1 repair or stability.**

Duplicates of liquid cultures of the indicated strains were grown mixotrophically to a cell density of  $2 \times 10^6$  cells/mL at  $30 \mu\text{E m}^{-2}\text{s}^{-1}$  of light. Subsequently, one of the cultures was supplemented with lincomycin and chloramphenicol for inhibition of plastidic protein synthesis before both cultures were shifted to  $800 \mu\text{E m}^{-2}\text{s}^{-1}$  of light for 1.5 h. Samples were taken at the indicated time points. Whole cell proteins were separated via SDS-PAGE and D1 levels were analyzed by immunoblot.

To analyze this further, PSII degradation was induced by sulfur deprivation for 48 h in the *dla2* mutant, the DLA2-HA strain and the two DLA2 acetylation strains. Afterwards, the reaccumulation of D1 by *de novo* synthesis was analyzed through 24 h of sulfur repletion (Figure 31, Muranaka et al., 2016). Immunoblot analysis indicated slightly lower accumulation of D1 in the *dla2* mutant (Figure 31a). Quantification of the D1 signal and normalization on the signal intensity of the HSP70B loading control showed that there were no significant differences in D1 accumulation between the lines during 48 h of sulfur depletion (Figure 31b). In contrast to the complemented DLA2 lines which all showed an increasing D1 accumulation within 8 h of sulfur repletion, the *dla2* mutant still displayed decreasing D1 levels at this point. This indicates that the response to sulfur repletion in respect to D1 accumulation in the *dla2*

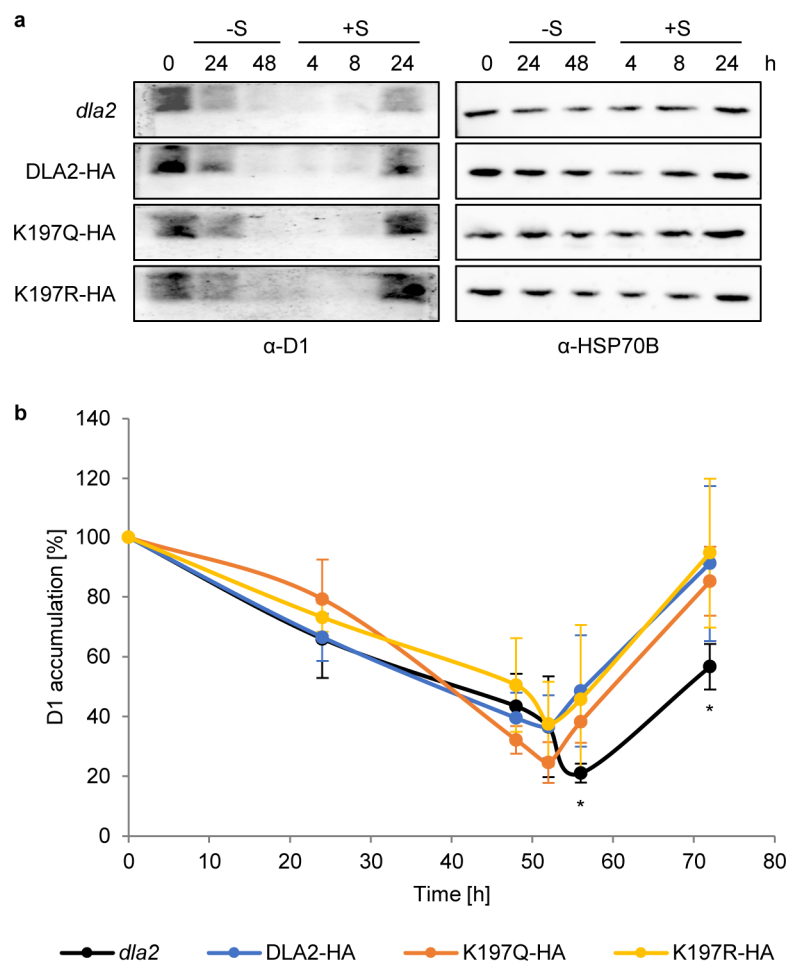


**Figure 31: Loss of DLA2 leads to slower accumulation of D1 for PSII *de novo* biogenesis.**

Liquid cultures of the indicated strains were grown in TAPS to a cell density of about  $2 \times 10^6$  cells/mL at constant light of about  $30 \mu\text{E m}^{-2}\text{s}^{-1}$ . Afterwards cells were shifted to medium lacking sulfur (-S). After 48 h under -S conditions, cultures were shifted back to TAPS medium containing sulfur (+S) for another 24 h. **a**, Whole cell proteins from samples taken at the indicated time points were separated via SDS-PAGE and D1 abundance was measured using immunoblot analysis and HSP70B as loading control. **b**, Quantification of the immunoblot signals was performed using ImageJ software and D1 signals were normalized to the respective HSP70B signals. The values obtained for the time point 0 were set to 100 %. All mean and standard deviation values are calculated from at least three independent experiments. An asterisk indicates a significant difference ( $p < 0.05$ ) of the D1 accumulation to that of the DLA2-HA line at the respective time point using a two-sample *t*-test.

knock out mutant might be delayed or impaired. This delayed response together with a slightly lower D1 accumulation rate during the subsequent 16 h led to a significant lower D1 accumulation in the *dla2* mutant of just about 55 % after 24 h of sulfur repletion compared to before the treatment. In contrast, the D1 accumulation of the DLA2-HA as well as of the two DLA2 acetylation lines was restored to 85 to 95 % after 24 h of sulfur repletion indicating that the loss of DLA2 leads to a decreased rate of D1 synthesis for PSII *de novo* biogenesis.

Taken together, these data clearly show that DLA2 is not involved in D1 stability or PSII repair. In fact, DLA2 is involved in D1 synthesis for PSII *de novo* biogenesis demonstrated by the sulfur depletion experiment. Moreover, the delayed D1 accumulation response upon sulfur repletion in the *dla2* mutant suggests that the delivery of *psbA* mRNA to T-zones mediated by DLA2 is a prerequisite to enable fast adaptation processes to these kinds of environmental transitions and DLA2 itself might be even involved in sensing them.

## IV. DISCUSSION

### IV.1. Mode of RNA-binding of DLA2

Bohne et al. (2013) showed that DLA2 possesses an intrinsic RNA-binding activity with a high affinity for the *psbA* mRNA. However, the precise binding mode and the regulation of the DLA2 functions remained elusive. Bioinformatical predictions identified two regions with high potential for RNA-binding within the mature DLA2 protein (compare Figure 9; Bohne et al., 2013). The first region covers almost the whole E3BD spanning from amino acid 188 – 224 while the second region is located at the C-terminus within the catalytic domain spanning from amino acid 450 – 457 (compare Figure 9). The comprehensive MST analysis of various DLA2 mutant proteins performed in course of this study indeed confirmed that both domains are important for binding of the *psbA* mRNA (Figure 11).

Deletion of the E3BD led to a decrease of RNA-binding affinity of more than 50 % of the wild-type affinity and to the loss of specificity to the A-stretch within the *psbA* 5' UTR (Figure 12). Moreover, deletion of the last 33 amino acids of the catalytic domain ( $\Delta$ Cat 462) resulted in a dramatic decrease of RNA-binding affinity. Nevertheless, the  $\Delta$ Cat 462 deletion protein could still confer recognition of the A-stretch as its substitution by a C-stretch resulted in an additional decrease of the RNA-binding affinity. The massive decrease of the RNA binding capacity of the  $\Delta$ Cat 462 protein was very unexpected as amino acid residues predicted in the catalytic domain to be probably important for RNA binding were not deleted in this mutant protein. However, the proximity of the deletion to this region or an altered protein folding might have an impact on its RNA binding capacity. It also needs to be considered that the efficient RNA binding by DLA2 may require a homooligomerization of the protein as the C-terminus of E2 subunits, which is partially deleted in  $\Delta$ Cat 462, is known to be responsible for self-assembly and organization of the cubic inner core of the PDC (Izard et al., 1999; Jung et al., 2002; Jung et al., 2002). However, increasing deletions of the catalytic domain resulted in a gradual decrease of RNA-binding affinity indicating that independently of higher order structural assemblies the catalytic domain itself is interacting with the *psbA* mRNA. Certainly, deletions can cause structural alterations within the protein which might affect RNA-binding as well. Nevertheless, analysis of protein structural models created *in silico* using the Phyre2 web tool indicate that larger rearrangements caused by the deletions concerning the catalytic domain are unlikely also because the domains are connected by large flexible linker regions (Supplemental Figure S10). However, the algorithms these tools use are usually biased as they mainly look for sequence similarity to known proteins. Therefore, a detailed analysis of possible

structural changes upon partial deletion of the DLA2 protein might be helpful using additional experiments like circular dichroism spectroscopy. Still, the results suggest that reduction of binding affinity observed upon partial deletion of the catalytic domain might be the consequence of missing RNA-binding activity of the deleted peptides. Interestingly, deletion of the third domain of DLA2, the lipoyl-binding domain, did not affect RNA-binding at all.

Additionally, MST analysis of the DLA2 proteins having substitutions mimicking acetylation at the three lysine residues within the E3BD showed that the K193 substitution to glutamine (K193Q), led to a drastic reduction of RNA-binding affinity (Figure 16). This reduction is most likely caused by a loss of the positive charge of the lysine residue as preservation of the positive charge by substitution of K193 to arginine had no effect on RNA-binding affinity compared to the wild-type DLA2 protein. This shows that the positive charge K193 within the E3BD is crucial for RNA-binding.

In summary, the results show that two domains are crucial for RNA-binding to the *psbA* mRNA, the E3BD and the catalytic domain (Figure 32). While the latter, and especially the last 33 amino acids, seem to have a decisive function for determination of overall RNA-binding capacity of DLA2, the E3BD is responsible for RNA recognition by binding to the A-stretch within the 5' UTR of the *psbA* mRNA. Interestingly, the lipoyl-binding domain is not involved in RNA-binding.

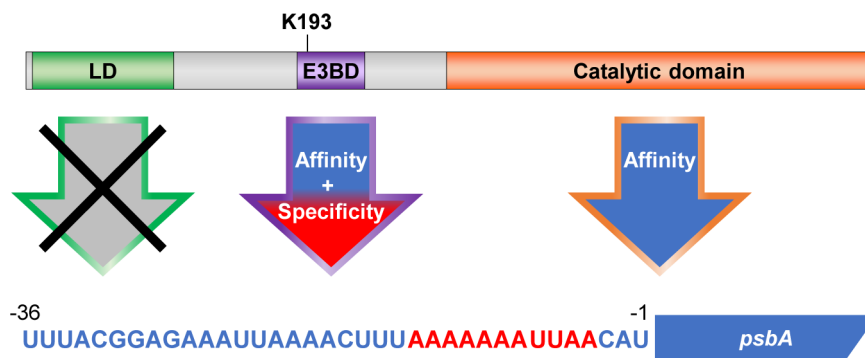


**Figure 32: *In vitro* binding mode of DLA2 to the 5' UTR of the *psbA* mRNA.**

Catalytic domain (orange) was shown to be crucial for affinity to the 5' UTR of the *psbA* mRNA. E3BD (purple) is responsible for affinity and specificity to a poly-A stretch (red) within the 5' UTR of the *psbA* mRNA. Positions relative to the start codon are marked above the sequence. Especially K193 within the E3BD seems to be crucial for the RNA-binding activity of this domain. In contrast, the lipoyl-binding domain (LD, green) has no influence on the RNA-binding affinity and/or specificity of DLA2.

## IV.2. DLA2 is essential for growth of *C. reinhardtii* under photoautotrophic growth conditions

As all experiments performed by Bohne et al. (2013) were conducted using *DLA2*-RNAi lines, the generation of a *dla2* knock out mutant was crucial for the characterization of DLA2's function in more detail. Hence, the recently established CRISPR/Cas9 system was used for the generation of a *dla2* mutant in collaboration with the group of Prof. Dr. Peter Hegemann. Loss of DLA2 led to an acetate requiring phenotype which allowed no growth in Minimal medium. This phenotype could be complemented by reintegration of the *DLA2* gene fused to a triple HA-tag confirming that the phenotype is DLA2-dependent and not caused by a second site mutation (Figure 19). That inhibition of growth under photoautotrophic conditions is a result of a lack of cpPDC activity is supported by data from Shtaida et al. (2014) who showed that downregulation of the *C. reinhardtii* E1 $\alpha$  subunit, PDC2, resulted in a significantly impaired growth under these conditions.

In line with this, acetate as external carbon source could complement the phenotype completely resulting in a wild-type-like growth under various temperature and light conditions in the presence of acetate (Table 8, Figure 20). This shows that inhibition of photoautotrophic growth is due to a lack of acetyl-CoA usually provided by the cpPDC. Under mixotrophic conditions, acetyl-CoA can be synthesized by two cpPDC-independent systems, the acetate synthetase (ACS) and the acetyl-kinase/phosphate acetyltransferase (ACK/PAT) system which both use acetate as substrate (Spalding, 2009; Yang et al., 2014).

To elucidate if the loss of DLA2, and with that cpPDC activity, leads to alterations regarding acetyl-CoA-driven fatty acid and lipid synthesis, liquid cultures were analyzed per mass spectrometry during a shift from heterotrophic to mixotrophic conditions. The general response to this shift was very similar in the wild type and the *dla2* mutant and was characterized by a massive decrease in storage lipids (TAG) which were previously reported to accumulate in the dark (Figure 21; Liu et al., 2011; Singh et al., 2014; Juergens et al., 2016). However, comparative analysis of the wild type and the *dla2* mutant revealed only slight differences for a few lipids, showing that the loss of DLA2 does not lead to altered fatty acid and lipid accumulation in the presence of acetate. This is supported by Shtaida et al. (2014) who showed that downregulation of *PDC2* in *C. reinhardtii* led to impaired TAG accumulation in photoautotrophic growth but is fully complemented in the presence of acetate.

Taken together, DLA2, and with that cpPDC activity, seems to be essential under photoautotrophic conditions but can be fully complemented by the addition of acetate.

### IV.3. Lysine acetylation is regulating the moonlighting function of DLA2

Analysis of acetylome data of various organisms indicated a general role of acetylation in the regulation of E2 subunits. Therefore, the role of lysine acetylation in the regulation of DLA2's functions was elucidated by analyzing the acetylome of *C. reinhardtii* under different growth conditions together with the group of Prof. Dr. Iris Finkemeier (König et al., manuscript in preparation). This led to the identification of a lysine residue (K197) which was significantly differentially acetylated under mixo- and heterotrophic conditions compared to photoautotrophic conditions and was predicted to have a high potential for RNA-binding (compare Figures 9, 13). Nevertheless, *in vitro* experiments indicated that amino acid substitutions that mimic acetylation at K197 do not influence the RNA-binding affinity of DLA2, suggesting that K197 is not crucial for *psbA*-binding (Figure 16).

#### IV.3.1. Acetylation of K197 leads to cpPDC disassembly

For analysis of acetylation effects on DLA2's function *in vivo*, several DLA2 acetylation mutants were created by complementation of the *dla2* mutant with DLA2 versions mimicking constitutive acetylation at K193, K197 and K200 (K193Q-HA, K197Q-HA and K200Q-HA, respectively) or constitutive deacetylation at K197 (K197R-HA).

Analysis of the DLA2 acetylation lines showed that all investigated DLA2 mutant versions could restore photoautotrophic growth, indicating restored cpPDC activity (Tables 9, 10). Unexpectedly, cpPDC activity was dramatically decreased in the K197Q-HA and K193Q-HA lines compared to the DLA2-HA line (Figure 24). In contrast, the cpPDC activity in the K197R-HA line was increased, indicating that a complete lack of acetylation at K197 can even increase stability of the cpPDC. Quantification of cpPDC subunit levels showed that neither changes in DLA2 accumulation nor accumulation of the other cpPDC subunits is responsible for altered cpPDC activity in the various lines (Figures 22, 23). Thus, decreased cpPDC activities are a result of lysine acetylation within the E3BD which is also reflected by decreased growth rates under photoautotrophic conditions. In agreement with this assumption, these effects can be negated by the addition of acetate. However, the growth rate differences under photoautotrophic conditions are rather small compared to the drastic changes in cpPDC activity indicating that other factors like CO<sub>2</sub> or light supply might limit growth under the tested conditions as well.

Co-immunoprecipitation experiments revealed that the altered cpPDC activity is a result of changes in complex stability due to the acetylation state of lysines K193 and K197 (Figure 25). Acetylation at each of the two lysine residues led to a massive reduction of co-

precipitated cpPDC subunits compared to the DLA2-HA strain suggesting decreased complex assembly or stability in these lines. While acetylation at K197 resulted in a decreased co-precipitation of cpPDC subunits of 50-80 %, acetylation of K193 even led to a reduction of up to 80-90 % compared to the DLA2-HA line. This shows that K197 and especially K193 are crucial for interaction with PDC2, PDH2 and DLD2. *In vitro* studies using a recombinant peptide of the E2 subunit from *E. coli* support this finding as charge-reverse substitution of the arginine residue corresponding to K193 in DLA2 (compare AceF in Figure 14) resulted in a dramatic reduction of binding affinity to the respective E1 and E3 proteins (Park et al., 2004). Moreover, mutations of the *Bacillus stearothermophilus* E2 subunit obliterating the positive charge of the arginine residues corresponding to K193 and K197 in DLA2, showed that in particular mutation of the former arginine residue led to a massive reduction of E3-binding while mutation of the latter position resulted in a smaller but still significant decrease (Jung et al., 2002).

In contrast to acetylation, the simulation of constitutive deacetylation at K197 (K197R-HA) resulted in an increased co-precipitation of cpPDC subunits suggesting increased complex stability and assembly compared to the DLA2-HA strain. The fact that the acetylation-dependent alterations in complex stability could be detected under photoautotrophic and mixotrophic conditions suggests that the acetylation state of K197 of the native DLA2 is intermediate, i.e. no complete acetylation or deacetylation of the DLA2 pool under both growth conditions. In line with the unaffected growth rate and cpPDC activity, acetylation at K200 did not lead to altered cpPDC assembly, showing that this residue is not involved in interaction with the other cpPDC subunits, as it was also not involved in RNA-binding. This might be explained by the position of the amino acids in the protein structural models created with the Phyre2 web tool (Supplemental Figures S10, S11). In this model, K193 and K197 are positioned at an exposed  $\alpha$ -helix which would enable interaction with E1 and E3, while K200 is located within a loop structure facing the protein's core.

Taken together, the data show that differentially acetylated lysine K197 regulates cpPDC complex formation and with that cpPDC activity. Constitutive acetylation of the complete DLA2 pool leads to drastically decreased cpPDC formation/assembly, cpPDC activity and a concomitantly reduction of growth rates under conditions where cpPDC activity is essential. Constitutive acetylation at K193 showed the same effects but decreases *psbA* mRNA-binding affinity at the same time. This shows that this lysine residue is crucial for both DLA2 functions which is reflected by a high conservation of the positive charge at this position among E2 subunits of various organisms (compare Figure 14). The fact that K197 is only critical for

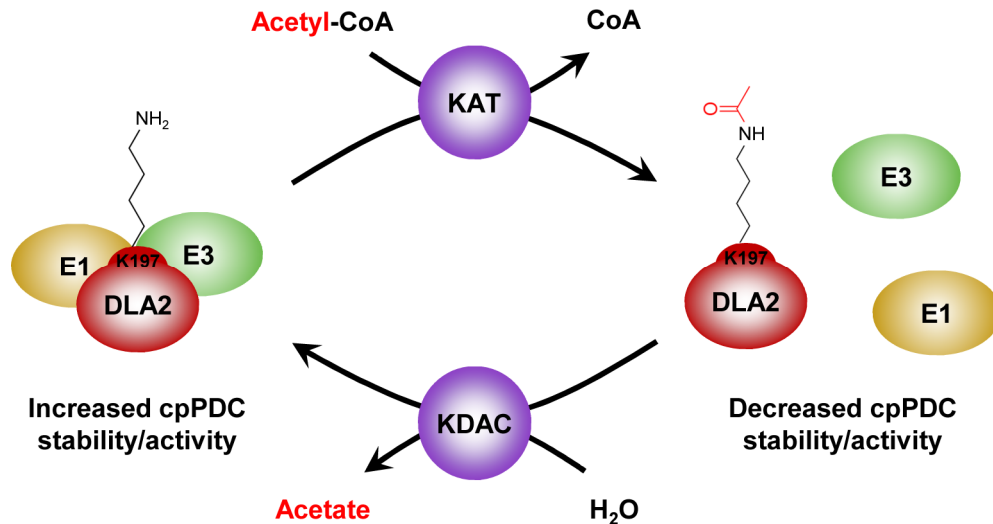


**Figure 33: Acetylation at K197 of DLA2 leads to increased disassembly of the cpPDC.**

Acetylation of the lysine residue at position 197 of DLA2 by a protein Lys-N<sup>ε</sup>-acetyltransferase (KAT) leads to decreased stability of the cpPDC and thereby to an increased disassembly of the complex. The acetyl moiety transferred to the  $\epsilon$ -amino group of the lysine side chain is depicted in red. Deacetylation of K197 is performed by a protein Lys-N<sup>ε</sup>-deacetylase (KDAC) resulting in an increased stability of the cpPDC.

binding to the other cpPDC subunits is making it the perfect target for shifting DLA2 function from cpPDC to RNP complex formation and vice versa.

#### IV.3.2. Acetylation of K197 leads to RNP complex formation

In contrast to the mainly soluble cpPDC, the RNP complex is membrane associated. Thus, membrane attachment of DLA2 in the K197 acetylation lines and the DLA2-HA reference strain was analyzed (Figure 26; Ossenbühl et al., 2002; Bohne et al., 2013). Increased membrane association of DLA2 in the K197Q-HA line compared to the DLA2-HA line under both growth conditions tested, suggested an increased RNP complex formation. On the other hand, membrane association was decreased in the K197R-HA line under both growth conditions. An increase in membrane association of DLA2 in the DLA2-HA line under mixotrophic conditions compared to photoautotrophic conditions could also be detected, suggesting that increased acetylation and with that reduced complex stability under mixotrophic conditions automatically leads to membrane association of DLA2. This might be caused by hydrophobic protein surfaces of DLA2 which are exposed upon disassembly of the cpPDC. Furthermore, other factors might be involved in the association of DLA2 to membranes. The fact that the increased membrane association is accompanied by increased RNP formation was supported by the results of the size exclusion chromatography (Figure 27). Constitutive acetylation of K197 clearly led to increased RNA association under mixotrophic and photoautotrophic conditions. In the constitutive deacetylated K197R-HA line, no RNA

association of DLA2 could be detected. However, there was only a slight size shift of DLA2 in the DLA2-HA line which was not as prominent as seen in Kleinknecht (2018). It cannot be excluded that this is due to a decreased RNP complex stability caused by the fusion of the triple HA-tag at the C-terminus of DLA2. This could lead to increased degradation of the complex during the time-consuming process of chloroplast isolation and sample preparation. As it was shown that the catalytic domain and especially the C-terminal part is crucial for *psbA* mRNA-binding, a negative effect of the HA-tag on RNA-binding seems likely. However, as all complemented lines possess an HA-tagged DLA2 version, the observed differences between the lines are most likely caused by the single remaining difference, i.e. the acetylation state of K197.

Final proof that the acetylation state of K197 influences RNP formation was given by the, to my knowledge, first report of Förster resonance energy transfer (FRET) microscopy analyzing protein-RNA interaction in *C. reinhardtii* (Figure 28). FRET analysis clearly showed that disassembly of the cpPDC upon acetylation of K197 indeed leads to a direct formation of the RNP complex involving DLA2 and the *psbA* mRNA. Constitutive acetylation at K197 resulted in a 50 % increase of the FRET signal while deacetylation led to a decrease to 80 % compared to the native state in the DLA2-HA line under mixotrophic conditions. Under photoautotrophic conditions, FRET signal intensity in the DLA2-HA line was decreased to 75 %. This is consistent with lower membrane association of DLA2 under these conditions showing that decreased acetylation of the native DLA2 leads to decreased RNP complex formation. Interestingly, FRET signal intensity under photoautotrophic conditions could be decreased even more by constitutive deacetylation in the K197R-HA line, indicating that there is low but distinct RNP formation in the native DLA2-HA line under photoautotrophic conditions, even though this could not be detected in the SEC analysis. This would be in line with increased cpPDC stability in the K197R-HA line under these conditions compared to the DLA2-HA line (Figure 25b). Even though SEC analysis could also not detect an RNP complex formation in the K197R-HA line under mixotrophic conditions, FRET signal intensity suggests that there is also low but obvious DLA2-*psbA* association under these conditions. These low amounts might be sufficient for proper D1 synthesis in the presence of acetate. Furthermore, the distribution of the FRET signal accumulating around the pyrenoid was in line with the fluorescence microscopy data from Bohne et al. (2013) as they saw a maximal colocalization of the *psbA* mRNA and the DLA2 signal around the pyrenoid.

The analysis of the FRET signal of the additional acetylation lines K193Q-HA and K200Q-HA supported the results of the previous experiments (Figure 28c). While mimicking

acetylation at K200 led to a FRET signal similar to that of the DLA2-HA strain, simulated acetylation at K193 resulted in increased RNP complex formation. Nevertheless, complex formation was lower in the K193Q-HA line compared to the K197Q-HA strain, although complex assembly was reduced resulting in an increased pool of free DLA2 and a high potential for *psbA* mRNA-binding. This could be caused by the negative effect of acetylation of K193 on RNA-binding affinity detected in the MST experiments (Figure 16). Furthermore, bromodomain proteins might specifically recognize acetylation at K197 and facilitate RNA binding and RNP complex formation (compare chapter I.6).

Increased RNP complex formation in acetylation lines in the presence of acetate suggests that there are additional factors or mechanisms facilitating cpPDC complex disassembly and/or RNP complex formation under mixotrophic conditions. A potential mechanism could involve differential acetylation at the other cpPDC subunits to facilitate disassembly of the complex under mixotrophic conditions. Analysis of several published acetylome studies revealed that all PDC subunits identified in these organisms were acetylated *in vivo* (Finkemeier et al., 2011; Henriksen et al., 2012; Kim et al., 2013; Zhang et al., 2013; König et al., 2014; Liu et al., 2014; Smith-Hammond et al., 2014; Smith-Hammond et al., 2014; Mo et al., 2015; Yan et al., 2020). Analysis of the *C. reinhardtii* acetylome data revealed no acetylation site for PDC2 or PDH2 while DLD2 was found to be acetylated although the identified acetylation site, K419 (according to the Cre01.g016514 sequence obtained from Phytozome v5.5), did not seem to be differentially acetylated under varying growth conditions. Nevertheless, K419 is located within the C-terminal dimerization domain and homodimer formation of E3 subunits was shown to be important for E3 function and E2 binding. This makes K419 a potential candidate for regulation of DLD2 function and affinity to DLA2 (Brautigam et al., 2005; Chandrasekhar et al., 2013; Patel et al., 2014).

However, additional regulation might also occur on the level of RNP complex formation. As MST experiments showed that the catalytic domain is crucial for RNA binding, the two identified acetylation sites here give rise for a potential regulation of RNA-binding affinity via reversible lysine acetylation within the catalytic domain. The detected acetylation pattern for K315 and K394 of DLA2 support this hypothesis even though the mean values were not significant. A decrease of acetylation specifically under mixotrophic growth conditions might lead to an increased RNA-binding affinity due to the positive charges of the deacetylated lysine residues. A more detailed analysis of these acetylation sites might lead to new insights regarding their role in RNA-binding. Moreover, experiments performed by Bohne et al. (2013) suggest that RNP complex formation is also depending on light indicating that there is also a

light-dependent regulation. This could involve phosphorylation as phosphorylation at E1 alpha is known to regulate PDC activity in humans (Korotchkina and Patel, 2001; Kato et al., 2008). Indeed, DLA2 was identified in three independent phosphoproteomic screens even leading to the identification of two phosphorylation sites (Wagner et al., 2006; Wang et al., 2014; Roustan and Weckwerth, 2018). Two serine residues, S44 and S290, were found to be phosphorylated under mixotrophic conditions. As S290 is located within the catalytic domain, phosphorylation at this site might influence RNA-binding. So far, all phosphoproteomic screens in *C. reinhardtii* were performed under mixotrophic growth conditions, thus additional data under varying growth conditions are needed to elucidate the role of this phosphorylation site in regulation of DLA2's function. Moreover, isoelectric focusing experiments might lead to new insights about the phosphorylation state of DLA2 under different growth conditions.

The enormous size of the RNP complex in the MDa range does not exclude that DLA2 forms homooligomeric structures which might be necessary for RNA-binding but also that other proteins are part of this complex thereby facilitating complex formation in an acetate and/or light-dependent manner. Interestingly, SEC analysis of chloroplast proteins from *A. thaliana* revealed that LTA2, the E2 subunit of its cpPDC, is part of a second HMW complex distinct from the cpPDC function (Olinares et al., 2010). The fraction characterized by this second HMW contained also several ribosomal and RNA-binding proteins, e.g. CSP41B, which was shown to interact with a number of mRNAs corresponding to photosynthetic proteins (Qi et al., 2011; Chevalier et al., 2015). The CSP41B homologue in *C. reinhardtii* was shown to associate with plastid 70S ribosomes making it a possible candidate being involved in the RNP complex including DLA2 and the *psbA* mRNA (Yamaguchi et al., 2003).

A common mechanism for light-dependent adaptations especially in the chloroplast is thioredoxin-based redox regulation. These thioredoxins are ubiquitous enzymes containing redox-active thiols for the reduction of disulfide bonds within or between target proteins, thereby regulating the structure and/or function of those proteins (for a review see Geigenberger et al., 2017). Interestingly, DLA2, DLD2 and PDH2 have been identified to be putative thioredoxin targets using an affinity chromatography approach with subsequent mass spectrometry analysis for *C. reinhardtii* (Pérez-Pérez et al., 2017). Furthermore, preliminary data suggest that co-immunoprecipitation experiments of DLA2 can co-precipitate the NADPH-dependent thioredoxin reductase C (NTRC) and vice versa (Neusius, Teh, Nickelsen unpublished). In *A. thaliana* NTRC was shown to be involved in redox regulation of proteins with target proteins in various chloroplast processes including translation and carbon metabolism (Michalska et al., 2009; Thormählen et al., 2015; González et al., 2019). This

indicates that redox-based mechanisms might be involved in the light-dependent regulation of PDC activity and/or RNP complex formation. Moreover, interactions with published redox-dependent components of *psbA* gene expression regulation (see chapter I.4.3) cannot be excluded.

In summary, the acetylation state of K197 is one factor regulating the moonlighting function of DLA2. Acetylation-dependent disassembly of the cpPDC leads directly to RNP complex formation involving DLA2 and the *psbA* mRNA mainly at membranes around the pyrenoid. However, other factors are most likely involved in facilitating RNP complex formation in the presence of acetate and light. Nevertheless, the function of the RNP complex does not seem to be limited to mixotrophic conditions, as minor amounts are also present under photoautotrophic growth conditions.

#### IV.3.3. DLA2 is regulating D1 synthesis for PSII *de novo* biogenesis

<sup>35</sup>S pulse labelling experiments showed that loss of DLA2 led to a strong reduction of D1 synthesis rates under mixotrophic conditions similar to what Bohne et al. (2013) detected for their *iDLA2* lines. This clearly strengthens the assumption that DLA2 is indeed involved in regulation of D1 synthesis (Figure 29). Highlight experiments and sulfur deprivation experiments revealed that the observed reduction of D1 synthesis could be attributed to synthesis for PSII *de novo* biogenesis and not for PSII repair (Figures 30, 31). This is supported by FRET signals locating the DLA2-*psbA* mRNA-complex mainly around the pyrenoid where PSII *de novo* biogenesis at T-zones is thought to take place (Figure 28; Sun et al., 2019). Interestingly, the D1 accumulation rate in the *dla2* mutant in the sulfur starvation experiment was just slightly decreased compared to the complemented strains but the response to sulfur repletion seemed to be significantly delayed. This suggests that DLA2 might be especially important for fast responses to changing environmental conditions. This is in line with the strong decrease of D1 synthesis in the *dla2* mutant seen in the <sup>35</sup>S pulse labeling experiment as these experiments detect protein synthesis in fast response to changed sulfur availability. Moreover, it was shown that translation of D1 is induced by the addition of acetate to the medium, i.e. under conditions where the RNP complex involving DLA2 and the *psbA* mRNA is accumulating (Michaels and Herrin, 1990). On the other hand, no change of D1 accumulation and PSII efficiency in the *dla2* mutant under steady state mixotrophic conditions suggest that other regulatory mechanisms can complement the DLA2 function for D1 synthesis in the presence of acetate. Moreover, it cannot be excluded that the decreased D1 accumulation rates observed for the *dla2* knock out mutant are rather a result of mislocalized D1 synthesis leading to fast degradation of newly synthesized D1 protein than of strongly decreased synthesis rates.

Additionally, a significant difference in respect to D1 synthesis between the DLA2 acetylation lines and the DLA2-HA reference strain could not be detected, leaving the influence of changing RNP complex formation on D1 synthesis uncertain. The massive increase of DLA2-*psbA* mRNA association in the K197Q-HA line might not directly lead to an increased D1 synthesis because other factors involved in the RNP complex formation might be limited. On the other hand, as there are other mechanisms promoting RNP complex formation in the presence of acetate, decreased DLA2-*psbA* mRNA association in the K197R-HA line might just lead to small differences in D1 synthesis which cannot be resolved with the methods used in this study. The combination of different PTMs might also be necessary for significant alterations in D1 synthesis. As it was shown that acetate was able to complement both DLA2 functions in different experimental approaches, future analysis of the DLA2 acetylation lines focusing on photoautotrophic growth conditions might lead to new insights concerning effects of changing RNP complex accumulation. Thus, the presumably mild effects on D1 synthesis in the DLA2 acetylation lines might become more obvious under conditions when photosynthesis is essential.

Taken together, DLA2 is involved in the regulation of D1 synthesis for PSII *de novo* biogenesis making it an integrator protein, coordinating carbon metabolism and gene expression in response to changing environmental conditions (Figure 34).

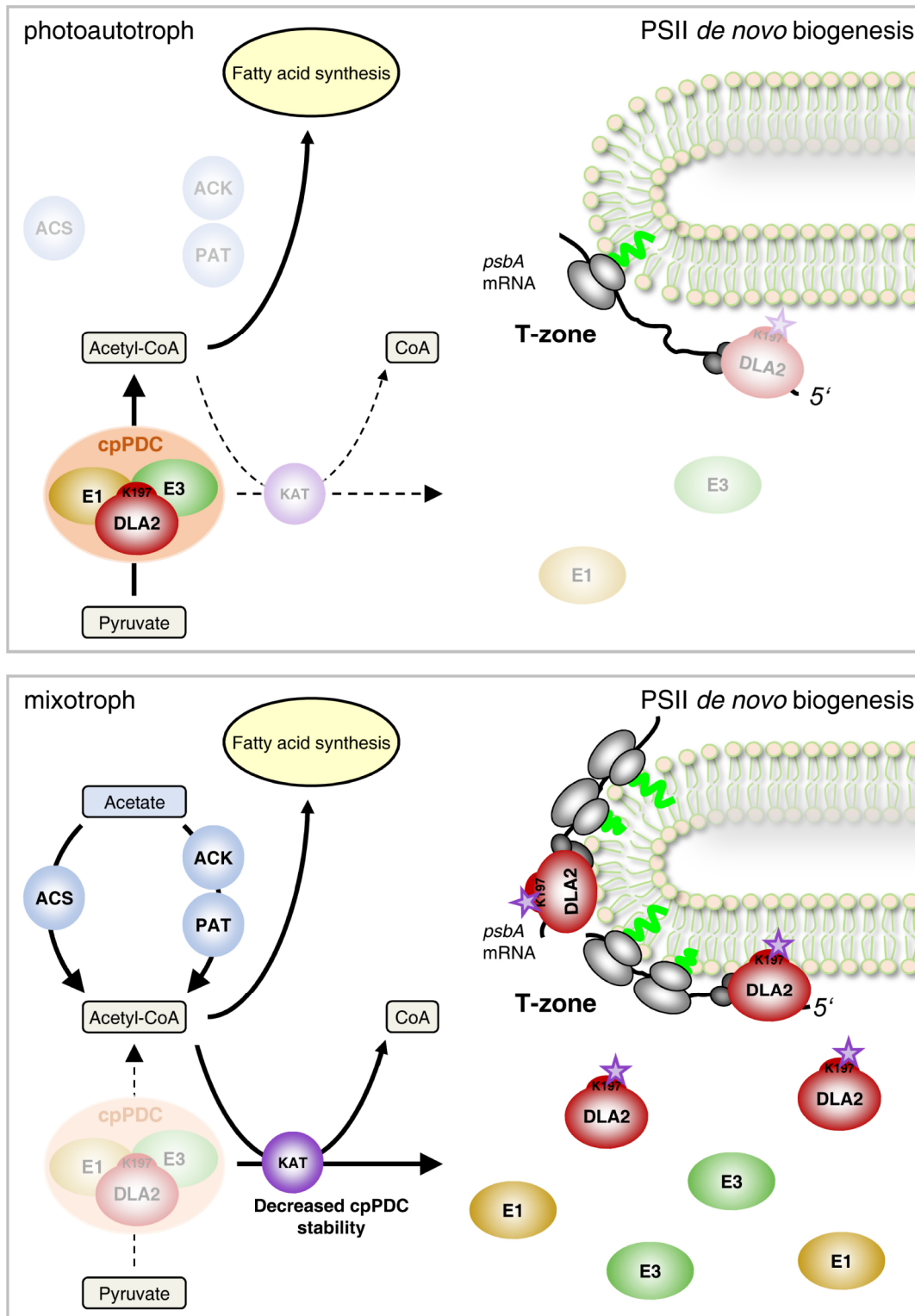


**Figure 34: Acetate-dependent regulation of *psbA* gene expression by DLA2 in *C. reinhardtii*.**

Under photoautotrophic growth conditions, DLA2 is mainly assembled within the cpPDC for production of acetyl-CoA which is needed for fatty acid synthesis (upper panel). Under mixotrophic growth conditions, external acetate can be incorporated by the cell and converted to acetyl-CoA by ACS and/or the ACK/PAT system (lower panel). Under these conditions, K197 within the E3BD of DLA2 is increasingly acetylated by a protein Lys-N<sup>ε</sup>-acetyltransferase (KAT) leading to decreased stability of the cpPDC thereby promoting disassembly of the complex. The released DLA2 binds to the *psbA* mRNA and localizing it to T-zones around the pyrenoid thereby enhancing D1 synthesis for PSII *de novo* biogenesis. Acetylation at K197 is depicted as a purple star. Kindly provided and adapted from (Bohne and Nickelsen, 2017).

#### IV.4. Evolutionary conservation of DLA2's moonlighting function and regulation

UV-crosslinking experiments with recombinant E2 subunits from various organisms performed by Bohne et al. (2013) showed that all of the analyzed E2 subunits possessed RNA-binding activity, suggesting moonlighting might be a conserved trait of E2 subunits. This is further supported by results from human adipocytes which show that the E1 and E2 subunits of the mtPDC are also localized to the nucleus and are involved in the control of gene transcription (Richard et al., 2017). The aforementioned SEC analysis of chloroplast proteins revealing the participation of LTA2 in a second HMW complex was not the only finding indicating an additional function of the plastid E2 subunit from *A. thaliana* (Olinares et al., 2010). Moreover, T-DNA insertion lines missing the LTA2 protein were shown to be lethal, while a line deficient of the E3 subunit was viable (Lin et al., 2003; Chen et al., 2010). Recent data by Kleinknecht (2018) even showed that, similar to the size exclusion experiments performed in this study, the E2 subunit from *Synechocystis* sp. PCC 6803 (sll1841) is part of an RNase-sensitive HMW complex. Taken together, this suggests that a moonlighting function of E2 subunits might be conserved from cyanobacteria to higher plants.

Alignments of the E3-binding domains of E2 subunits from various organisms showed that the lysine residue (K197), which was found to be involved in the regulation of DLA2 function, is especially conserved in E2 subunits of plastidic or photosynthetic prokaryotes' PDCs (Figure 14). This indicates that regulation of DLA2 function via reversible lysine acetylation might be a conserved mechanism in the green lineage. The analysis of acetylation at K193 showed that lysine residues at other positions could also be used for the regulation of E2 functions, however, an acetylation site for the three mitochondrial E2 isoforms (DLA1, DLA3 and DLA4) could not be identified in the acetylome analysis. Moreover, analysis of published mitochondrial acetylome data of various organisms did not reveal acetylation within the E3BD of any mitochondrial E2 subunit indicating that other regulation mechanisms might be involved here (Henriksen et al., 2012; Kim et al., 2013; Zhang et al., 2013; König et al., 2014; Liu et al., 2014; Smith-Hammond et al., 2014; Smith-Hammond et al., 2014; Mo et al., 2015; Chen et al., 2018; Wang et al., 2019; Yan et al., 2020). As almost all published acetylome data are generated from mitochondria or prokaryotes, analysis of acetylation sites within chloroplasts will be important to gain new insights into the conservation of this mechanism in plastids.

In summary, the data presented in this thesis together with published research suggest that moonlighting activities of E2 subunits of the pyruvate dehydrogenase complex are

evolutionary conserved. However, the regulation of E2's function probably involves different mechanisms among organisms with a potential for conserved reversible lysine acetylation in the green lineage.

#### **IV.5. Conclusion and future perspectives**

Despite the plethora of moonlighting enzymes identified in the last 20 years, only little is known about moonlighting enzymes in the chloroplast. The data presented in this thesis provide new insights into the working mode and regulation of DLA2, thereby adding its piece to the better understanding of moonlighting functions of metabolic enzymes in plastids. Especially the identification of reversible lysine acetylation for the regulation of moonlighting function might be valuable for future characterizations of moonlighting enzymes. Furthermore, the identified function in PSII *de novo* biogenesis substantiates DLA2's role as an integrator protein connecting carbon metabolism and plastid gene expression in response to environmental conditions. Besides these significant insights into DLA2 function, the establishment of the FRET microscopy assay should facilitate future *in vivo* analysis of RNA-protein interactions in *C. reinhardtii*.

However, some questions about DLA2's function remain elusive. Therefore, the major goal of research following this thesis should be to clarify the molecular mechanism of how DLA2 is changing D1 synthesis. Therefore, the identification of other components of the RNP complex might be essential. As all complemented lines contain DLA2 versions fused to a triple HA-tag they can be used for co-immunoprecipitation experiments on solubilized thylakoids. Moreover, determination of the structure of the recombinant DLA2-*psbA* mRNA complex using cryo-electron microscopy might lead to additional information about the binding mode in respect to the oligomeric state of DLA2 and involved amino acids. Furthermore, *de novo* biogenesis of PSII is a process involving the concerted synthesis of D1 and many other subunits, above all D2. Therefore, it might be interesting to analyze the influence of DLA2-dependent changes of D1 synthesis on the translation and maybe even localization of mRNAs corresponding to other PSII subunits.

**V. REFERENCES**

- Abolhassani Rad, S., E. J. Clayton, E. J. Cornelius, T. R. Howes and S. E. Kohalmi** (2018). "Moonlighting proteins: putting the spotlight on enzymes." *Plant signaling & behavior* **13**(10): e1517075.
- Aljaberi, A. M., J. R. Webster and S. P. Wheatley** (2015). "Mitotic activity of survivin is regulated by acetylation at K129." *Cell cycle (Georgetown, Tex.)* **14**(11): 1738-1747.
- Allen, J. F., W. B. de Paula, S. Puthiyaveetil and J. Nield** (2011). "A structural phylogenetic map for chloroplast photosynthesis." *Trends Plant Sci* **16**(12): 645-655.
- Allison, L. A.** (2000). "The role of sigma factors in plastid transcription." *Biochimie* **82**(6-7): 537-548.
- Archibald, John M.** (2015). "Endosymbiosis and Eukaryotic Cell Evolution." *Current Biology* **25**(19): R911-R921.
- Arjunan, P., J. Wang, N. S. Nemeria, S. Reynolds, I. Brown, K. Chandrasekhar, G. Calero, F. Jordan and W. Furey** (2014). "Novel binding motif and new flexibility revealed by structural analyses of a pyruvate dehydrogenase-dihydrolipoyl acetyltransferase subcomplex from the *Escherichia coli* pyruvate dehydrogenase multienzyme complex." *J Biol Chem* **289**(43): 30161-30176.
- Asamizu, E., et al.** (2004). "Establishment of publicly available cDNA material and information resource of *Chlamydomonas reinhardtii* (Chlorophyta) to facilitate gene function analysis." *Phycologia* **43**(6): 722-726.
- Auchincloss, A. H., W. Zerges, K. Perron, J. Girard-Bascou and J. D. Rochaix** (2002). "Characterization of Tbc2, a nucleus-encoded factor specifically required for translation of the chloroplast *psbC* mRNA in *Chlamydomonas reinhardtii*." *J Cell Biol* **157**(6): 953-962.
- Barbas, A., A. Popescu, C. Frazão, C. M. Arraiano and A. M. Fialho** (2013). "Rossmann-fold motifs can confer multiple functions to metabolic enzymes: RNA binding and ribonuclease activity of a UDP-glucose dehydrogenase." *Biochem Biophys Res Commun* **430**(1): 218-224.
- Barkan, A.** (2011). "Expression of Plastid Genes: Organelle-Specific Elaborations on a Prokaryotic Scaffold." *Plant Physiology* **155**(4): 1520-1532.
- Barkan, A. and M. Goldschmidt-Clermont** (2000). "Participation of nuclear genes in chloroplast gene expression." *Biochimie* **82**(6-7): 559-572.
- Bassham, J. A., A. A. Benson and M. Calvin** (1950). "The path of carbon in photosynthesis." *J Biol Chem* **185**(2): 781-787.
- Bennoun, P., A. Masson and M. Delosme** (1980). "A method for complementation analysis of nuclear and chloroplast mutants of photosynthesis in *Chlamydomonas*." *Genetics* **95**(1): 39-47.

- Bepperling, A., F. Alte, T. Kriehuber, N. Braun, S. Weinkauff, M. Groll, M. Haslbeck and J. Buchner** (2012). "Alternative bacterial two-component small heat shock protein systems." *Proc Natl Acad Sci U S A* **109**(50): 20407-20412.
- Bertani, G.** (1951). "Studies on lysogenesis. I. The mode of phage liberation by lysogenic *Escherichia coli*." *Journal of bacteriology* **62**(3): 293-300.
- Bock, R. and J. N. Timmis** (2008). "Reconstructing evolution: Gene transfer from plastids to the nucleus." *BioEssays* **30**(6): 556-566.
- Bohne, A.-V., C. Schwarz, M. Schottkowski, M. Lidschreiber, M. Piotrowski, W. Zerges and J. Nickelsen** (2013). "Reciprocal Regulation of Protein Synthesis and Carbon Metabolism for Thylakoid Membrane Biogenesis." *PLOS Biology* **11**(2): e1001482.
- Bohne, A. V. and J. Nickelsen** (2017). "Metabolic Control of Chloroplast Gene Expression: An Emerging Theme." *Mol Plant* **10**(1): 1-3.
- Bohne, A. V., C. Schwarz, A. Jalal, F. Ossenbühl and J. Nickelsen** (2009). "Control of organellar gene expression in *Chlamydomonas reinhardtii* – future perspectives." *Endocytobiosis Cell Res*(19): 70-80
- Bohne, A. V., S. Schwenkert, B. Grimm and J. Nickelsen** (2016). "Roles of Tetratricopeptide Repeat Proteins in Biogenesis of the Photosynthetic Apparatus." *Int Rev Cell Mol Biol* **324**: 187-227.
- Boudreau, E., J. Nickelsen, S. D. Lemaire, F. Ossenbühl and J.-D. Rochaix** (2000). "The *Nac2* gene of *Chlamydomonas* encodes a chloroplast TPR-like protein involved in *psbD* mRNA stability." *The EMBO Journal* **19**(13): 3366-3376.
- Bradford, M. M.** (1976). "A rapid and sensitive method for the quantitation of microgram quantities of protein utilizing the principle of protein-dye binding." *Anal Biochem* **72**: 248-254.
- Brautigam, C. A., J. L. Chuang, D. R. Tomchick, M. Machius and D. T. Chuang** (2005). "Crystal structure of human dihydrolipoamide dehydrogenase: NAD<sup>+</sup>/NADH binding and the structural basis of disease-causing mutations." *J Mol Biol* **350**(3): 543-552.
- Brilli, M. and R. Fani** (2004). "The origin and evolution of eucaryal HIS7 genes: from metabolon to bifunctional proteins?" *Gene* **339**: 149-160.
- Bross, C. D., T. R. Howes, S. Abolhassani Rad, O. Kljakic and S. E. Kohalmi** (2017). "Subcellular localization of Arabidopsis arogenate dehydratases suggests novel and non-enzymatic roles." *Journal of Experimental Botany* **68**(7): 1425-1440.
- Brown Jr., R. M. and H. J. Arnott** (1970). "Structure and Function of the Algal Pyrenoid. I. Ultrastructure and Cytochemistry during Zoosporogenesis of *Tetracystis Excentrica*." *Journal of Phycology* **6**(1): 14-22.
- Broz, A. K., A. Tovar-Mendez, B. P. Mooney, M. L. Johnston, J. A. Miernyk and D. D. Randall** (2014). "A novel regulatory mechanism based upon a dynamic core structure for the mitochondrial pyruvate dehydrogenase complex?" *Mitochondrion* **19 Pt B**: 144-153.

- Buchanan, B. B.** (2016). "The carbon (formerly dark) reactions of photosynthesis." *Photosynth Res* **128**(2): 215-217.
- Byron, O. and J. G. Lindsay** (2017). "The Pyruvate Dehydrogenase Complex and Related Assemblies in Health and Disease." *Subcell Biochem* **83**: 523-550.
- Camp, P. J., J. A. Miernyk and D. D. Randall** (1988). "Some kinetic and regulatory properties of the pea chloroplast pyruvate dehydrogenase complex." *Biochimica et Biophysica Acta (BBA) - Bioenergetics* **933**(2): 269-275.
- Camp, P. J. and D. D. Randall** (1985). "Purification and Characterization of the Pea Chloroplast Pyruvate Dehydrogenase Complex : A Source of Acetyl-CoA and NADH for Fatty Acid Biosynthesis." *Plant Physiology* **77**(3): 571-577.
- Carter, M. L., A. C. Smith, H. Kobayashi, S. Purton and D. L. Herrin** (2004). "Structure, circadian regulation and bioinformatic analysis of the unique sigma factor gene in *Chlamydomonas reinhardtii*." *Photosynthesis Research* **82**(3): 339-349.
- Cavaiuolo, M., R. Kuras, F.-A. Wollman, Y. Choquet and O. Vallon** (2017). "Small RNA profiling in *Chlamydomonas*: insights into chloroplast RNA metabolism." *Nucleic Acids Research* **45**(18): 10783-10799.
- Chandrasekhar, K., et al.** (2013). "Insight to the interaction of the dihydrolipoamide acetyltransferase (E2) core with the peripheral components in the *Escherichia coli* pyruvate dehydrogenase complex via multifaceted structural approaches." *J Biol Chem* **288**(21): 15402-15417.
- Chen, W., Y. Chi, N. L. Taylor, H. Lambers and P. M. Finnegan** (2010). "Disruption of *ptLPD1* or *ptLPD2*, genes that encode isoforms of the plastidial lipoamide dehydrogenase, confers arsenate hypersensitivity in *Arabidopsis*." *Plant Physiology* **153**(3): 1385-1397.
- Chen, Z., L. Luo, R. Chen, H. Hu, Y. Pan, H. Jiang, X. Wan, H. Jin and Y. Gong** (2018). "Acetylome Profiling Reveals Extensive Lysine Acetylation of the Fatty Acid Metabolism Pathway in the Diatom *Phaeodactylum tricoratum*." *Molecular & Cellular Proteomics* **17**(3): 399-412.
- Chevalier, F., M. M. Ghulam, D. Rondet, T. Pfannschmidt, L. Merendino and S. Lerbs-Mache** (2015). "Characterization of the *psbH* precursor RNAs reveals a precise endoribonuclease cleavage site in the *psbT/psbH* intergenic region that is dependent on *psbN* gene expression." *Plant Mol Biol* **88**(4-5): 357-367.
- Choquet, Y. and O. Vallon** (2000). "Synthesis, assembly and degradation of thylakoid membrane proteins." *Biochimie* **82**(6-7): 615-634.
- Choquet, Y., K. Wostrikoff, B. Rimbault, F. Zito, J. Girard-Bascou, D. Drapier and F. A. Wollman** (2001). "Assembly-controlled regulation of chloroplast gene translation." *Biochem Soc Trans* **29**(Pt 4): 421-426.
- Choudhary, C., C. Kumar, F. Gnad, M. L. Nielsen, M. Rehman, T. C. Walther, J. V. Olsen and M. Mann** (2009). "Lysine Acetylation Targets Protein Complexes and Co-Regulates Major Cellular Functions." *Science* **325**(5942): 834-840.

- Cohen, I., Y. Sapir and M. Shapira** (2006). "A Conserved Mechanism Controls Translation of Rubisco Large Subunit in Different Photosynthetic Organisms." *Plant Physiology* **141**(3): 1089-1097.
- de Boer, A. H., P. J. van Kleeff and J. Gao** (2013). "Plant 14-3-3 proteins as spiders in a web of phosphorylation." *Protoplasma* **250**(2): 425-440.
- Dekker, J. P. and E. J. Boekema** (2005). "Supramolecular organization of thylakoid membrane proteins in green plants." *Biochimica et Biophysica Acta (BBA) - Bioenergetics* **1706**(1): 12-39.
- Derelle, E., et al.** (2006). "Genome analysis of the smallest free-living eukaryote *Ostreococcus tauri* unveils many unique features." *Proc Natl Acad Sci U S A* **103**(31): 11647-11652.
- Douchi, D., Y. Qu, P. Longoni, L. Legendre-Lefebvre, X. Johnson, C. Schmitz-Linneweber and M. Goldschmidt-Clermont** (2016). "A Nucleus-Encoded Chloroplast Phosphoprotein Governs Expression of the Photosystem I Subunit PsaC in *Chlamydomonas reinhardtii*." *Plant Cell* **28**(5): 1182-1199.
- Drager, R. G., J. Girard-Bascou, Y. Choquet, K. L. Kindle and D. B. Stern** (1998). "*In vivo* evidence for 5'→3' exoribonuclease degradation of an unstable chloroplast mRNA." *Plant J* **13**(1): 85-96.
- Drapier, D., H. Suzuki, H. Levy, B. Rimbault, K. L. Kindle, D. B. Stern and F.-A. Wollman** (1998). "The chloroplast *atpA* gene cluster in *Chlamydomonas reinhardtii*. Functional analysis of a polycistronic transcription unit." *Functional Analysis of a Polycistronic Transcription Unit* **117**(2): 629-641.
- Drechsel, O. and R. Bock** (2010). "Selection of Shine-Dalgarno sequences in plastids." *Nucleic Acids Research* **39**(4): 1427-1438.
- Eberhard, S., D. Drapier and F. A. Wollman** (2002). "Searching limiting steps in the expression of chloroplast-encoded proteins: relations between gene copy number, transcription, transcript abundance and translation rate in the chloroplast of *Chlamydomonas reinhardtii*." *Plant J* **31**(2): 149-160.
- Eberhard, S., G. Finazzi and F. A. Wollman** (2008). "The dynamics of photosynthesis." *Annu Rev Genet* **42**: 463-515.
- Eberhard, S., C. Loiselay, D. Drapier, S. Bujaldon, J. Girard-Bascou, R. Kuras, Y. Choquet and F. A. Wollman** (2011). "Dual functions of the nucleus-encoded factor TDA1 in trapping and translation activation of *atpA* transcripts in *Chlamydomonas reinhardtii* chloroplasts." *Plant J* **67**(6): 1055-1066.
- Ferris, P. J. and U. W. Goodenough** (1994). "The mating-type locus of *Chlamydomonas reinhardtii* contains highly rearranged DNA sequences." *Cell* **76**(6): 1135-1145.
- Finkemeier, I., M. Laxa, L. Miguet, A. J. M. Howden and L. J. Sweetlove** (2011). "Proteins of Diverse Function and Subcellular Location Are Lysine Acetylated in Arabidopsis." *Plant Physiology* **155**(4): 1779-1790.

- Frank, R. A., J. V. Pratap, X. Y. Pei, R. N. Perham and B. F. Luisi** (2005). "The molecular origins of specificity in the assembly of a multienzyme complex." *Structure* **13**(8): 1119-1130.
- Gancedo, C. and C. L. Flores** (2008). "Moonlighting proteins in yeasts." *Microbiol Mol Biol Rev* **72**(1): 197-210, table of contents.
- Geigenberger, P., I. Thormählen, D. M. Daloso and A. R. Fernie** (2017). "The Unprecedented Versatility of the Plant Thioredoxin System." *Trends in Plant Science* **22**(3): 249-262.
- González, M., V. Delgado-Requerey, J. Ferrández, A. Serna and F. J. Cejudo** (2019). "Insights into the function of NADPH thioredoxin reductase C (NTRC) based on identification of NTRC-interacting proteins *in vivo*." *Journal of Experimental Botany* **70**(20): 5787-5798.
- Gould, S. B., R. F. Waller and G. I. McFadden** (2008). "Plastid evolution." *Annu Rev Plant Biol* **59**: 491-517.
- Gray, M. W. and P. H. Boer** (1988). "Organization and expression of algal (*Chlamydomonas reinhardtii*) mitochondrial DNA." *Philos Trans R Soc Lond B Biol Sci* **319**(1193): 135-147.
- Greiner, A., S. Kelterborn, H. Evers, G. Kreimer, I. Sizova and P. Hegemann** (2017). "Targeting of Photoreceptor Genes in *Chlamydomonas reinhardtii* via Zinc-Finger Nucleases and CRISPR/Cas9." *The Plant Cell* **29**(10): 2498-2518.
- Grote, A., K. Hiller, M. Scheer, R. Münch, B. Nörtemann, D. C. Hempel and D. Jahn** (2005). "JCat: a novel tool to adapt codon usage of a target gene to its potential expression host." *Nucleic Acids Res* **33**(Web Server issue): W526-531.
- Gudi, R., M. M. Bowker-Kinley, N. Y. Kedishvili, Y. Zhao and K. M. Popov** (1995). "Diversity of the pyruvate dehydrogenase kinase gene family in humans." *J Biol Chem* **270**(48): 28989-28994.
- Hammani, K., G. Bonnard, A. Bouchoucha, A. Gobert, F. Pinker, T. Salinas and P. Giegé** (2014). "Helical repeats modular proteins are major players for organelle gene expression." *Biochimie* **100**: 141-150.
- Hammani, K., W. B. Cook and A. Barkan** (2012). "RNA binding and RNA remodeling activities of the half-a-tetratricopeptide (HAT) protein HCF107 underlie its effects on gene expression." *Proc Natl Acad Sci U S A* **109**(15): 5651-5656.
- Harris, E. H.** (1989). "The *Chlamydomonas* Sourcebook. A Comprehensive Guide to Biology and Laboratory Use. Academic Press, San Diego, CA, 1989. xiv, 780 pp., illus." *Science* **246**(4936): 1503-1504.
- Harwood, J. L.** (1996). "Recent advances in the biosynthesis of plant fatty acids." *Biochimica et Biophysica Acta (BBA) - Lipids and Lipid Metabolism* **1301**(1): 7-56.
- Harwood, J. L. and A. L. Jones** (1989). *Lipid Metabolism in Algae. Advances in Botanical Research.* J. A. Callow, Academic Press. **16**: 1-53.

- Hashimoto, M., T. Endo, G. Peltier, M. Tasaka and T. Shikanai** (2003). "A nucleus-encoded factor, CRR2, is essential for the expression of chloroplast *ndhB* in Arabidopsis." *Plant J* **36**(4): 541-549.
- Heinz, S., J. Hamm, B. Rengstl, A. Stengel, A. Rast, M. Ostermeier, C. Funk and J. Nickelsen** (manuscript in preparation). "Identification of periplasmic interaction partners of the manganese-delivering protein PrtA in *Synechocystis* sp. PCC 6803."
- Henriksen, P., et al.** (2012). "Proteome-wide Analysis of Lysine Acetylation Suggests its Broad Regulatory Scope in *Saccharomyces cerevisiae*." *Molecular & Cellular Proteomics* **11**(11): 1510-1522.
- Herrin, D. L. and J. Nickelsen** (2004). "Chloroplast RNA processing and stability." *Photosynth Res* **82**(3): 301-314.
- Hess, W. R., A. Prombona, B. Fieder, A. R. Subramanian and T. Börner** (1993). "Chloroplast *rps15* and the *rpoB/C1/C2* gene cluster are strongly transcribed in ribosome-deficient plastids: evidence for a functioning non-chloroplast-encoded RNA polymerase." *EMBO J* **12**(2): 563-571.
- Hirose, T. and M. Sugiura** (1996). "Cis-acting elements and trans-acting factors for accurate translation of chloroplast *psbA* mRNAs: development of an *in vitro* translation system from tobacco chloroplasts." *EMBO J* **15**(7): 1687-1695.
- Hohmann-Marriott, M. F. and R. E. Blankenship** (2011). "Evolution of photosynthesis." *Annu Rev Plant Biol* **62**: 515-548.
- Hollender, C. and Z. Liu** (2008). "Histone deacetylase genes in Arabidopsis development." *J Integr Plant Biol* **50**(7): 875-885.
- Huang, B., R. Gudi, P. Wu, R. A. Harris, J. Hamilton and K. M. Popov** (1998). "Isoenzymes of pyruvate dehydrogenase phosphatase. DNA-derived amino acid sequences, expression, and regulation." *J Biol Chem* **273**(28): 17680-17688.
- Huranová, M., J. A. Jablonski, A. Benda, M. Hof, D. Stanek and M. Caputi** (2009). "*In vivo* detection of RNA-binding protein interactions with cognate RNA sequences by fluorescence resonance energy transfer." *Rna* **15**(11): 2063-2071.
- Imbard, A., et al.** (2011). "Molecular characterization of 82 patients with pyruvate dehydrogenase complex deficiency. Structural implications of novel amino acid substitutions in E1 protein." *Molecular genetics and metabolism* **104**(4): 507-516.
- Itakura, A. K., et al.** (2019). "A Rubisco-binding protein is required for normal pyrenoid number and starch sheath morphology in *Chlamydomonas reinhardtii*." *Proc Natl Acad Sci U S A* **116**(37): 18445-18454.
- Izard, T., A. Aevansson, M. D. Allen, A. H. Westphal, R. N. Perham, A. de Kok and W. G. Hol** (1999). "Principles of quasi-equivalence and Euclidean geometry govern the assembly of cubic and dodecahedral cores of pyruvate dehydrogenase complexes." *Proc Natl Acad Sci U S A* **96**(4): 1240-1245.

- Jalal, A., C. Schwarz, C. Schmitz-Linneweber, O. Vallon, J. Nickelsen and A. V. Bohne** (2015). "A small multifunctional pentatricopeptide repeat protein in the chloroplast of *Chlamydomonas reinhardtii*." *Mol Plant* **8**(3): 412-426.
- Jarvis, P. and J. Soll** (2002). "Toc, tic, and chloroplast protein import." *Biochim Biophys Acta* **1590**(1-3): 177-189.
- Jeffery, C. J.** (1999). "Moonlighting proteins." *Trends Biochem Sci* **24**(1): 8-11.
- Jeffery, C. J.** (2003). "Moonlighting proteins: old proteins learning new tricks." *Trends Genet* **19**(8): 415-417.
- Jeffery, C. J.** (2018). "Protein moonlighting: what is it, and why is it important?" *Philos Trans R Soc Lond B Biol Sci* **373**(1738).
- Jeoung, N. H., C. R. Harris and R. A. Harris** (2014). "Regulation of pyruvate metabolism in metabolic-related diseases." *Rev Endocr Metab Disord* **15**(1): 99-110.
- Jiang, X. and D. Stern** (2009). "Mating and Tetrad Separation of *Chlamydomonas reinhardtii* for Genetic Analysis." *Journal of Visualized Experiments : JoVE*(30): 1274.
- Johnston, M. L., M. H. Luethy, J. A. Miernyk and D. D. Randall** (1997). "Cloning and molecular analyses of the *Arabidopsis thaliana* plastid pyruvate dehydrogenase subunits." *Biochim Biophys Acta* **1321**(3): 200-206.
- Juergens, M. T., B. Disbrow and Y. Shachar-Hill** (2016). "The Relationship of Triacylglycerol and Starch Accumulation to Carbon and Energy Flows during Nutrient Deprivation in *Chlamydomonas reinhardtii*." *Plant Physiology* **171**(4): 2445-2457.
- Jung, H.-I., A. Cooper and R. N. Perham** (2002). "Identification of Key Amino Acid Residues in the Assembly of Enzymes into the Pyruvate Dehydrogenase Complex of *Bacillus stearothermophilus*: A Kinetic and Thermodynamic Analysis." *Biochemistry* **41**(33): 10446-10453.
- Jung, H. I., S. J. Bowden, A. Cooper and R. N. Perham** (2002). "Thermodynamic analysis of the binding of component enzymes in the assembly of the pyruvate dehydrogenase multienzyme complex of *Bacillus stearothermophilus*." *Protein Sci* **11**(5): 1091-1100.
- Kato, M., R. M. Wynn, J. L. Chuang, S. C. Tso, M. Machius, J. Li and D. T. Chuang** (2008). "Structural basis for inactivation of the human pyruvate dehydrogenase complex by phosphorylation: role of disordered phosphorylation loops." *Structure* **16**(12): 1849-1859.
- Kelley, L. A., S. Mezulis, C. M. Yates, M. N. Wass and M. J. E. Sternberg** (2015). "The Pyre2 web portal for protein modeling, prediction and analysis." *Nature Protocols* **10**(6): 845-858.
- Kim, D., B. J. Yu, J. A. Kim, Y.-J. Lee, S.-G. Choi, S. Kang and J.-G. Pan** (2013). "The acetylproteome of Gram-positive model bacterium *Bacillus subtilis*." *Proteomics* **13**(10-11): 1726-1736.

- Kitajima, M. and W. L. Butler** (1975). "Quenching of chlorophyll fluorescence and primary photochemistry in chloroplasts by dibromothymoquinone." *Biochim Biophys Acta* **376**(1): 105-115.
- Kleinknecht, L.** (2018). Molecular analysis of nucleus-encoded regulators of plastid protein synthesis. Fakultät für Biologie, Ludwig-Maximilians-Universität München.
- Klinkert, B., F. Ossenbühl, M. Sikorski, S. Berry, L. Eichacker and J. Nickelsen** (2004). "PratA, a periplasmic tetratricopeptide repeat protein involved in biogenesis of photosystem II in *Synechocystis* sp. PCC 6803." *J Biol Chem* **279**(43): 44639-44644.
- Komine, Y., E. Kikis, G. Schuster and D. Stern** (2002). "Evidence for *in vivo* modulation of chloroplast RNA stability by 3'-UTR homopolymeric tails in *Chlamydomonas reinhardtii*." *Proc Natl Acad Sci U S A* **99**(6): 4085-4090.
- Komine, Y., L. Kwong, M. C. Anguera, G. Schuster and D. B. Stern** (2000). "Polyadenylation of three classes of chloroplast RNA in *Chlamydomonas reinhardtii*." *Rna* **6**(4): 598-607.
- König, A.-C., M. Hartl, P. J. Boersema, M. Mann and I. Finkemeier** (2014). "The mitochondrial lysine acetylome of Arabidopsis." *Mitochondrion* **19**: 252-260.
- König, A.-C., L. Kleinknecht, J. Nickelsen and I. Finkemeier** (manuscript in preparation). "The acetylome of *Chlamydomonas reinhardtii* influenced by acetate and light".
- Korotchkina, L. G. and M. S. Patel** (2001). "Probing the mechanism of inactivation of human pyruvate dehydrogenase by phosphorylation of three sites." *J Biol Chem* **276**(8): 5731-5738.
- Laemmli, U. K.** (1970). "Cleavage of structural proteins during the assembly of the head of bacteriophage T4." *Nature* **227**(5259): 680-685.
- Lei, Y., L. Lu, H.-Y. Liu, S. Li, F. Xing and L.-L. Chen** (2014). "CRISPR-P: A Web Tool for Synthetic Single-Guide RNA Design of CRISPR-System in Plants." *Molecular Plant* **7**(9): 1494-1496.
- Li-Beisson, Y., F. Beisson and W. Riekhof** (2015). "Metabolism of acyl-lipids in *Chlamydomonas reinhardtii*." *Plant J* **82**(3): 504-522.
- Li-Beisson, Y., J. J. Thelen, E. Fedosejevs and J. L. Harwood** (2019). "The lipid biochemistry of eukaryotic algae." *Prog Lipid Res* **74**: 31-68.
- Li, X., et al.** (2016). "An Indexed, Mapped Mutant Library Enables Reverse Genetics Studies of Biological Processes in *Chlamydomonas reinhardtii*." *The Plant Cell* **28**(2): 367.
- Lin, M., R. Behal and D. J. Oliver** (2003). "Disruption of *pLE2*, the gene for the E2 subunit of the plastid pyruvate dehydrogenase complex, in Arabidopsis causes an early embryo lethal phenotype." *Plant Molecular Biology* **52**(4): 865-872.
- Lin, M. and D. J. Oliver** (2008). "The role of acetyl-coenzyme a synthetase in Arabidopsis." *Plant Physiology* **147**(4): 1822-1829.

- Liu, F., M. Yang, X. Wang, S. Yang, J. Gu, J. Zhou, X.-E. Zhang, J. Deng and F. Ge** (2014). "Acetylome analysis reveals diverse functions of lysine acetylation in *Mycobacterium tuberculosis*." *Molecular & Cellular Proteomics* **13**(12): 3352-3366.
- Liu, J., J. Huang, Z. Sun, Y. Zhong, Y. Jiang and F. Chen** (2011). "Differential lipid and fatty acid profiles of photoautotrophic and heterotrophic *Chlorella zofingiensis*: Assessment of algal oils for biodiesel production." *Bioresource Technology* **102**(1): 106-110.
- Loiselay, C., N. J. Gumpel, J. Girard-Bascou, A. T. Watson, S. Purton, F. A. Wollman and Y. Choquet** (2008). "Molecular identification and function of cis- and trans-acting determinants for *petA* transcript stability in *Chlamydomonas reinhardtii* chloroplasts." *Mol Cell Biol* **28**(17): 5529-5542.
- Lorenz, M.** (2009). "Visualizing protein-RNA interactions inside cells by fluorescence resonance energy transfer." *Rna* **15**(1): 97-103.
- Maier, U. G., A. Bozarth, H. T. Funk, S. Zauner, S. A. Rensing, C. Schmitz-Linneweber, T. Borner and M. Tillich** (2008). "Complex chloroplast RNA metabolism: just debugging the genetic programme?" *BMC Biol* **6**: 36.
- Malnoë, A., F. Wang, J. Girard-Bascou, F.-A. Wollman and C. de Vitry** (2014). "Thylakoid FtsH Protease Contributes to Photosystem II and Cytochrome *b<sub>6</sub>f* Remodeling in *Chlamydomonas reinhardtii* under Stress Conditions." *The Plant Cell* **26**(1): 373-390.
- Mande, S. S., S. Sarfaty, M. D. Allen, R. N. Perham and W. G. J. Hol** (1996). "Protein-protein interactions in the pyruvate dehydrogenase multienzyme complex: dihydrolipoamide dehydrogenase complexed with the binding domain of dihydrolipoamide acetyltransferase." *Structure* **4**(3): 277-286.
- Mani, M., et al.** (2015). "MoonProt: a database for proteins that are known to moonlight." *Nucleic Acids Res* **43**(Database issue): D277-282.
- Margulis, L.** (1967). "On the origin of mitosing cells." *J Theor Biol* **14**(3): 255-274.
- Marin-Navarro, J., A. L. Manuell, J. Wu and P. M. S** (2007). "Chloroplast translation regulation." *Photosynth Res* **94**(2-3): 359-374.
- Martinez, A., J. A. Traverso, B. Valot, M. Ferro, C. Espagne, G. Ephritikhine, M. Zivy, C. Giglione and T. Meinnel** (2008). "Extent of N-terminal modifications in cytosolic proteins from eukaryotes." *Proteomics* **8**(14): 2809-2831.
- Maul, J. E., J. W. Lilly, L. Cui, C. W. dePamphilis, W. Miller, E. H. Harris and D. B. Stern** (2002). "The *Chlamydomonas reinhardtii* plastid chromosome: islands of genes in a sea of repeats." *Plant Cell* **14**(11): 2659-2679.
- Mayfield, S. P., A. Cohen, A. Danon and C. B. Yohn** (1994). "Translation of the *psbA* mRNA of *Chlamydomonas reinhardtii* requires a structured RNA element contained within the 5' untranslated region." *J Cell Biol* **127**(6 Pt 1): 1537-1545.
- McFadden, G. I. and G. G. van Dooren** (2004). "Evolution: red algal genome affirms a common origin of all plastids." *Curr Biol* **14**(13): R514-516.

- Melkozernov, A. N., J. Barber and R. E. Blankenship** (2006). "Light Harvesting in Photosystem I Supercomplexes." *Biochemistry* **45**(2): 331-345.
- Merchant, S. S., et al.** (2007). "The *Chlamydomonas* genome reveals the evolution of key animal and plant functions." *Science* **318**(5848): 245-250.
- Mereschkowsky, C.** (1905). "Über Natur und Ursprung der Chromatophoren im Pflanzenreiche." *Biologisches Centralblatt* **25**(18): 593-604.
- Michaels, A. and D. L. Herrin** (1990). "Translational regulation of chloroplast gene expression during the light-dark cell cycle of *Chlamydomonas*: evidence for control by ATP/energy supply." *Biochem Biophys Res Commun* **170**(3): 1082-1088.
- Michalska, J., H. Zauber, B. B. Buchanan, F. J. Cejudo and P. Geigenberger** (2009). "NTRC links built-in thioredoxin to light and sucrose in regulating starch synthesis in chloroplasts and amyloplasts." *Proc Natl Acad Sci U S A* **106**(24): 9908-9913.
- Michelet, L., et al.** (2013). "Redox regulation of the Calvin-Benson cycle: something old, something new." *Front Plant Sci* **4**: 470.
- Min, S.-W., et al.** (2015). "Critical role of acetylation in tau-mediated neurodegeneration and cognitive deficits." *Nature medicine* **21**(10): 1154-1162.
- Minagawa, J. and R. Tokutsu** (2015). "Dynamic regulation of photosynthesis in *Chlamydomonas reinhardtii*." *Plant J* **82**(3): 413-428.
- Minai, L., K. Wostrikoff, F.-A. Wollman and Y. Choquet** (2006). "Chloroplast Biogenesis of Photosystem II Cores Involves a Series of Assembly-Controlled Steps That Regulate Translation." *The Plant Cell* **18**(1): 159-175.
- Mo, R., et al.** (2015). "Acetylome analysis reveals the involvement of lysine acetylation in photosynthesis and carbon metabolism in the model cyanobacterium *Synechocystis* sp. PCC 6803." *J Proteome Res* **14**(2): 1275-1286.
- Moon, M. H., T. A. Hilimire, A. M. Sanders and J. S. Schneekloth** (2018). "Measuring RNA-Ligand Interactions with Microscale Thermophoresis." *Biochemistry* **57**(31): 4638-4643.
- Mooney, B. P., J. A. Miernyk and D. D. Randall** (1999). "Cloning and characterization of the dihydrolipoamide S-acetyltransferase subunit of the plastid pyruvate dehydrogenase complex (E2) from *Arabidopsis*." *Plant Physiology* **120**(2): 443-452.
- Mooney, B. P., J. A. Miernyk and D. D. Randall** (2002). "The complex fate of alpha-ketoacids." *Annu Rev Plant Biol* **53**: 357-375.
- Mulo, P.** (2011). "Chloroplast-targeted ferredoxin-NADP<sup>+</sup> oxidoreductase (FNR): Structure, function and location." *Biochimica et Biophysica Acta (BBA) - Bioenergetics* **1807**(8): 927-934.
- Mulo, P., I. Sakurai and E.-M. Aro** (2012). "Strategies for *psbA* gene expression in cyanobacteria, green algae and higher plants: From transcription to PSII repair." *Biochimica et Biophysica Acta (BBA) - Bioenergetics* **1817**(1): 247-257.

- Muranaka, L. S., M. Rütgers, S. Bujaldon, A. Heublein, S. Geimer, F.-A. Wollman and M. Schroda** (2016). "TEF30 Interacts with Photosystem II Monomers and Is Involved in the Repair of Photodamaged Photosystem II in *Chlamydomonas reinhardtii*." *Plant Physiology* **170**(2): 821-840.
- Nagy, E., T. Henics, M. Eckert, A. Miseta, R. N. Lightowlers and M. Kellermayer** (2000). "Identification of the NAD<sup>+</sup>-Binding Fold of Glyceraldehyde-3-Phosphate Dehydrogenase as a Novel RNA-Binding Domain." *Biochemical and Biophysical Research Communications* **275**(2): 253-260.
- Nakagawa, S., Y. Niimura and T. Gojobori** (2017). "Comparative genomic analysis of translation initiation mechanisms for genes lacking the Shine-Dalgarno sequence in prokaryotes." *Nucleic Acids Res* **45**(7): 3922-3931.
- Nelson, N.** (2011). "Photosystems and global effects of oxygenic photosynthesis." *Biochim Biophys Acta* **1807**(8): 856-863.
- Nelson, N. and A. Ben-Shem** (2005). "The structure of photosystem I and evolution of photosynthesis." *BioEssays* **27**(9): 914-922.
- Nelson, N. and W. Junge** (2015). "Structure and energy transfer in photosystems of oxygenic photosynthesis." *Annu Rev Biochem* **84**: 659-683.
- Nelson, N. and C. F. Yocum** (2006). "Structure and function of photosystems I and II." *Annu Rev Plant Biol* **57**: 521-565.
- Neupert, J., D. Karcher and R. Bock** (2009). "Generation of *Chlamydomonas* strains that efficiently express nuclear transgenes." *Plant J* **57**(6): 1140-1150.
- Nickelsen, J., M. Fleischmann, E. Boudreau, M. Rahire and J. D. Rochaix** (1999). "Identification of cis-acting RNA leader elements required for chloroplast *psbD* gene expression in *Chlamydomonas*." *Plant Cell* **11**(5): 957-970.
- Nickelsen, J. and U. Kuck** (2000). "The unicellular green alga *Chlamydomonas reinhardtii* as an experimental system to study chloroplast RNA metabolism." *Naturwissenschaften* **87**(3): 97-107.
- Nickelsen, J. and B. Rengstl** (2013). "Photosystem II assembly: from cyanobacteria to plants." *Annu Rev Plant Biol* **64**: 609-635.
- Nour-Eldin, H. H., E. A. Specht and S. P. Mayfield** (2016). "An improved ARG7-based selection cassette with highly efficient transformation rates and a small size suitable for complex expression constructs." *Algal Research* **16**: 383-386.
- Olinares, P. D., L. Ponnala and K. J. van Wijk** (2010). "Megadalton complexes in the chloroplast stroma of *Arabidopsis thaliana* characterized by size exclusion chromatography, mass spectrometry, and hierarchical clustering." *Mol Cell Proteomics* **9**(7): 1594-1615.
- Ossenbühl, F., K. Hartmann and J. Nickelsen** (2002). "A chloroplast RNA binding protein from stromal thylakoid membranes specifically binds to the 5' untranslated region of the *psbA* mRNA." *Eur J Biochem* **269**(16): 3912-3919.

- Ozawa, S. I., M. Cavaiuolo, D. Jarrige, R. Kuras, M. Rutgers, S. Eberhard, D. Drapier, F. A. Wollman and Y. Choquet** (2020). "The OPR Protein MTHI1 Controls the Expression of Two Different Subunits of ATP Synthase CFo in *Chlamydomonas reinhardtii*." *Plant Cell* **32**(4): 1179-1203.
- Pandey, R., A. Müller, C. A. Napoli, D. A. Selinger, C. S. Pikaard, E. J. Richards, J. Bender, D. W. Mount and R. A. Jorgensen** (2002). "Analysis of histone acetyltransferase and histone deacetylase families of *Arabidopsis thaliana* suggests functional diversification of chromatin modification among multicellular eukaryotes." *Nucleic Acids Research* **30**(23): 5036-5055.
- Park, Y. H., W. Wei, L. Zhou, N. Nemeria and F. Jordan** (2004). "Amino-terminal residues 1-45 of the *Escherichia coli* pyruvate dehydrogenase complex E1 subunit interact with the E2 subunit and are required for activity of the complex but not for reductive acetylation of the E2 subunit." *Biochemistry* **43**(44): 14037-14046.
- Patel, K. P., T. W. O'Brien, S. H. Subramony, J. Shuster and P. W. Stacpoole** (2012). "The spectrum of pyruvate dehydrogenase complex deficiency: clinical, biochemical and genetic features in 371 patients." *Molecular genetics and metabolism* **106**(3): 385-394.
- Patel, M. S., N. S. Nemeria, W. Furey and F. Jordan** (2014). "The pyruvate dehydrogenase complexes: structure-based function and regulation." *The Journal of biological chemistry* **289**(24): 16615-16623.
- Pérez-Pérez, M. E., A. Mauriès, A. Maes, N. J. Tourasse, M. Hamon, S. D. Lemaire and C. H. Marchand** (2017). "The Deep Thioredoxome in *Chlamydomonas reinhardtii*: New Insights into Redox Regulation." *Molecular Plant* **10**(8): 1107-1125.
- Phillips, D. M.** (1963). "The presence of acetyl groups of histones." *Biochem J* **87**: 258-263.
- Piatigorsky, J.** (1998). "Gene sharing in lens and cornea: facts and implications." *Prog Retin Eye Res* **17**(2): 145-174.
- Piperno, G. and M. T. Fuller** (1985). "Monoclonal antibodies specific for an acetylated form of alpha-tubulin recognize the antigen in cilia and flagella from a variety of organisms." *J Cell Biol* **101**(6): 2085-2094.
- Plant, A. L. and J. C. Gray** (1988). "Introns in chloroplast protein-coding genes of land plants." *Photosynthesis Research* **16**(1): 23-39.
- Qi, Y., U. Armbruster, C. Schmitz-Linneweber, E. Delannoy, A. F. de Longevialle, T. Rühle, I. Small, P. Jahns and D. Leister** (2011). "Arabidopsis CSP41 proteins form multimeric complexes that bind and stabilize distinct plastid transcripts." *Journal of Experimental Botany* **63**(3): 1251-1270.
- Rahire, M., F. Laroche, L. Cerutti and J. D. Rochaix** (2012). "Identification of an OPR protein involved in the translation initiation of the PsaB subunit of photosystem I." *Plant J* **72**(4): 652-661.
- Ran, F. A., et al.** (2015). "*In vivo* genome editing using *Staphylococcus aureus* Cas9." *Nature* **520**(7546): 186-191.

- Rao, R. S., J. J. Thelen and J. A. Miernyk** (2014). "Is Lys-N $\epsilon$ -acetylation the next big thing in post-translational modifications?" *Trends Plant Sci* **19**(9): 550-553.
- Rao, R. S. P., J. J. Thelen and J. A. Miernyk** (2014). "*In silico* analysis of protein Lys-N." *Frontiers in Plant Science* **5**(381).
- Rao, S. T. and M. G. Rossmann** (1973). "Comparison of super-secondary structures in proteins." *J Mol Biol* **76**(2): 241-256.
- Rast, A., S. Heinz and J. Nickelsen** (2015). "Biogenesis of thylakoid membranes." *Biochim Biophys Acta* **1847**(9): 821-830.
- Rawsthorne, S.** (2002). "Carbon flux and fatty acid synthesis in plants." *Prog Lipid Res* **41**(2): 182-196.
- Ren, Q. and M. A. Gorovsky** (2001). "Histone H2A.Z Acetylation Modulates an Essential Charge Patch." *Molecular Cell* **7**(6): 1329-1335.
- Richard, A. J., H. Hang and J. M. Stephens** (2017). "Pyruvate dehydrogenase complex (PDC) subunits moonlight as interaction partners of phosphorylated STAT5 in adipocytes and adipose tissue." *J Biol Chem* **292**(48): 19733-19742.
- Riekhof, W. R., B. B. Sears and C. Benning** (2005). "Annotation of genes involved in glycerolipid biosynthesis in *Chlamydomonas reinhardtii*: discovery of the betaine lipid synthase BTA1<sub>Cr</sub>." *Eukaryotic cell* **4**(2): 242-252.
- Röttig, A. and A. Steinbüchel** (2013). "Acyltransferases in Bacteria." *Microbiology and Molecular Biology Reviews* **77**(2): 277-321.
- Roustan, V. and W. Weckwerth** (2018). "Quantitative Phosphoproteomic and System-Level Analysis of TOR Inhibition Unravel Distinct Organellar Acclimation in *Chlamydomonas reinhardtii*." *Front Plant Sci* **9**: 1590.
- Rungrat, T., et al.** (2016). "Using Phenomic Analysis of Photosynthetic Function for Abiotic Stress Response Gene Discovery." *The arabidopsis book* **14**: e0185-e0185.
- Sager, R. and S. Granick** (1953). "Nutritional studies with *Chlamydomonas reinhardtii*." *Ann N Y Acad Sci* **56**(5): 831-838.
- Salomé, P. A. and S. S. Merchant** (2019). "A Series of Fortunate Events: Introducing *Chlamydomonas* as a Reference Organism." *The Plant Cell* **31**(8): 1682-1707.
- Salvato, F., J. F. Havelund, M. Chen, R. S. P. Rao, A. Rogowska-Wrzesinska, O. N. Jensen, D. R. Gang, J. J. Thelen and I. M. Møller** (2014). "The Potato Tuber Mitochondrial Proteome." *Plant Physiology* **164**(2): 637-653.
- Sato, S., Y. Nakamura, T. Kaneko, E. Asamizu and S. Tabata** (1999). "Complete structure of the chloroplast genome of *Arabidopsis thaliana*." *DNA Res* **6**(5): 283-290.
- Schägger, H. and G. von Jagow** (1987). "Tricine-sodium dodecyl sulfate-polyacrylamide gel electrophoresis for the separation of proteins in the range from 1 to 100 kDa." *Anal Biochem* **166**(2): 368-379.

- Scharff, L. B., L. Childs, D. Walther and R. Bock** (2011). "Local absence of secondary structure permits translation of mRNAs that lack ribosome-binding sites." *PLoS Genet* **7**(6): e1002155.
- Scharff, L. B., M. Ehrnthaler, M. Janowski, L. H. Childs, C. Hasse, J. Gremmels, S. Ruf, R. Zoschke and R. Bock** (2017). "Shine-Dalgarno Sequences Play an Essential Role in the Translation of Plastid mRNAs in Tobacco." *Plant Cell* **29**(12): 3085-3101.
- Schmid, L. M., L. Ohler, T. Möhlmann, A. Brachmann, J. M. Muiño, D. Leister, J. Meurer and N. Manavski** (2019). "PUMPKIN, the Sole Plastid UMP Kinase, Associates with Group II Introns and Alters Their Metabolism." *Plant Physiol* **179**(1): 248-264.
- Schneider, C. A., W. S. Rasband and K. W. Eliceiri** (2012). "NIH Image to ImageJ: 25 years of image analysis." *Nature Methods* **9**(7): 671-675.
- Schottkowski, M., S. Gkalypoudis, N. Tzekova, C. Stelljes, D. Schünemann, E. Ankele and J. Nickelsen** (2009). "Interaction of the periplasmic PrtA factor and the PsbA (D1) protein during biogenesis of photosystem II in *Synechocystis* sp. PCC 6803." *J Biol Chem* **284**(3): 1813-1819.
- Schreier, T. B., et al.** (2018). "Plastidial NAD-Dependent Malate Dehydrogenase: A Moonlighting Protein Involved in Early Chloroplast Development through Its Interaction with an FtsH12-FtsHi Protease Complex." *Plant Cell* **30**(8): 1745-1769.
- Schwarz, C., A. V. Bohne, F. Wang, F. J. Cejudo and J. Nickelsen** (2012). "An intermolecular disulfide-based light switch for chloroplast *psbD* gene expression in *Chlamydomonas reinhardtii*." *Plant J* **72**(3): 378-389.
- Schwarz, C., I. Elles, J. Kortmann, M. Piotrowski and J. Nickelsen** (2007). "Synthesis of the D2 protein of photosystem II in *Chlamydomonas* is controlled by a high molecular mass complex containing the RNA stabilization factor Nac2 and the translational activator RBP40." *Plant Cell* **19**(11): 3627-3639.
- Sekine, K., T. Hase and N. Sato** (2002). "Reversible DNA compaction by sulfite reductase regulates transcriptional activity of chloroplast nucleoids." *J Biol Chem* **277**(27): 24399-24404.
- Shine, J. and L. Dalgarno** (1974). "The 3'-terminal sequence of *Escherichia coli* 16S ribosomal RNA: complementarity to nonsense triplets and ribosome binding sites." *Proceedings of the National Academy of Sciences of the United States of America* **71**(4): 1342-1346.
- Shtaida, N., I. Khozin-Goldberg, A. Solovchenko, K. Chekanov, S. Didi-Cohen, S. Leu, Z. Cohen and S. Boussiba** (2014). "Downregulation of a putative plastid PDC E1 $\alpha$  subunit impairs photosynthetic activity and triacylglycerol accumulation in nitrogen-starved photoautotrophic *Chlamydomonas reinhardtii*." *Journal of Experimental Botany* **65**(22): 6563-6576.
- Singh, H., M. R. Shukla, K. V. Chary and B. J. Rao** (2014). "Acetate and bicarbonate assimilation and metabolite formation in *Chlamydomonas reinhardtii*: a <sup>13</sup>C-NMR study." *PLoS One* **9**(9): e106457.

- Smith-Hammond, C. L., E. Hoyos and J. A. Miernyk** (2014). "The pea seedling mitochondrial N<sup>ε</sup>-lysine acetylome." *Mitochondrion* **19**: 154-165.
- Smith-Hammond, C. L., K. N. Swatek, M. L. Johnston, J. J. Thelen and J. A. Miernyk** (2014). "Initial description of the developing soybean seed protein Lys-N<sup>ε</sup>-acetylome." *Journal of Proteomics* **96**: 56-66.
- Soppa, J.** (2010). "Protein Acetylation in Archaea, Bacteria, and Eukaryotes." *Archaea* **2010**: 820681.
- Spalding, M.** (2009). The CO<sub>2</sub>-Concentrating Mechanism and Carbon Assimilation. **2**: 257-301.
- Stengel, A., I. L. Gügel, D. Hilger, B. Rengstl, H. Jung and J. Nickelsen** (2012). "Initial steps of photosystem II *de novo* assembly and preloading with manganese take place in biogenesis centers in *Synechocystis*." *Plant Cell* **24**(2): 660-675.
- Stern, D. B. and R. G. Drager** (1998). Chloroplast RNA Synthesis and Processing. The Molecular Biology of Chloroplasts and Mitochondria in *Chlamydomonas*. J. D. Rochaix, M. Goldschmidt-Clermont and S. Merchant. Dordrecht, Springer Netherlands: 165-181.
- Stern, D. B., M. Goldschmidt-Clermont and M. R. Hanson** (2010). "Chloroplast RNA metabolism." *Annu Rev Plant Biol* **61**: 125-155.
- Stoppel, R., L. Lezhneva, S. Schwenkert, S. Torabi, S. Felder, K. Meierhoff, P. Westhoff and J. Meurer** (2011). "Recruitment of a ribosomal release factor for light- and stress-dependent regulation of *petB* transcript stability in *Arabidopsis* chloroplasts." *Plant Cell* **23**(7): 2680-2695.
- Strittmatter, P., J. Soll and B. Bolter** (2010). "The chloroplast protein import machinery: a review." *Methods Mol Biol* **619**: 307-321.
- Suga, M., et al.** (2015). "Native structure of photosystem II at 1.95 Å resolution viewed by femtosecond X-ray pulses." *Nature* **517**(7532): 99-103.
- Sun, Y., M. Valente-Paterno, S. Bakhtiari, C. Law, Y. Zhan and W. Zerges** (2019). "Photosystem Biogenesis Is Localized to the Translation Zone in the Chloroplast of *Chlamydomonas*." *Plant Cell* **31**(12): 3057-3072.
- Sun, Y. and W. Zerges** (2015). "Translational regulation in chloroplasts for development and homeostasis." *Biochim Biophys Acta* **1847**(9): 809-820.
- Tardif, M., et al.** (2012). "PredAlgo: a new subcellular localization prediction tool dedicated to green algae." *Mol Biol Evol* **29**(12): 3625-3639.
- Theis, J. and M. Schroda** (2016). "Revisiting the photosystem II repair cycle." *Plant signaling & behavior* **11**(9): e1218587-e1218587.
- Thompson, M. D., T. M. Mittelmeier and C. L. Dieckmann** (2017). *Chlamydomonas: The Eyespot. Chlamydomonas: Molecular Genetics and Physiology*. M. Hippler. Cham, Springer International Publishing: 257-281.

- Thompson, P., E. E. Reid, C. R. Lyttle and D. T. Dennis** (1977). "Pyruvate dehydrogenase complex from higher plant mitochondria and proplastids: regulation." *Plant Physiol* **59**(5): 854-858.
- Thormählen, I., T. Meitzel, J. Groysman, A. B. Öchsner, E. von Roepenack-Lahaye, B. Naranjo, F. J. Cejudo and P. Geigenberger** (2015). "Thioredoxin f1 and NADPH-Dependent Thioredoxin Reductase C Have Overlapping Functions in Regulating Photosynthetic Metabolism and Plant Growth in Response to Varying Light Conditions." *Plant Physiology* **169**(3): 1766-1786.
- Tillich, M., S. Beick and C. Schmitz-Linneweber** (2010). "Chloroplast RNA-binding proteins: repair and regulation of chloroplast transcripts." *RNA Biol* **7**(2): 172-178.
- Tovar-Mendez, A., J. A. Miernyk and D. D. Randall** (2003). "Regulation of pyruvate dehydrogenase complex activity in plant cells." *Eur J Biochem* **270**(6): 1043-1049.
- Uniacke, J., D. Colón-Ramos and W. Zerges** (2011). FISH and Immunofluorescence Staining in *Chlamydomonas*. *RNA Detection and Visualization: Methods and Protocols*. J. E. Gerst. Totowa, NJ, Humana Press: 15-29.
- Uniacke, J. and W. Zerges** (2007). "Photosystem II assembly and repair are differentially localized in *Chlamydomonas*." *Plant Cell* **19**(11): 3640-3654.
- Uniacke, J. and W. Zerges** (2009). "Chloroplast protein targeting involves localized translation in *Chlamydomonas*." *Proc Natl Acad Sci U S A* **106**(5): 1439-1444.
- Vaistij, F. E., E. Boudreau, S. D. Lemaire, M. Goldschmidt-Clermont and J. D. Rochaix** (2000). "Characterization of Mbb1, a nucleus-encoded tetratricopeptide-like repeat protein required for expression of the chloroplast *psbB/psbT/psbH* gene cluster in *Chlamydomonas reinhardtii*." *Proc Natl Acad Sci U S A* **97**(26): 14813-14818.
- Vijayakrishnan, S., S. M. Kelly, R. J. Gilbert, P. Callow, D. Bhella, T. Forsyth, J. G. Lindsay and O. Byron** (2010). "Solution structure and characterisation of the human pyruvate dehydrogenase complex core assembly." *J Mol Biol* **399**(1): 71-93.
- Viola, S., M. Cavaiuolo, D. Drapier, S. Eberhard, O. Vallon, F. A. Wollman and Y. Choquet** (2019). "MDA1, a nucleus-encoded factor involved in the stabilization and processing of the *atpA* transcript in the chloroplast of *Chlamydomonas*." *Plant J* **98**(6): 1033-1047.
- Wagner, G. R. and R. M. Payne** (2013). "Widespread and enzyme-independent N<sup>ε</sup>-acetylation and N<sup>ε</sup>-succinylation of proteins in the chemical conditions of the mitochondrial matrix." *J Biol Chem* **288**(40): 29036-29045.
- Wagner, V., G. Gessner, I. Heiland, M. Kaminski, S. Hawat, K. Scheffler and M. Mittag** (2006). "Analysis of the phosphoproteome of *Chlamydomonas reinhardtii* provides new insights into various cellular pathways." *Eukaryotic cell* **5**(3): 457-468.
- Wang, D., N. Kon, G. Lasso, L. Jiang, W. Leng, W.-G. Zhu, J. Qin, B. Honig and W. Gu** (2016). "Acetylation-regulated interaction between p53 and SET reveals a widespread regulatory mode." *Nature* **538**(7623): 118-122.

- Wang, F., X. Johnson, M. Cavaiuolo, A. V. Bohne, J. Nickelsen and O. Vallon (2015). "Two Chlamydomonas OPR proteins stabilize chloroplast mRNAs encoding small subunits of photosystem II and cytochrome *b<sub>6</sub>f*." *Plant J* **82**(5): 861-873.
- Wang, H., B. Gau, W. O. Slade, M. Juergens, P. Li and L. M. Hicks (2014). "The global phosphoproteome of *Chlamydomonas reinhardtii* reveals complex organellar phosphorylation in the flagella and thylakoid membrane." *Mol Cell Proteomics* **13**(9): 2337-2353.
- Wang, Y., D. J. Stessman and M. H. Spalding (2015). "The CO<sub>2</sub> concentrating mechanism and photosynthetic carbon assimilation in limiting CO<sub>2</sub>: how *Chlamydomonas* works against the gradient." *The Plant Journal* **82**(3): 429-448.
- Wang, Z.-X., R.-S. Hu, C.-X. Zhou, J.-J. He, H. M. Elsheikha and X.-Q. Zhu (2019). "Label-Free Quantitative Acetylome Analysis Reveals *Toxoplasma gondii* Genotype-Specific Acetylomic Signatures." *Microorganisms* **7**(11): 510.
- Wang, Z. and C. Benning (2012). "Chloroplast lipid synthesis and lipid trafficking through ER-plastid membrane contact sites." *Biochem Soc Trans* **40**(2): 457-463.
- Wienken, C. J., P. Baaske, U. Rothbauer, D. Braun and S. Duhr (2010). "Protein-binding assays in biological liquids using microscale thermophoresis." *Nature Communications* **1**(1): 100.
- Wollman, F. A., L. Minai and R. Nechushtai (1999). "The biogenesis and assembly of photosynthetic proteins in thylakoid membranes." *Biochim Biophys Acta* **1411**(1): 21-85.
- Wostrikoff, K., J. Girard-Bascou, F. A. Wollman and Y. Choquet (2004). "Biogenesis of PSI involves a cascade of translational autoregulation in the chloroplast of *Chlamydomonas*." *EMBO J* **23**(13): 2696-2705.
- Wunder, T., Z. G. Oh and O. Mueller-Cajar (2019). "CO<sub>2</sub> -fixing liquid droplets: Towards a dissection of the microalgal pyrenoid." *Traffic* **20**(6): 380-389.
- Xing, S. and Y. Poirier (2012). "The protein acetylome and the regulation of metabolism." *Trends Plant Sci* **17**(7): 423-430.
- Xiong, J. and C. E. Bauer (2002). "Complex evolution of photosynthesis." *Annu Rev Plant Biol* **53**: 503-521.
- Yamaguchi, K., M. V. Beligni, S. Prieto, P. A. Haynes, W. H. McDonald, J. R. Yates and S. P. Mayfield (2003). "Proteomic Characterization of the *Chlamydomonas reinhardtii* Chloroplast Ribosome: Identification of Proteins Unique to the 70 S Ribosome." *Journal of Biological Chemistry* **278**(36): 33774-33785.
- Yan, Z., Z. Shen, Z.-F. Gao, Q. Chao, C.-R. Qian, H. Zheng and B.-C. Wang (2020). "A comprehensive analysis of the lysine acetylome reveals diverse functions of acetylated proteins during de-etiolation in *Zea mays*." *Journal of Plant Physiology* **248**: 153158.
- Yang, C., J. Wu, S. H. Sinha, J. M. Neveu and Y. G. Zheng (2012). "Autoacetylation of the MYST lysine acetyltransferase MOF protein." *J Biol Chem* **287**(42): 34917-34926.

- Yang, D., J. Song, T. Wagenknecht and T. E. Roche** (1997). "Assembly and full functionality of recombinantly expressed dihydrolipoyl acetyltransferase component of the human pyruvate dehydrogenase complex." *J Biol Chem* **272**(10): 6361-6369.
- Yang, W., et al.** (2014). "Alternative acetate production pathways in *Chlamydomonas reinhardtii* during dark anoxia and the dominant role of chloroplasts in fermentative acetate production." *The Plant Cell* **26**(11): 4499-4518.
- Yehudai-Resheff, S., S. L. Zimmer, Y. Komine and D. B. Stern** (2007). "Integration of chloroplast nucleic acid metabolism into the phosphate deprivation response in *Chlamydomonas reinhardtii*." *The Plant Cell* **19**(3): 1023.
- Zerges, W. and J. D. Rochaix** (1998). "Low density membranes are associated with RNA-binding proteins and thylakoids in the chloroplast of *Chlamydomonas reinhardtii*." *The Journal of cell biology* **140**(1): 101-110.
- Zhan, Y., et al.** (2018). "Pyrenoid functions revealed by proteomics in *Chlamydomonas reinhardtii*." *PLoS One* **13**(2): e0185039.
- Zhang, K., S. Zheng, J. S. Yang, Y. Chen and Z. Cheng** (2013). "Comprehensive Profiling of Protein Lysine Acetylation in *Escherichia coli*." *Journal of Proteome Research* **12**(2): 844-851.
- Zhao, S., et al.** (2010). "Regulation of Cellular Metabolism by Protein Lysine Acetylation." *Science* **327**(5968): 1000-1004.
- Zhou, Z. H., D. B. McCarthy, C. M. O'Connor, L. J. Reed and J. K. Stoops** (2001). "The remarkable structural and functional organization of the eukaryotic pyruvate dehydrogenase complexes." *Proc Natl Acad Sci U S A* **98**(26): 14802-14807.
- Zimmer, S. L., A. Schein, G. Zipor, D. B. Stern and G. Schuster** (2009). "Polyadenylation in Arabidopsis and *Chlamydomonas* organelles: the input of nucleotidyltransferases, poly(A) polymerases and polynucleotide phosphorylase." *Plant J* **59**(1): 88-99.

## VI. APPENDIX

Supplemental Table S1: Oligonucleotides used in this study.

| Construct / Description  | Oligonucleotide name and sequence (5'→3')   | Protein    | Amino acid coverage     |
|--------------------------|---|------------|-------------------------|
| pSUMO: DLA2 WT           | DLA2 cDNA fw 2 <i>Bam</i> HI (TGGTGGATCCAATGCGGTTAAAGA)<br>DLA2 cDNA rev <i>Sal</i> I (CTCGAGGCGCGTCGACGAATTCTTA)   | DLA2       | Aa 32-494 <sup>e</sup>  |
| pSUMO: DLA2 ΔLip         | DLA2-Lip fw <i>Bam</i> HI (GGATCCGAAGAGGCGAAAAAGAAAGC)<br>DLA2 cDNA rev <i>Sal</i> I (CTCGAGGCGCGTCGACGAATTCTTA)  | ΔLip       | Aa 116-494 <sup>e</sup> |
| pSUMO: DLA2 ΔE3B         | DLA2 cDNA fw 2 <i>Bam</i> HI (TGGTGGATCCAATGCGGTTAAAGA)<br>DLA2-E3B rev <i>Sal</i> I (GTCGACCCCGTCTGCACGGCCAAC)   | ΔE3B       | Aa 32-184 <sup>e</sup>  |
| pSUMO: DLA2 ΔE3B         | DLA2-E3B fw <i>Sal</i> I (5'-GTCGACGCAGCAGGCAAGGCTGTT)<br>DLA2 cDNA rev <i>Sal</i> I (5'-CTCGAGGCGCGTCGACGAATTCTTA)   | ΔE3B       | Aa 224-494 <sup>e</sup> |
| pSUMO: DLA2 ΔCat Aa461   | DLA2 cDNA fw 2 <i>Bam</i> HI (TGGTGGATCCAATGCGGTTAAAGA)<br>DLA2 Cat Domain rev4 <i>Sal</i> I (GCTGTCGACTTAGACGTTTCATAACCTTCTTAACAC)   | ΔCat Aa461 | Aa 32-461 <sup>e</sup>  |
| pSUMO: DLA2 ΔCat Aa449   | DLA2 cDNA fw 2 <i>Bam</i> HI (TGGTGGATCCAATGCGGTTAAAGA)<br>DLA2 Cat Domain rev3 <i>Sal</i> I (GCTGTCGACTTAGCGGAGACGCCACAACGGT)  | ΔCat Aa449 | Aa 32-449 <sup>e</sup>  |
| pSUMO: DLA2 ΔCat Aa393   | DLA2 cDNA fw 2 <i>Bam</i> HI (TGGTGGATCCAATGCGGTTAAAGA)<br>DLA2 Cat Domain rev2 <i>Sal</i> I (GCTGTCGACTTAGACGTTTCAGGCCCAGTT)   | ΔCat Aa393 | Aa 32-393 <sup>e</sup>  |
| pSUMO: DLA2 ΔCat Aa314   | DLA2 cDNA fw 2 <i>Bam</i> HI (TGGTGGATCCAATGCGGTTAAAGA)<br>DLA2 Cat Domain rev1 <i>Sal</i> I (GCTGTCGACTTAGACGTTTCAGGCCCAGTT)   | ΔCat Aa314 | Aa 32-314 <sup>e</sup>  |
| pSUMO: DLA2 ΔCat Domain  | DLA2 cDNA fw 2 <i>Bam</i> HI (TGGTGGATCCAATGCGGTTAAAGA)<br>DLA2-Cat rev <i>Sal</i> I (GTCGACCTCGAGTTAGAGTTTCGGAGACCGTGGTA)  | ΔCat       | Aa 32-269 <sup>e</sup>  |
| pSumo: DLA2 K193R        | DLA2 K193R fw (GGTCCTTGCCAGCTGACGGGCATACGGGGTAGCC)<br>DLA2 K193R rev (GGTACCCCGTATGCCCGTCAGCTGGCCAAGGACC)   | DLA2 K193R | Aa 32-494 <sup>e</sup>  |
| pSumo: DLA2 K193Q        | DLA2 K193Q fw (CTTGCCAGCTGTTGGGCATACGGGGTAG)<br>DLA2 K193Q rev (CTACCCCGTATGCCCAACAGCTGGCCAAG)  | DLA2 K193Q | Aa 32-494 <sup>e</sup>  |
| pSumo: DLA2 K197R        | DLA2 K197R fw (CCAGGTCCACTTTCAGGTCACGGGCCAGCTGTTGGCATAAC)<br>DLA2 K197R rev (GTATGCCAAACAGCTGGCCCGTGACCTGAAAGTGGACCTGG)   | DLA2 K197R | Aa 32-494 <sup>e</sup>  |
| pSumo: DLA2 K197Q        | DLA2 K197Q fw (CCACTTTCAGGTCCTGGGCCAGCTGTTTGGC)<br>DLA2 K197Q rev (GCCAAACAGCTGGCCAGGACCTGAAAGTGG)  | DLA2 K197Q | Aa 32-494 <sup>e</sup>  |
| pSumo: DLA2 K200R        | DLA2 K200R fw (GGTCCTTGCCAGCTGACGGGCATACGGGGTAGCC)<br>DLA2 K200R rev (GCTGGCCAAGGACCTGCGTGTGGACCTGGCGACTG)  | DLA2 K200R | Aa 32-494 <sup>e</sup>  |
| pSumo: DLA2 K200Q        | DLA2 K200Q fw (GCCAGGTCCACTTGCAGGTCCTTGCC)<br>DLA2 K200Q rev (GGCCAAGGACCTGCAAGTGGACCTGGC)  | DLA2 K200Q | Aa 32-494 <sup>e</sup>  |
| pBC1:DLA2-HA             | DLA2 5' UTR fw <i>Bam</i> HI (GGATCCCTGGGGCTTGCCGATCATT)<br>DLA2 Exon 3 rev <i>Sfi</i> I (AGTGATGCGGCCGTTGGG)   |            |                         |
| pBC1:DLA2 cDNA-HA        | DLA2 fw <i>Nde</i> I (AACATATGCAGGCCACGACCCG)<br>DLA2-3xHA rev <i>Eco</i> RI (GAATTCCTTAGGCGTAGTCCGGCACGTCGTACGGGTAGG<br>CGTAGTCCGGCACGTCGTACGGGTAGGCGTAGTCCGGCACGTCGTACGGGTACA<br>GCAGCTGGTCCGGGT) |            |                         |
| pBC1: DLA2 K193Q-HA      | DLA2 gDNA K193Q fw (GCGACCCCTACGCTCAGCAGCTGG)<br>DLA2 gDNA K193Q rev (CCAGTGTGAGCGTAGGGGGTTCG)  |            |                         |
| pBC1: DLA2 K197R-HA      | DLA2 gDNA K197R fw (TCACCTTCAGGTCCTAGCCAGCTGCTTAGC)<br>DLA2 gDNA K197R rev (GCTAAGCAGCTGGCTAGGGACCTGAAGGTGA)  |            |                         |
| pBC1: DLA2 K197Q-HA      | DLA2 gDNA K197Q fw (CTTCAGGTCCTGAGCCAGCTGCTTAGCGTAGGG)<br>DLA2 gDNA K197Q rev (CCCTACGCTAAGCAGCTGGCTCAGGACCTGAAG)   |            |                         |
| pBC1: DLA2 K200Q-HA      | DLA2 gDNA K200Q fw (TGGCTAAGGACCTGCAGGTGACTGGGTTCG)<br>DLA2 gDNA K200Q rev (CGACCCAGTCACTGCAGGTCTTAGCCA)  |            |                         |
| CRISPR mutation oligo    | EMX1-1-FLAGv3 insert (TTAGCTAAGCCTCCCAAAGCCTGGCCAGGGTCTAG)<br>EMX1-1-FLAGv3 insert RC (CTAGACCTGGCCAGGCTTTGGGGAGGCTTAGCTAA)   |            |                         |
| CRISPR mutant screen     | DLA2 short locus fw (CCGCGTGCCCGCCAAGTC)<br>DLA2 short locus rev (GCCTCGCCCTTCTTGACCTTGT)   |            |                         |
| CRISPR mutant generation | DLA2 KO crRNA (UGUUCUGGUGUCCCCAACG + 16 bp complementary to the tracrRNA)   |            |                         |

Restriction sites introduced for cloning are underlined. Amino acid coverage given is related to the *C. reinhardtii* protein sequences obtained from Phytozome (v5.5): <sup>a</sup>PDH2, Cre03.g194200; <sup>b</sup>DLD2, Cre01.g016514; <sup>c</sup>DLA2, Cre03.g158900. The *Synechocystis* sp. PCC 6803 protein sequence of <sup>p</sup>ratA (*slr2048*) was obtained from cyanobase.

**Supplemental Table S2: Plasmids used in this study.**

| Plasmid                 | Description   | Reference  |
|-------------------------|---|--|
| pJET1.2/blunt           | Cloning vector; confers ampicillin resistance in <i>E. coli</i>   | Thermo Fisher Scientific   |
| pET28-Sumo              | pET28 vector for the expression of recombinant 6xHis-Sumo fusion proteins in <i>E. coli</i> ; confers kanamycin resistance in <i>E. coli</i>  | Bepperling et al. (2012)   |
| pARG7 (pHR11)           | Contains ARG7 gene for complementation of arginine auxotrophic <i>C. reinhardtii</i> strains; confers ampicillin resistance in <i>E. coli</i>   | Nour-Eldin et al. (2016); Chlamydomonas resource center                            |
| pBC1-CrGFP              | pBC1 expression vector containing the <i>C. reinhardtii</i> codon adapted GFP coding sequence (CrGFP) under control of the <i>PsaD</i> 5' and 3' UTRs; confers paromomycin resistance in <i>C. reinhardtii</i>  | Neupert et al. (2009)  |
| pSUMO: DLA2 WT          | pSumo vector containing the <i>DLA2</i> cDNA codon adapted to <i>E. coli</i> . For overexpression of the recombinant DLA2 protein.  | Generated during this work and used for MST analysis.                              |
| pSUMO: DLA2 ΔLip        | pSumo vector containing part of the <i>DLA2</i> cDNA codon adapted to <i>E. coli</i> . For overexpression of the recombinant DLA2 protein without the lipoyl domain.  | Generated during this work and used for MST analysis.                              |
| pSUMO: DLA2 ΔE3B        | pSumo vector containing part of the <i>DLA2</i> cDNA codon adapted to <i>E. coli</i> . For overexpression of the recombinant DLA2 protein without the E3-binding domain.  | Generated during this work and used for MST analysis.                              |
| pSUMO: DLA2 ΔCat Aa461  | pSumo vector containing part of the <i>DLA2</i> cDNA codon adapted to <i>E. coli</i> . For overexpression of the recombinant DLA2 protein with a truncated catalytic domain.  | Generated during this work and used for MST analysis.                              |
| pSUMO: DLA2 ΔCat Aa449  | pSumo vector containing part of the <i>DLA2</i> cDNA codon adapted to <i>E. coli</i> . For overexpression of the recombinant DLA2 protein with a truncated catalytic domain.  | Generated during this work and used for MST analysis.                              |
| pSUMO: DLA2 ΔCat Aa393  | pSumo vector containing part of the <i>DLA2</i> cDNA codon adapted to <i>E. coli</i> . For overexpression of the recombinant DLA2 protein with a truncated catalytic domain.  | Generated during this work and used for MST analysis.                              |
| pSUMO: DLA2 ΔCat Aa314  | pSumo vector containing part of the <i>DLA2</i> cDNA codon adapted to <i>E. coli</i> . For overexpression of the recombinant DLA2 protein with a truncated catalytic domain.  | Generated during this work and used for MST analysis.                              |
| pSUMO: DLA2 ΔCat Domain | pSumo vector containing part of the <i>DLA2</i> cDNA codon adapted to <i>E. coli</i> . For overexpression of the recombinant DLA2 protein without the catalytic domain.   | Generated during this work and used for MST analysis.                              |
| pSUMO: Prata            | pSumo vector containing the PrataA cDNA from <i>Synechocystis</i> spp. For overexpression of the recombinant PrataA protein.  | (Heinz et al., manuscript in preparation)  |
| pSUMO: DLA2 K193R       | pSumo vector containing the <i>DLA2</i> cDNA codon adapted to <i>E. coli</i> with a single nucleotide mutation leading to an amino acid change. For overexpression of the recombinant DLA2 protein with K193 mutated to R.  | Generated during this work and used for MST analysis.                              |
| pSUMO: DLA2 K193Q       | pSumo vector containing the <i>DLA2</i> cDNA codon adapted to <i>E. coli</i> with a single nucleotide mutation leading to an amino acid change. For overexpression of the recombinant DLA2 protein with K193 mutated to Q.  | Generated during this work and used for MST analysis.                              |
| pSUMO: DLA2 K197R       | pSumo vector containing the <i>DLA2</i> cDNA codon adapted to <i>E. coli</i> with a single nucleotide mutation leading to an amino acid change. For overexpression of the recombinant DLA2 protein with K197 mutated to R.  | Generated during this work and used for MST analysis.                              |
| pSUMO: DLA2 K197Q       | pSumo vector containing the <i>DLA2</i> cDNA codon adapted to <i>E. coli</i> with a single nucleotide mutation leading to an amino acid change. For overexpression of the recombinant DLA2 protein with K197 mutated to Q.  | Generated during this work and used for MST analysis.                              |
| pSUMO: DLA2 K200R       | pSumo vector containing the <i>DLA2</i> cDNA codon adapted to <i>E. coli</i> with a single nucleotide mutation leading to an amino acid change. For overexpression of the recombinant DLA2 protein with K200 mutated to R.  | Generated during this work and used for MST analysis.                              |
| pSUMO: DLA2 K200Q       | pSumo vector containing the <i>DLA2</i> cDNA codon adapted to <i>E. coli</i> with a single nucleotide mutation leading to an amino acid change. For overexpression of the recombinant DLA2 protein with K200 mutated to Q.  | Generated during this work and used for MST analysis.                              |
| pBC1:DLA2-HA            | pBC1 vector containing the 5' UTR, the whole cDNA and the first two introns of the <i>DLA2</i> gene. A triple HA-tag sequence was added to the end of the last exon for the expression of a HA-tagged version of the native DLA2 protein in <i>C. reinhardtii</i> . | Generated during this work and used for complementation of the <i>dla2</i> mutant. |
| pBC1: DLA2 K197R-HA     | pBC1:DLA2-HA vector with a single nucleotide mutation leading to an amino acid change. For expression of a DLA2 protein with K197 mutated to R in <i>C. reinhardtii</i> .   | Generated during this work and used for complementation of the <i>dla2</i> mutant. |
| pBC1: DLA2 K197Q-HA     | pBC1:DLA2-HA vector with a single nucleotide mutation leading to an amino acid change. For expression of a DLA2 protein with K197 mutated to Q in <i>C. reinhardtii</i> .   | Generated during this work and used for complementation of the <i>dla2</i> mutant. |

|                     |   |  |
|---------------------|---|--|
| pBC1: DLA2 K193Q-HA | pBC1:DLA2-HA vector with a single nucleotide mutation leading to an amino acid change. For expression of a DLA2 protein with K193 mutated to Q in <i>C. reinhardtii</i> . | Generated during this work and used for complementation of the <i>dla2</i> mutant. |
| pBC1: DLA2 K200Q-HA | pBC1:DLA2-HA vector with a single nucleotide mutation leading to an amino acid change. For expression of a DLA2 protein with K200 mutated to Q in <i>C. reinhardtii</i> . | Generated during this work and used for complementation of the <i>dla2</i> mutant. |

**Supplemental Table S3: Mass spectrometry analysis of K-acetylation sites within DLA2 under various growth conditions.**

| Acetyl (K) Peptides | Position in peptide | Position within protein | Hetero / Photo R1 | Hetero / Photo R2 | Hetero / Photo R3 | average log2 fold change | -LOG10 p-value |
|---------------------|---------------------|-------------------------|-------------------|-------------------|-------------------|--------------------------|----------------|
| NVGDK(ac)VK         | 5                   | 61                      | -0.43059          | -0.17007          | -0.12644          | -0.24237                 | 0.95762        |
| QLAK(ac)DLK         | 4                   | 197                     | 1.98554           | 1.53057           | 1.46450           | 1.66020                  | <b>5.32110</b> |
| LDALYQQLK(ac)PK     | 9                   | 315                     | -0.56648          |                   | -0.13396          | -0.35022                 | 1.16801        |
| NWADLVK(ac)R        | 7                   | 394                     | -0.04561          | 0.11250           | -0.07066          | -0.00126                 | 0.00318        |
|                     |                     |                         | Mixo / Photo R1   | Mixo / Photo R2   | Mixo / Photo R3   |                          |                |
| NVGDK(ac)VK         | 5                   | 61                      | -0.02803          | -1.49932          | 0.28588           | -0.41382                 | 0.62918        |
| QLAK(ac)DLK         | 4                   | 197                     | 2.15721           | 1.67577           | 2.24393           | 2.02564                  | <b>3.41925</b> |
| LDALYQQLK(ac)PK     | 9                   | 315                     | -0.53349          |                   | -1.08617          | -0.80983                 | 1.11660        |
| NWADLVK(ac)R        | 7                   | 394                     | -0.91667          | -0.47945          | -0.49344          | -0.62986                 | 1.05347        |
|                     |                     |                         | Hetero / Mixo R1  | Hetero / Mixo R2  | Hetero / Mixo R3  |                          |                |
| NVGDK(ac)VK         | 5                   | 61                      | -0.26111          | 1.62491           | -0.09653          | 0.42242                  | 0.54259        |
| QLAK(ac)DLK         | 4                   | 197                     | -0.05561          | -0.03295          | -0.43381          | -0.17412                 | 0.19720        |
| LDALYQQLK(ac)PK     | 9                   | 315                     | 0.21245           |                   | 1.01768           | 0.61507                  | 0.69757        |
| NWADLVK(ac)R        | 7                   | 394                     | 0.91007           | 0.70689           | 0.41585           | 0.67760                  | 1.02233        |

Identified acetylated peptides are given together with their log<sub>2</sub> fold change in three biological replicates. Positions of acetylated lysins within the protein correspond to the *C. reinhardtii* protein sequence (Cre03.g158900) obtained from Phytozome (v5.5). Comparison of heterotrophic to photoautotrophic growth conditions (Hetero / Photo) is marked in blue. Comparison of mixotrophic to photoautotrophic growth conditions (Mixo / Photo) is marked in green. Comparison of heterotrophic to mixotrophic growth conditions (Hetero / Mixo) is marked in orange. High values are marked in red and low values in blue. -LOG<sub>10</sub> p-values indicating significance of the corresponding log<sub>2</sub> fold change are written in bold numbers ( $p < 0.05$ ). Acetylome analysis was performed in collaboration with the group of Prof. Dr. Iris Finkemeier (Westfälische Wilhelms-Universität Münster)

**Supplemental Table S4: Mass spectrometry analysis of DLA2 protein abundance under various growth conditions.**

| Protein IDs | Protein name | Peptides | Unique peptides | Sequence coverage [%] | Score  | Hetero / Photo   |                | Mixo / Photo     |                | Hetero / Mixo    |                |
|-------------|--------------|----------|-----------------|-----------------------|--------|------------------|----------------|------------------|----------------|------------------|----------------|
|             |              |          |                 |                       |        | log2 fold-change | -LOG10 p-value | log2 fold-change | -LOG10 p-value | log2 fold-change | -LOG10 p-value |
| A8J7F6      | DLA2         | 18       | 18              | 40                    | 105.29 | -0.48113         | <b>2.04915</b> | 0.19334          | 0.66935        | -0.45332         | <b>2.03824</b> |

Values are the mean of three biological replicates. Comparison of heterotrophic to photoautotrophic growth conditions (Hetero / Photo) is marked in blue. Comparison of mixotrophic to photoautotrophic growth conditions (Mixo / Photo) is marked in green. Comparison of heterotrophic to mixotrophic growth conditions (Hetero / Mixo) is marked in orange. High values are marked in red and low values in blue. -LOG10 p-values indicating significance of the corresponding log2 fold change are written in bold numbers ( $p < 0.05$ ). Acetylome analysis was performed in collaboration with the group of Prof. Dr. Iris Finkemeier (Westfälische Wilhelms-Universität Münster)

**Supplemental Table S5: Mass spectrometry analysis of lipids and fatty acids in the cc-3403 strain and the *dla2* knock out mutant under heterotrophic and mixotrophic growth conditions.**

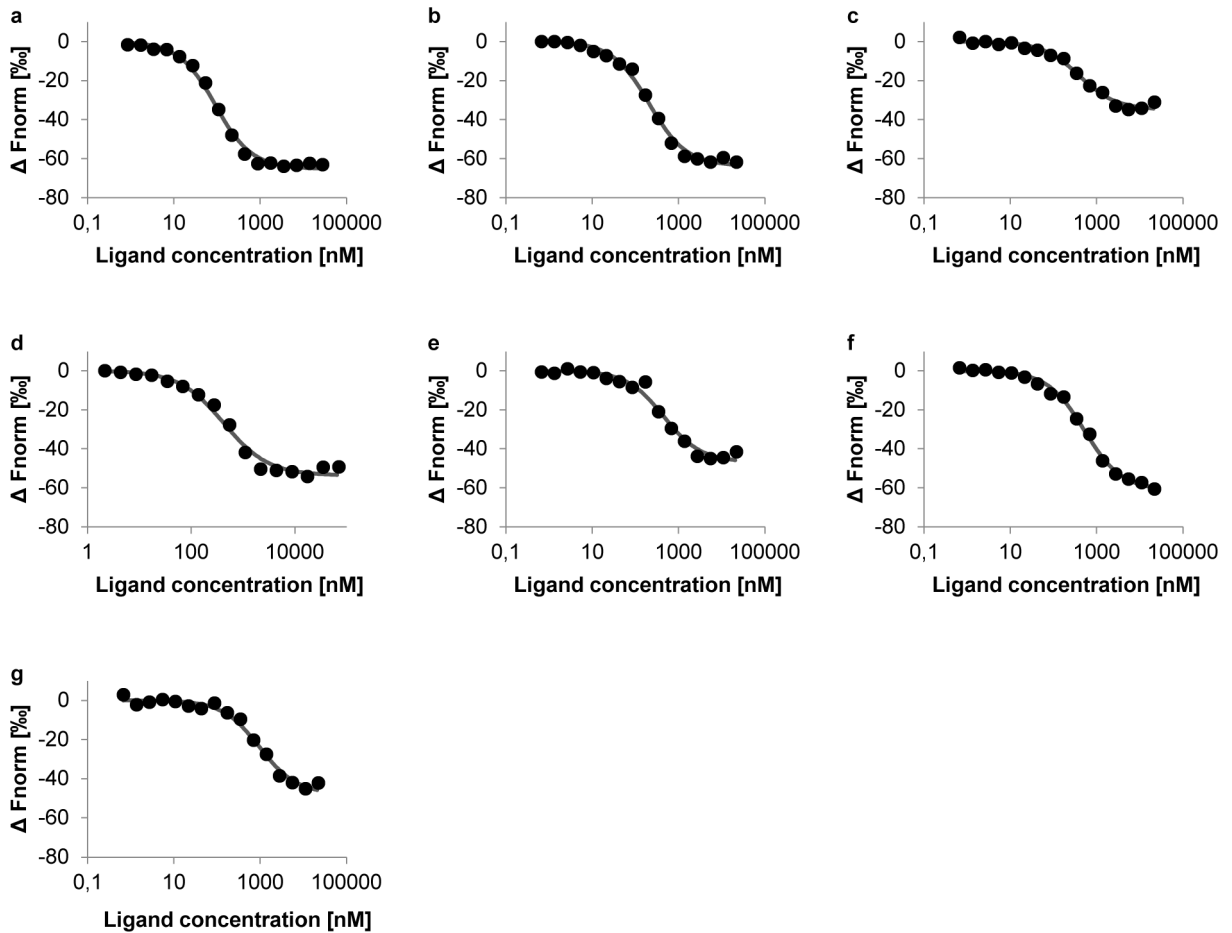
| NAME          | Formula      | Mean        |             |           |             | Stdev       |             |           |             |
|---------------|--------------|-------------|-------------|-----------|-------------|-------------|-------------|-----------|-------------|
|               |              | heterotroph |             | mixotroph |             | heterotroph |             | mixotroph |             |
|               |              | cc-3403     | <i>dla2</i> | cc-3403   | <i>dla2</i> | cc-3403     | <i>dla2</i> | cc-3403   | <i>dla2</i> |
| Chlorophyll a | C55H72N4O5Mg | 1549169     | 1798061     | 967520    | 921092      | 134604      | 39698       | 10968     | 27006       |
| Chlorophyll b | C55H70N4O6Mg | 331174      | 382373      | 247022    | 235517      | 31746       | 16714       | 8250      | 11269       |
| DAG 34:1      | C37H70O5     | 229596      | 193276      | 90024     | 81022       | 45160       | 22600       | 35016     | 31319       |
| DAG 34:2      | C37H68O5     | 298317      | 322732      | 70841     | 110617      | 21017       | 10438       | 8488      | 17303       |
| DAG 34:3      | C37H66O5     | 181776      | 211634      | 36521     | 62264       | 8794        | 16995       | 3779      | 12686       |
| DAG 34:4      | C37H64O5     | 354576      | 383165      | 134065    | 183277      | 18755       | 15690       | 12701     | 21248       |
| DAG 34:6      | C37H60O5     | 702527      | 792254      | 489377    | 447066      | 27145       | 33160       | 24276     | 18493       |
| DAG 36:1      | C39H74O5     | 5036        | 6157        | 3065      | 3607        | 837         | 165         | 1088      | 1223        |
| DAG 36:3      | C39H70O5     | 2996        | 3725        | 339       | 418         | 198         | 105         | 32        | 30          |
| DAG 36:3      | C39H70O5     | 58998       | 46684       | 32124     | 24970       | 13082       | 9614        | 8828      | 4102        |
| DAG 36:4      | C39H68O5     | 8040        | 8930        | 2296      | 1962        | 1265        | 867         | 250       | 83          |
| DAG 36:5      | C39H66O5     | 10320       | 12277       | 3000      | 2395        | 899         | 945         | 261       | 85          |
| DAG 36:6      | C39H64O5     | 49574       | 58876       | 10514     | 11343       | 6969        | 7407        | 563       | 1378        |
| TAG 54:5      | C57H100O6    | 6289        | 6319        | 173       | 247         | 508         | 1819        | 23        | 79          |
| MGDG 34:5     | C43H72O10    | 98069       | 108248      | 53927     | 53627       | 6516        | 3068        | 3325      | 1675        |
| MGDG 34:6     | C43H70O10    | 103629      | 121070      | 74496     | 68225       | 6198        | 451         | 2900      | 2262        |
| MGDG 36:1     | C45H84O10    | 3983        | 4869        | 3204      | 3703        | 454         | 296         | 429       | 138         |
| MGDG 36:4     | C45H78O10    | 2260        | 2847        | 233       | 275         | 234         | 307         | 14        | 57          |
| DGDG 32:3     | C47H82O15    | 51990       | 91210       | 36302     | 35711       | 11445       | 26053       | 6520      | 3730        |
| DGDG 34:1     | C49H90O15    | 4653        | 4534        | 1816      | 1642        | 601         | 520         | 136       | 141         |
| DGDG 34:2     | C49H88O15    | 2581        | 2860        | 1687      | 1713        | 391         | 262         | 166       | 121         |
| DGDG 34:3     | C49H86O15    | 1461        | 1609        | 1277      | 1203        | 171         | 310         | 58        | 34          |
| DGDG 34:4     | C49H84O15    | 1510        | 1510        | 1283      | 1197        | 257         | 79          | 57        | 106         |
| DGDG 34:5     | C49H82O15    | 315         | 329         | 582       | 511         | 34          | 53          | 20        | 78          |
| DGDG 34:6     | C49H80O15    | 780         | 840         | 2307      | 2155        | 125         | 170         | 124       | 183         |
| DGDG 36:4     | C51H88O15    | 3283        | 3440        | 1836      | 1734        | 768         | 863         | 302       | 334         |
| DGTS 32:1     | C42H79NO7    | 3345840     | 3040503     | 2354434   | 2144444     | 373318      | 86479       | 148120    | 120264      |
| DGTS 32:2     | C42H77NO7    | 231589      | 256575      | 396728    | 345600      | 18600       | 19284       | 24072     | 38291       |
| DGTS 32:3     | C42H75NO7    | 552970      | 649471      | 636913    | 611230      | 41995       | 88174       | 42942     | 15503       |
| DGTS 32:4     | C42H73NO7    | 584934      | 657490      | 786314    | 749362      | 47763       | 107738      | 49910     | 24130       |
| DGTS 32:5     | C42H71NO7    | 38145       | 44348       | 162783    | 96383       | 6028        | 4185        | 13217     | 20420       |
| DGTS 34:1     | C44H83NO7    | 945913      | 1019051     | 395287    | 364647      | 193463      | 215839      | 35355     | 20765       |
| DGTS 34:2     | C44H81NO7    | 7642481     | 8712294     | 4707714   | 4231713     | 755845      | 623530      | 169451    | 460087      |
| DGTS 34:4     | C44H77NO7    | 2955519     | 3113531     | 2233317   | 1977939     | 296076      | 503710      | 102584    | 57038       |
| DGTS 34:5     | C44H75NO7    | 776402      | 839220      | 1028327   | 815651      | 71423       | 43341       | 56089     | 79691       |
| DGTS 34:6     | C44H73NO7    | 424337      | 546015      | 1147390   | 825843      | 60870       | 68320       | 51648     | 128118      |
| DGTS 36:1     | C46H87NO7    | 125448      | 178387      | 214755    | 222364      | 7512        | 12141       | 10987     | 13985       |
| DGTS 36:5     | C46H79NO7    | 3738977     | 3555303     | 2302702   | 1962482     | 306544      | 184362      | 114903    | 195648      |
| DGTS 36:6     | C46H77NO7    | 8709602     | 9242224     | 4880694   | 4095142     | 768364      | 356241      | 37408     | 256627      |
| LysoPE 18:3   | C23H42NO7P   | 15828       | 13546       | 14936     | 17872       | 3425        | 1252        | 3706      | 5251        |
| UAC 1         | C42H76NO8P   | 134996      | 252328      | 174108    | 180933      | 19110       | 29635       | 61736     | 6258        |
| UAC 2         | C42H74NO8P   | 3636        | 5833        | 9489      | 8133        | 332         | 585         | 4409      | 338         |
| UAC 3         | C44H86NO8P   | 14248       | 14716       | 13517     | 11275       | 1496        | 1422        | 159       | 739         |
| UAC 4         | C44H78NO8P   | 9721        | 18335       | 12212     | 10411       | 1430        | 2384        | 4274      | 407         |
| UAC 5         | C44H76NO8P   | 15030       | 31110       | 38365     | 29596       | 1845        | 3820        | 16375     | 3474        |
| UAC 6         | C46H82NO8P   | 3219        | 4262        | 2757      | 2420        | 513         | 453         | 340       | 258         |
| PE 34:3       | C39H72NO8P   | 3018        | 3174        | 1408      | 1402        | 546         | 340         | 425       | 369         |
| PE 34:4       | C39H70NO8P   | 1337        | 1937        | 1523      | 1393        | 255         | 263         | 366       | 174         |
| PE 36:3       | C41H76NO8P   | 353840      | 354493      | 157882    | 160633      | 26301       | 49782       | 38604     | 20777       |
| PE 36:4       | C41H74NO8P   | 13143       | 14388       | 12084     | 11218       | 1052        | 694         | 728       | 768         |
| PE 36:5       | C41H72NO8P   | 2232        | 2515        | 1367      | 1364        | 199         | 622         | 188       | 104         |
| PE 38:3       | C43H80NO8P   | 990613      | 1183132     | 203078    | 334109      | 40572       | 49216       | 17903     | 63987       |
| PE 38:4       | C43H78NO8P   | 1787754     | 1919905     | 670935    | 904910      | 86305       | 89854       | 53915     | 104052      |
| PE 38:5       | C43H76NO8P   | 7579        | 9906        | 5078      | 4187        | 551         | 1989        | 1411      | 287         |
| FA 16:1       | C16H30O2     | 50702       | 54728       | 74409     | 51656       | 11788       | 4251        | 11646     | 8562        |

|         |            |         |         |         |         |        |        |        |        |
|---------|------------|---------|---------|---------|---------|--------|--------|--------|--------|
| FA 18:1 | C18H34O2   | 4149056 | 4417661 | 2658419 | 2817317 | 578272 | 280827 | 160263 | 53009  |
| FA 18:2 | C18H32O2   | 2650556 | 3236282 | 3995312 | 3418212 | 353287 | 154461 | 195657 | 378720 |
| FA 18:3 | C18H30O2   | 6652018 | 7780135 | 5453854 | 5123503 | 844009 | 256048 | 88006  | 175773 |
| FA 20:1 | C20H38O2   | 39173   | 44322   | 55685   | 61650   | 7271   | 1283   | 4301   | 6236   |
| FA 20:2 | C20H36O2   | 11038   | 12128   | 30524   | 30534   | 2187   | 484    | 2259   | 4644   |
| FA 22:1 | C21H41COOH | 1111    | 950     | 405     | 434     | 242    | 192    | 71     | 43     |
| FA 22:4 | C21H35COOH | 1216    | 1337    | 2342    | 1821    | 389    | 475    | 372    | 294    |
| FA 16:0 | C16H32O2   | 3080089 | 3339523 | 2718213 | 2047928 | 8008   | 196104 | 354169 | 301767 |
| FA 18:0 | C18H36O2   | 3925507 | 3706889 | 2533618 | 1700969 | 115385 | 356802 | 665725 | 413847 |
| FA 20:0 | C20H40O2   | 107046  | 78570   | 33579   | 18569   | 17345  | 7627   | 16349  | 6485   |
| FA 22:0 | C22H44O2   | 20576   | 11437   | 7703    | 3731    | 6086   | 609    | 4319   | 1122   |
| FA 24:0 | C24H48O2   | 4321    | 3391    | 1840    | 1234    | 728    | 322    | 739    | 209    |

Mean and standard deviation (Stdev) of three biological replicates are given. Lipids were identified according to their retention time and the respective specific. Numbers behind the lipids and fatty acids (FA) indicate the number of carbon atoms followed by the number of double bonds. Lipids are: DAG, diacylglycerol; MGDG, monogalactosyldiacylglycerol; DGDG, digalactosyldiacylglycerol; DGTS, diacylglyceryl-3-O-4'-(N,N,N-trimethyl)-homoserine; UAC, unknown apolar compound; PE, phosphatidylethanolamine. Mass spectrometry was performed by Dr. Martin Lehmann of the mass spec service unit of the LMU (MSBioLMU).

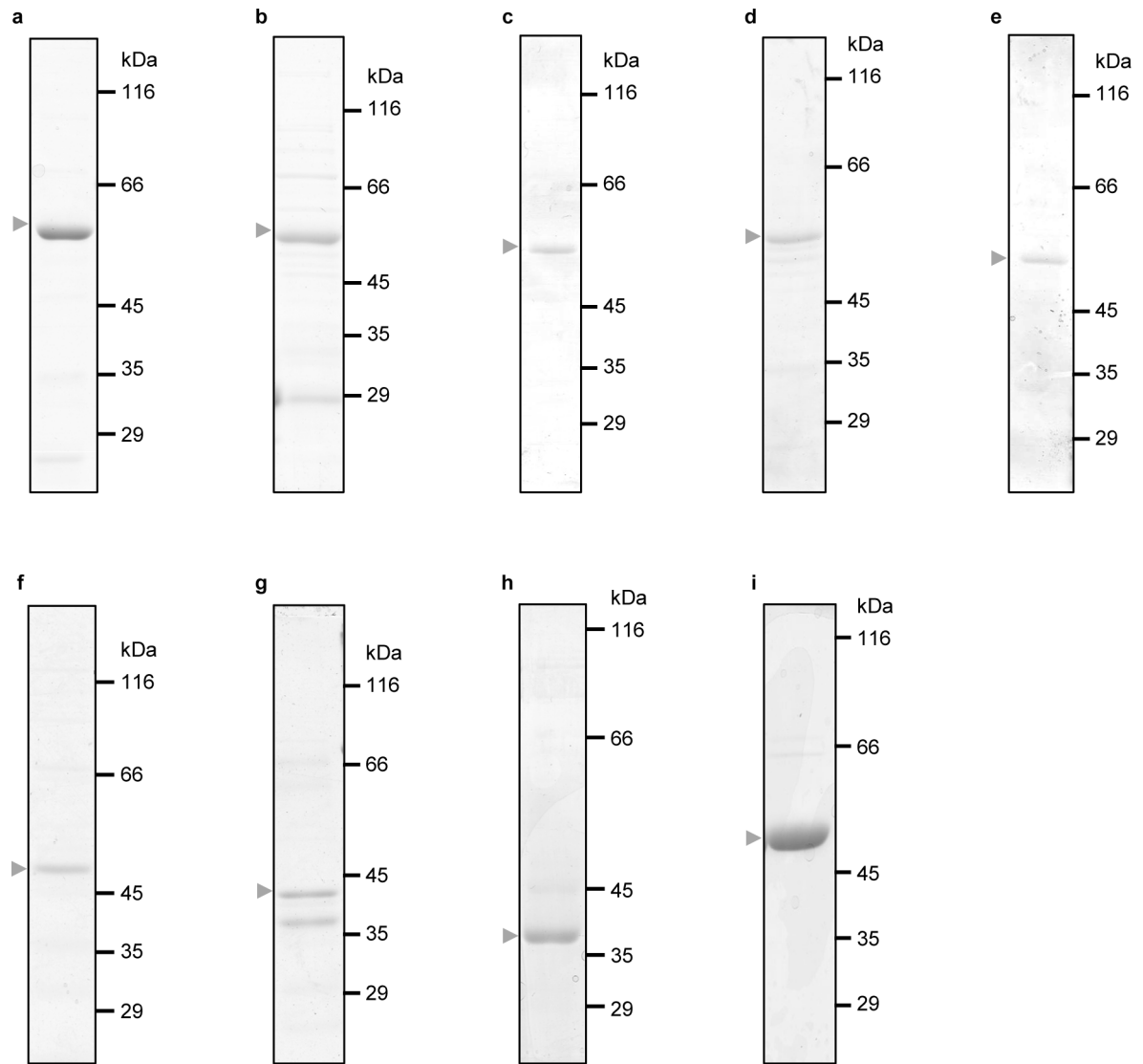
**Supplemental Table 6: Doubling times of the DLA2-HA strain, the *dla2* knock out mutant as well as the K197 acetylation mutants under mixotrophic growth conditions illuminated with  $100 \mu\text{E m}^{-2}\text{s}^{-1}$  of light. Values are means from at least 3 biological replicates.**

| <b>strain</b> | <b>doubling time [h]</b> |
|---------------|--------------------------|
| DLA2-HA       | $10.2 \pm 0.4$           |
| <i>dla2</i>   | $9.8 \pm 0.5$            |
| K197Q-HA      | $9.8 \pm 0.4$            |
| K197R-HA      | $10.0 \pm 0.5$           |



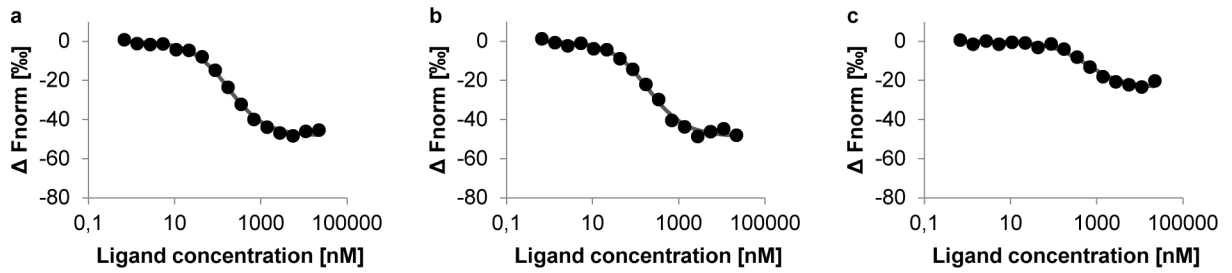
**Supplemental Figure S1: MST-binding curves resulting from interaction of the DLA2 mutant versions with the native *psbA* 5'-UTR probe.**

Binding curves for the (a)  $\Delta$ Lip, (b)  $\Delta$ E3B, (c)  $\Delta$ Cat 462, (d)  $\Delta$ Cat 450, (e)  $\Delta$ Cat 394, (f)  $\Delta$ Cat 315 and (g) the  $\Delta$ Cat protein to a Cy5-labeled RNA probe are shown. Evaluation of MST traces in respect to differences in fluorescence ( $\Delta$ Fnorm) was done after 15 sec and is depicted as black dots while the „Fit“ generated by the NanoTemper software is displayed as a dark grey line. Curves are representative for 3 independent experiments.



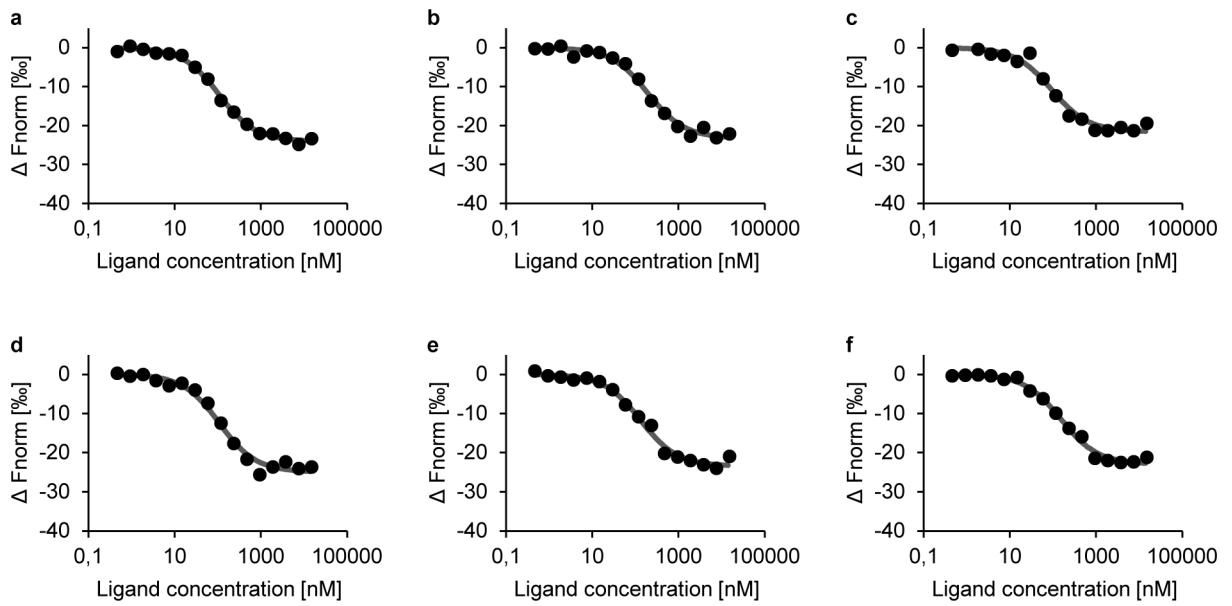
**Supplemental Figure S2: Coomassie brilliant blue-stained SDS gels demonstrating the purification of recombinant proteins used for MST analysis.**

Elution fractions of recombinant (a) wild-type DLA2, (b)  $\Delta$ Lip, (c)  $\Delta$ E3B, (d)  $\Delta$ Cat 315, (e)  $\Delta$ Cat 394, (f)  $\Delta$ Cat 450, (g)  $\Delta$ Cat 462, (h)  $\Delta$ Cat and (i) PratA were separated by SDS-PAGE and subsequently stained with Coomassie brilliant blue R-250. Samples were run alongside a molecular mass marker indicated in kDa. The arrow indicates the respective protein.



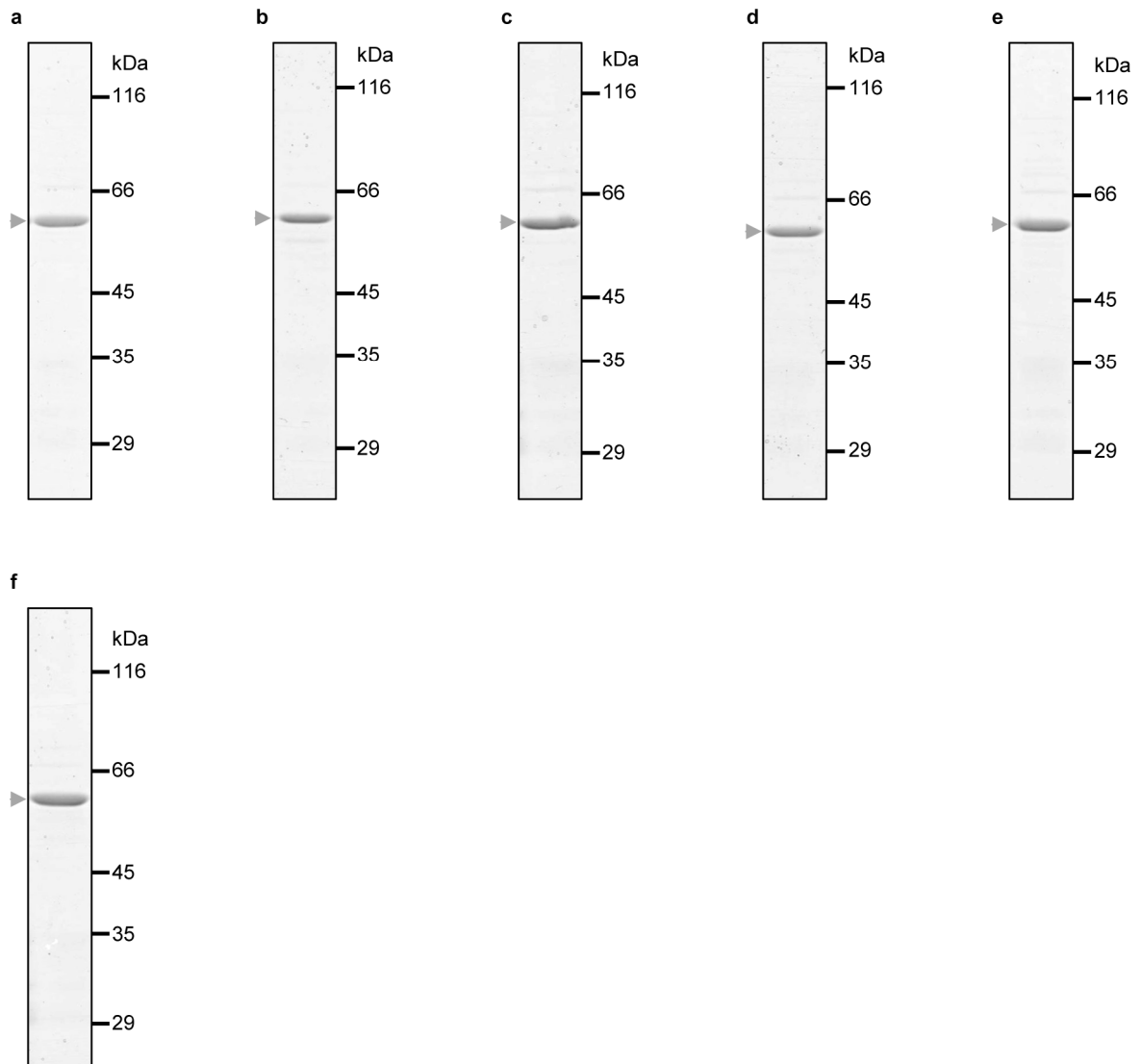
**Supplemental Figure S3: MST-binding curves resulting from interaction of different DLA2 versions with the mutated C-stretch *psbA* probe.**

Binding curves for the (a) wild-type DLA2, (b)  $\Delta E3B$ , and (c)  $\Delta \text{Cat } 462$  protein to the mutated Cy5-labeled RNA probe are shown. Evaluation of MST traces in respect to differences in fluorescence ( $\Delta F_{\text{norm}}$ ) was done after 15 sec and is depicted as black dots while the „Fit“ generated by the NanoTemper software is displayed as a dark grey line. Curves are representative for 3 independent experiments.



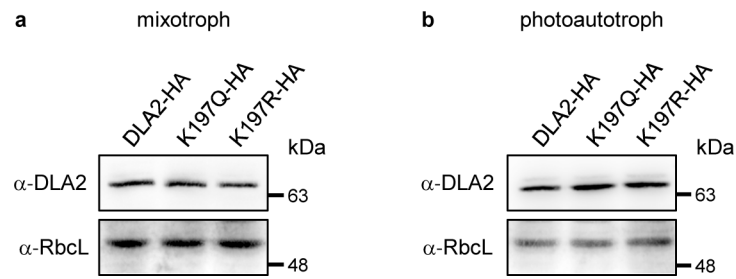
**Supplemental Figure S4: MST-binding curves resulting from interaction of the DLA2 acetylation mutant proteins with the native *psbA* 5'-UTR probe.**

Three lysine residues within the E3BD (K193, K197 and K200) were substituted to arginine or glutamine for mimicking of the deacetylated or acetylated state, respectively. RNA-binding affinity of the DLA2 acetylation mutant proteins to the native *psbA* 5'-UTR probe was determined using MST. Evaluation of MST traces in respect to differences in fluorescence ( $\Delta F_{\text{norm}}$ ) was done after 5 sec and is depicted as black dots while the „Fit“ generated by the NanoTemper software is displayed as a dark grey line. Curves are representative for 3 independent experiments. Shown are the binding curves for the (a) K193R, (b) K193Q, (c) K197R, (d) K197Q, (e) K200R and the (g) K200Q protein.



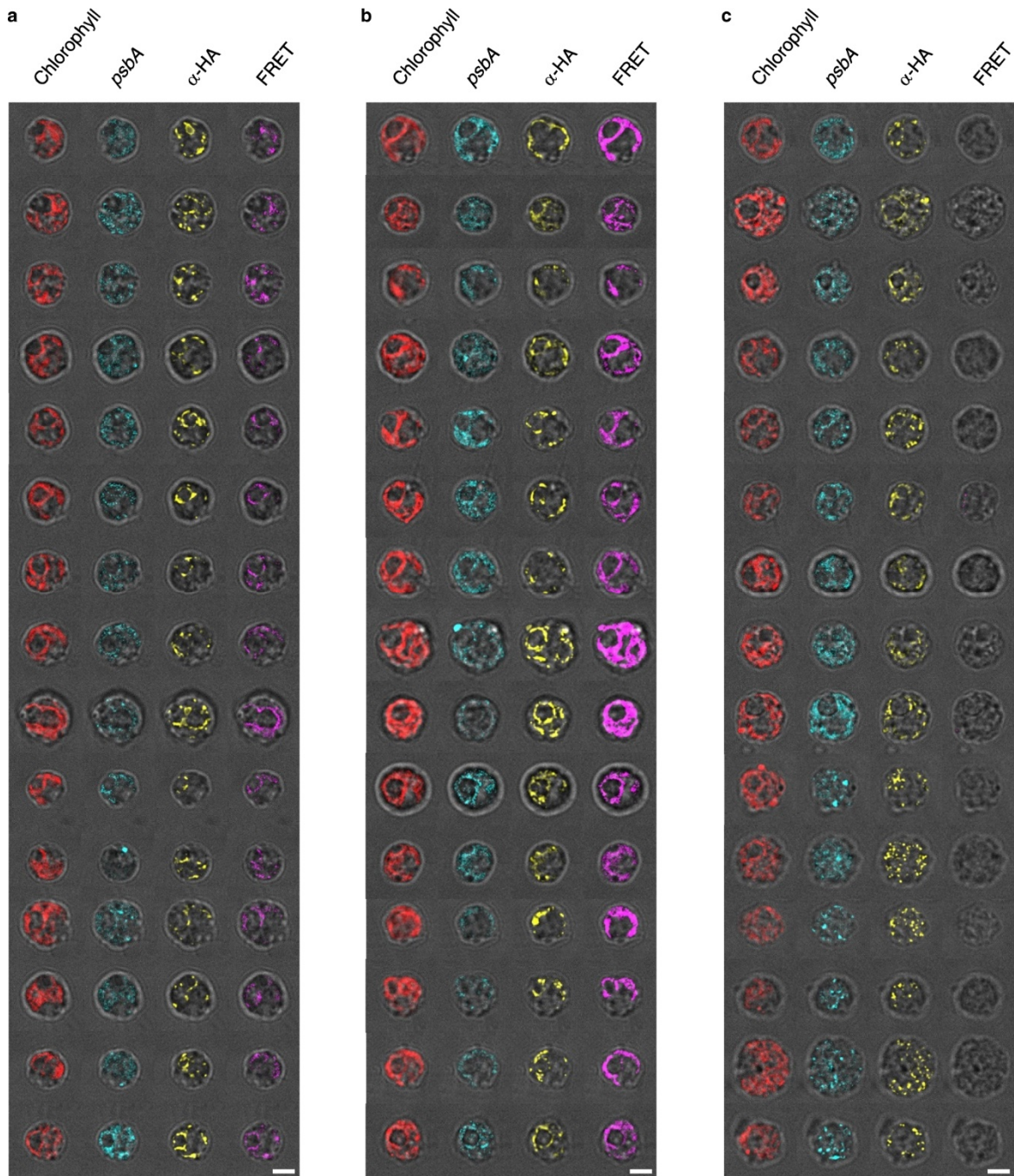
**Supplemental Figure S5: Coomassie brilliant blue-stained SDS gels demonstrating the purification of recombinant acetylation mimicking proteins used for MST analysis.**

Elution fractions of recombinant (a) K193R, (b) K193Q, (c) K197R, (d) K197Q, (e) K200R and (f) K200Q were separated by SDS-PAGE and subsequently stained with Coomassie brilliant blue R-250. Samples were run alongside a molecular mass marker indicated in kDa. The arrow indicates the respective protein.



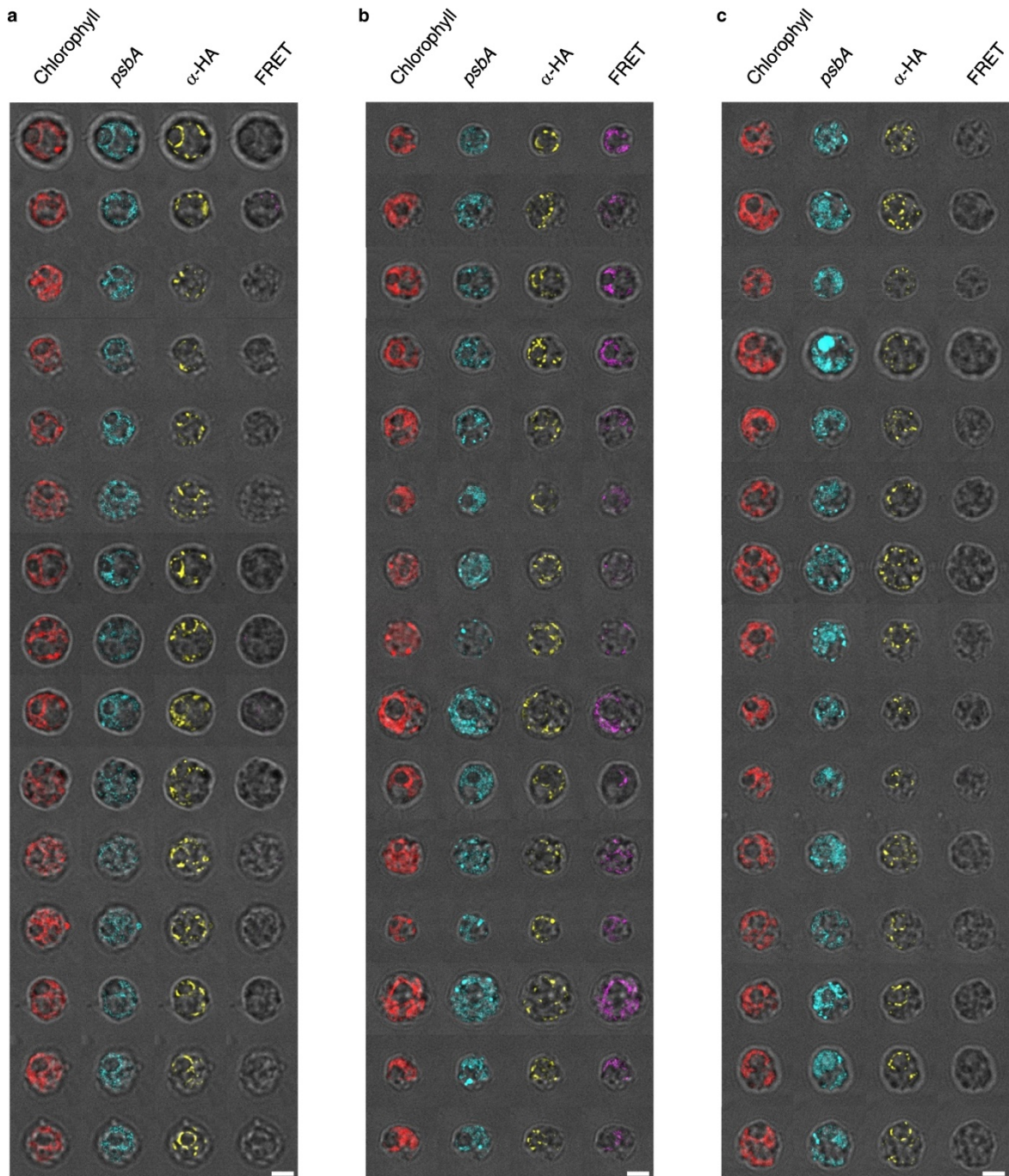
**Supplemental Figure S6: DLA2 accumulation in soluble fractions of various strains.**

10  $\mu$ g of soluble proteins of the DLA2-HA and both K197 acetylation strains were separated via SDS-PAGE and subjected to Western blot analysis to obtain the DLA2 accumulation in comparison to the RbcL accumulation. Strains were grown under (a) mixotrophic or (b) photoautotrophic conditions.



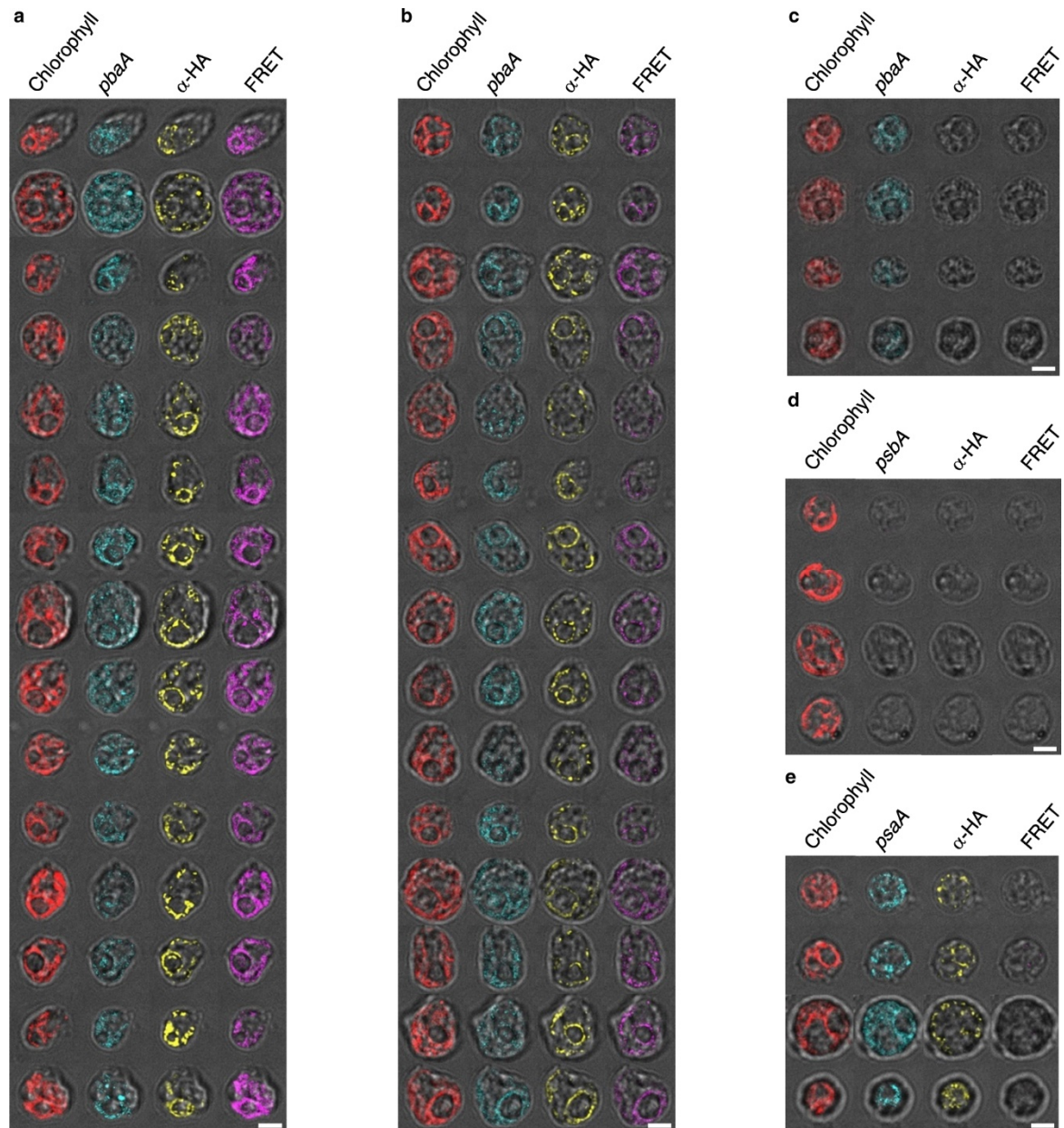
**Supplemental Figure S7: Fluorescence microscopic pictures of various strains under mixotrophic growth conditions.**

(a) DLA2-HA and the acetylation strains (b) K197Q-HA and (c) K197R-HA were grown under mixotrophic growth conditions. Chlorophyll autofluorescence (red), fluorescence in situ hybridization (FISH) of the *psbA* mRNA (cyan), immunofluorescence (IF) of the DLA2-HA protein (yellow) and Förster resonance energy transfer signals (FRET), visualizing DLA2-*psbA* interaction (purple), are depicted. Scale bars = 2  $\mu\text{m}$ . FRET microscopy was performed by Matthias Ostermeier (AG Nickelsen, LMU Munich).



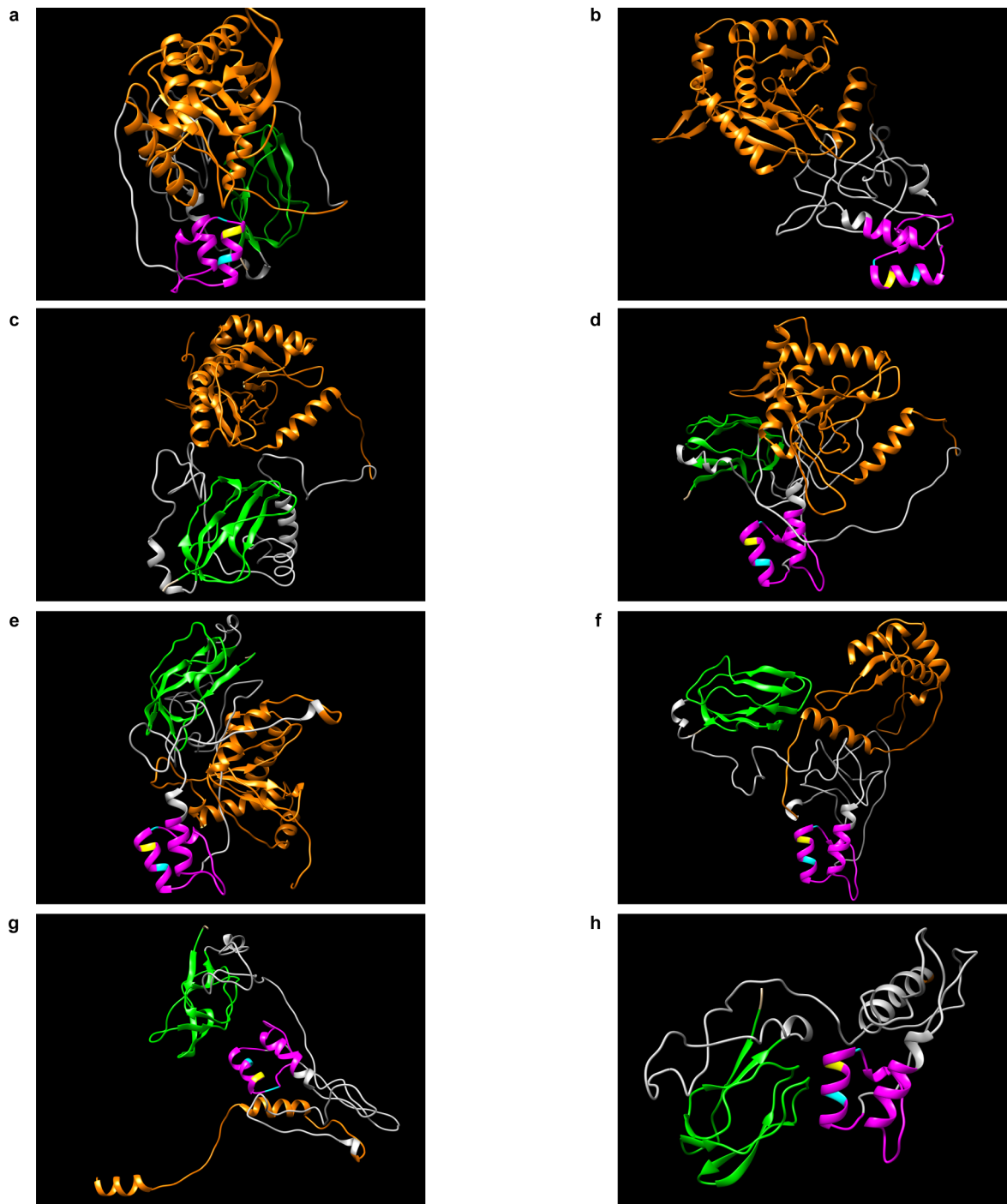
**Supplemental Figure S8: Fluorescence microscopic pictures of various strains under photoautotrophic growth conditions.**

(a) DLA2-HA and the acetylation strains (b) K197Q-HA and (c) K197R-HA were grown under photoautotrophic growth conditions. Chlorophyll autofluorescence (red), fluorescence in situ hybridization (FISH) of the *psbA* mRNA (cyan), immunofluorescence (IF) of the DLA2-HA protein (yellow) and Förster resonance energy transfer signals (FRET), visualizing DLA2-*psbA* interaction (purple), are depicted. Scale bars = 2 μm. FRET microscopy was performed by Matthias Ostermeier (AG Nickelsen, LMU Munich).



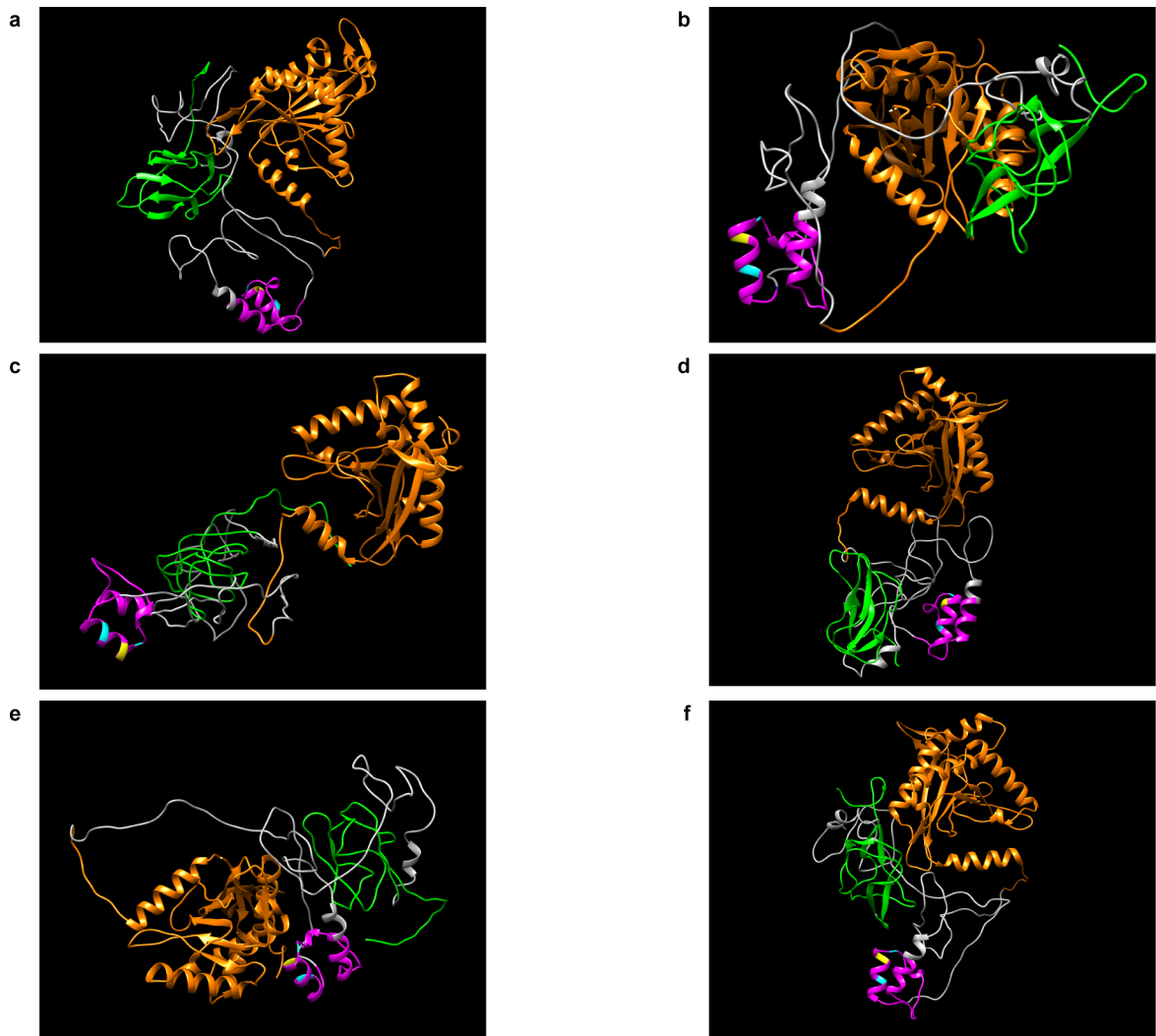
**Supplemental Figure S9: Fluorescence microscopic pictures of various strains under mixotrophic growth conditions.**

K193Q-HA (a) and K200Q-HA (b) strains were analyzed as controls for the effect of a lysine acetylation within the E3BD on *psbA* mRNA-binding of DLA2. (c) *dla2* mutant served as a control for the IF signal and (d) the FuD7 mutant served as a control for the *psbA* mRNA FISH signal. e, DLA2-HA line with oligonucleotides binding to the *psaA* mRNA for obtaining the FISH signal served as a control for the specificity of the FRET signal. Chlorophyll autofluorescence (red), fluorescence in situ hybridization (FISH) of the *psbA* mRNA (cyan), immunofluorescence (IF) of the DLA2-HA protein (yellow) and Förster resonance energy transfer signals (FRET), visualizing DLA2-*psbA* interaction (purple), are depicted. Scale bars = 2  $\mu\text{m}$ . FRET microscopy was performed by Matthias Ostermeier (AG Nickelsen, LMU Munich).



**Supplementary Figure S10: Protein structural models of DLA2 mutant proteins.**

Structural models of the DLA2 mutant proteins used in the MST analysis (compare Figure 11). Models were generated using the Phyre2 web portal for protein modeling, prediction and analysis and the intensive modelling mode (Kelley et al., 2015). The lipoyl-binding domain is depicted in green while the E3BD and the catalytic domain are depicted in purple and orange, respectively. Intrinsically disordered linker regions are depicted in grey. The lysine residues K193 and K200 are depicted in cyan while the *in vivo* acetylated lysine K197 is depicted in yellow. **a**,  $\Delta$ DLA2; **b**,  $\Delta$ Lip; **c**,  $\Delta$ E3B; **d**,  $\Delta$ Cat 462; **e**,  $\Delta$ Cat 450; **f**,  $\Delta$ Cat 394; **g**,  $\Delta$ Cat 315; **h**,  $\Delta$ Cat. Due to the unpredictable disordered linker regions, repeated modeling of the same protein leads to different overall structures but is not affecting the intrinsic structure of the domains.



**Supplementary Figure S11: Protein structural models of the DLA2 acetylation mutant proteins.** Structural models of the DLA2 acetylation mutant proteins used in the MST analysis (compare Figure 15). Models were generated using the Phyre2 web portal for protein modeling, prediction and analysis and the intensive modelling mode (Kelley et al., 2015). The lipoyl-binding domain is depicted in green while the E3BD and the catalytic domain are depicted in purple and orange, respectively. Intrinsically disordered linker regions are depicted in grey. The amino acids at positions 193 and 200 are depicted in cyan while the substituted amino acid at position 197 is depicted in yellow **a**, DLA2 K193R; **b**, DLA2 K193Q; **c**, DLA2 K197R; **d**, DLA2K197Q; **e**, DLA2 K200R; **f**, DLA2 K200Q. Due to the unpredictable disordered linker regions, repeated modeling of the same protein leads to different overall structures but is not affecting the intrinsic structure of the domains.

**LIST OF ABBREVIATIONS**

|                 |  |
|-----------------|--|
| <sup>35</sup> S | radioactive sulfur isotope                         |
| ACK/PAT         | acetyl-kinase/phosphate acetyltransferase          |
| ACS             | acetate synthetase                                 |
| ADP             | adenosine diphosphate                              |
| APS             | ammonium persulfate                                |
| ATP             | adenosine triphosphate                             |
| BRD             | bromodomain  |
| CES             | control by epistasy of synthesis                   |
| CoA             | Coenzym A  |
| cp              | chloroplast  |
| C-terminus      | carboxyl-terminus                                  |
| DAG             | Diacylglycerols                                    |
| DGTS            | diacylglyceryl-3-O-4'-(N,N,N-trimethyl)-homoserine |
| DLA2            | dihydrolipoamide acetyltransferase                 |
| DLD2            | dihydrolipoamide dehydrogenase                     |
| DNA             | deoxyribonucleic acid                              |
| E3BD            | E3-binding domain                                  |
| E3BP            | E3-binding protein                                 |
| ECL             | enhanced chemiluminescence                         |
| FAS             | Fatty acid synthase                                |
| FISH            | fluorescence in situ hybridization                 |
| FRET            | Förster resonance energy transfer                  |
| h               | hours  |
| HA              | hemagglutinin                                      |
| HMW             | high-molecular-weight                              |
| HSM             | high salt medium                                   |
| IF              | Immunofluorescence                                 |
| KATs            | protein Lys-N <sup>ε</sup> -acetyltransferases     |
| KDACs           | protein Lys-N <sup>ε</sup> -deacetylases           |
| LD              | lipoyl domain                                      |
| LHCs            | light-harvesting complexes                         |

|                  |  |
|------------------|--|
| MGDG             | monogalactosyldiacylglycerol                       |
| min              | minutes  |
| mRNA             | messenger RNA                                      |
| MST              | microscale thermophoresis                          |
| mt               | mating type  |
| mt               | mitochondrial                                      |
| NAD <sup>+</sup> | oxidized form of nicotinamide adenine dinucleotide |
| NADH             | reduced form of nicotinamide adenine dinucleotide  |
| NEP              | nuclear-encoded RNA polymerase                     |
| N-terminus       | amino-terminus                                     |
| OPR              | octotricopeptide repeat                            |
| PCR              | polymerase chain reaction                          |
| PDC              | pyruvate dehydrogenase complex                     |
| PDK              | pyruvate dehydrogenase kinase                      |
| PDP              | pyruvate dehydrogenase phosphatase                 |
| PE               | phosphatidylethanolamine                           |
| PEP              | plastid-encoded RNA polymerase                     |
| PNPase           | polynucleotide phosphorylase                       |
| PPR              | pentatricopeptide repeat                           |
| PratA            | processing-associated TPR protein                  |
| PSI              | photosystem I                                      |
| PSII             | photosystem II                                     |
| PTM              | post-transcriptional modification                  |
| RNA              | ribonucleic acid                                   |
| RNP              | ribonucleoprotein                                  |
| ROS              | reactive oxygen species                            |
| rRNA             | ribosomal RNA                                      |
| RT               | room temperature                                   |
| Rubisco          | ribulose-1,5-bisphosphate carboxylase/oxygenase    |
| s                | seconds  |
| SD               | Shine-Dalgarno                                     |
| SDS              | sodium dodecyl sulfate                             |
| TAE              | tris-acetate-EDTA                                  |
| TAG              | triacylglycerols                                   |

---

|        |  |
|--------|--|
| TAP    | tris-acetate-phosphate                           |
| ThDP   | thiamin diphosphate                              |
| TIC    | Translocon at the inner envelope of chloroplasts |
| TOC    | Translocon at the outer envelope of chloroplasts |
| TPP    | thiamine pyrophosphate                           |
| TPR    | tetratricopeptide repeat                         |
| tRNA   | transfer RNA                                     |
| T-zone | translation zone                                 |
| UAC    | unknown apolar compound                          |
| UTR    | untranslated region                              |

## DANKSAGUNG

Zuallererst möchte ich mich bei Herrn Prof. Dr. Jörg Nickelsen bedanken, für die Möglichkeit meine Dissertation in seiner Arbeitsgruppe anzufertigen. Besonders möchte ich mich für die sehr gute Zusammenarbeit, die stundenlangen Diskussionen, die immer zu neuen und hilfreichen Ansätzen führten, sowie für die permanente Unterstützung bedanken.

Vielen Dank auch an Herrn Prof. Dr. Geigenberger für das Übernehmen des Zweitgutachtens meiner Dissertation.

Ein besonderer Dank geht auch an Steffen Heinz, den zweitbesten Blobby Volley Spieler in unserer Gruppe. Deine ununterbrochen gute Laune und stets positive Sichtweise hat mich oftmals vor depressiven Zuständen nach negativen Ergebnissen bewahrt – und manchmal waren deine wissenschaftlichen Ideen auch gar nicht so dumm.

Ganz herzlich möchte ich mich auch bei Laura Kleinknecht bedanken, die mich in die Welt der Wissenschaft eingeführt hat und mich DLA2 lieben als auch hassen gelehrt hat. Deine stete Bereitschaft dir meine wissenschaftlichen Probleme anzuhören und mir immer mit Rat und Tat zur Seite zu stehen, hat mir sehr geholfen.

Ich möchte auch den weiteren Mitarbeitern unserer Gruppe für die gute Zusammenarbeit und die ständige Unterstützung danken. Allen voran Alexandra Bohne, für die vielen hilfreichen Anregungen bezüglich meines Projekts und die zahlreichen guten Gespräche. Den „New Kids on the Chlamy Block“ Tsong und Korbi, für die vielen lustigen Momente und die ständige Tolerierung meines großartigen Musikgeschmacks. Tsong vor allem auch für die Durchführung der Radioaktivexperimente. Matthias für ebenfalls lustige Gespräche und die Durchführung der Mikroskopie. Bei Karin Findeisen und Simone Boos, die die guten Geister der Gruppe während meiner Zeit hier waren, möchte ich mich ebenfalls bedanken.

Des Weiteren möchte ich mich bei den Kollegen der AG Soll für die nette Zusammenarbeit im dritten Stock bedanken sowie bei allen Mitarbeitern in der Botanik, mit denen immer ein sehr freundschaftlicher und produktiver Umgang herrschte. Auch beim SFB TRR175 möchte ich mich bedanken. Vor allem für die Bezahlung, aber auch bei allen involvierten Kollegen, die die jährlichen Meetings immer zu einem Ereignis gemacht haben, das wissenschaftliches Arbeiten und Diskutieren perfekt mit Spaß verbunden hat.

Ein Riesendank geht an meine Mutter und meine Großeltern, die mir meine akademische Ausbildung erst durch konstante finanzielle und moralische Unterstützung ermöglicht haben.

Mein allergrößter Dank geht an meine Frau Marie. Du warst diejenige, die das viele Arbeiten und die oftmals schlechte Laune aushalten und mittragen musste. Ohne deine positive Art und deine ununterbrochene Unterstützung hätte ich es nicht geschafft. Du bist die Beste!

Zuletzt möchte ich meinen Dank und Hass zugleich an *Chlamydomonas reinhardtii* (ja, extra nicht kursiv, hoffe der Seitenhieb kommt an) richten. Du hast mir während der wohl intensivsten Jahre meines Lebens größtmöglichen Frust als auch Glücksgefühle beschert. Irgendwann kriegst du zumindest den ersten Teil zurück. Man sieht sich bekanntlich zweimal im Leben.

**„I’ll be back!“**

## EIDESSTATTLICHE ERKLÄRUNG

Ich versichere hiermit an Eides statt, dass die vorgelegte Dissertation von mir selbständig und ohne unerlaubte Hilfe angefertigt ist.

München, 28. Juli 2020

---

Daniel Neusius

## ERKLÄRUNG

Hiermit erkläre ich, dass die Dissertation nicht ganz oder in wesentlichen Teilen einer anderen Prüfungskommission vorgelegt worden ist. Des Weiteren habe ich mich **nicht** anderweitig einer Doktorprüfung ohne Erfolg unterzogen.

München, 28. Juli 2020

---

Daniel Neusius